

#25

Hydrogeology and Preliminary Calibration of a Preliminary Three-Dimensional Finite-Element Ground-Water Flow Model of the Site Saturated Zone, Yucca Mountain, Nevada

by John B. Czarnecki, Claudia C. Faunt, Carl W. Gable, and George A. Zyvoloski

U.S. Geological Survey
Yucca Mountain Project Milestone Report SP23NM3

Prepared in cooperation with the
NEVADA OPERATIONS OFFICE of the
U.S. DEPARTMENT OF ENERGY, under
Interagency Agreement DE-AI08-92NV10874

DF03⁰/1
102
wm-11

Denver, Colorado
1997

240035

9804240373 971231
PDR WASTE
WM-11 PDR

6

Executive summary	1
Abstract	9
Introduction	10
Purpose and scope	10
Previous work	12
Acknowledgments	14
Quality Assurance Considerations	14
Conceptual model	15
Geologic Setting	15
Hydrologic Setting	21
Potentiometric data	21
Vertical gradients	22
Steady-state conditions	23
Potentiometric surface	25
Large hydraulic gradient	26
Potential perched water occurrence	29
USW UZ-14	29
USW G-2	30
UE-25 WT#6	34
UE-29 a#2	34
Hydraulic properties	36
Aquifer tests	37
Ranges of hydraulic properties	38
Recharge	41
Discharge	44
Hydrochemistry	45
Temperature	48
Hydrogeologic framework model	52
Surface Information	54
Subsurface Information	55
Representation of Faults	55
Structure Contour Maps	56
Assembling the Framework Model	57
Incorporation of Potentiometric Surface	59
Modeling approach	60
Description of FEHMN Computer Code	60
Conservation Equations	61
Constitutive Relations	67
Numerical Methods	69
Features Used in Current Model	70
Parameter Estimation	71
Saturated-Zone Flow-Model Construction	72
3D Finite-Element Mesh	72
Assumptions	76
Description of numerical flow model	77
Permeability	79

Model Zonal Definitions and Variable Values Used in Final Simulation	80
Large Hydraulic Gradient Zone	83
Solitario Canyon Fault Zone	84
Fortymile Wash Recharge Zone	84
Specified-Head Boundary Condiuons	85
Model calibration procedure	88
Model evaluation	90
Simulated Hydraulic Head	90
Simulated Fluxes	93
Sources of error	96
Uses and limitations of the model	99
Summary and conclusions	102
References	105
Figures	113
List of tables	114
Appendices	114

HYDROGEOLOGY AND PRELIMINARY THREE-DIMENSIONAL FINITE-ELEMENT GROUND-WATER FLOW MODEL OF THE SITE SATURATED ZONE, YUCCA MOUNTAIN, NEVADA

by John B. Czarnecki¹, Claudia C. Faunt¹, Carl W. Gable², and George A. Zyvoloski²

EXECUTIVE SUMMARY

Yucca Mountain, Nevada is being characterized by the U.S. Department of Energy and its contractors as to its suitability as a potential site for a repository for high-level nuclear waste. As part of this characterization, numerous studies of the ground-water flow system in the vicinity of Yucca Mountain have been completed or are underway. Development of a preliminary ground-water flow model presented in this report represents a combined effort by personnel from the U.S. Geological Survey and Los Alamos National Laboratory. This report documents the progress of the understanding of the site saturated-zone ground-water flow system at Yucca Mountain based on data analyses and ground-water flow-model simulations through September, 1997.

This report discusses the development of a fully three-dimensional, finite-element model of the Yucca Mountain saturated-zone flow system. The following components are included: (1) description of the conceptual models of the flow system, which differ mainly in terms of the representation of a large hydraulic gradient; (2) description of the numerical code of ground-water flow and heat transport; (3) construction of a three-dimensional, hydrogeo-

¹U.S. Geological Survey, Box 25046, MS 421, Lakewood, Colorado 80225

²Los Alamos National Laboratory, EES-5, MS 665, Los Alamos, New Mexico 87545

logic-framework model; (4) interfacing the framework model with a fully three-dimensional finite-element mesh; (5) hydrologic data and properties assigned within the model domain; (6) interfacing the finite-element numerical model with a parameter-estimation routine; (7) initial calibration of the model; and (8) uses, limitations and capabilities of the hydrogeologic framework and numerical models. The purposes for developing the model of the saturated zone of Yucca Mountain and vicinity are to: (1) estimate ground-water flow direction and magnitude from beneath the design repository area to the accessible environment; (2) characterize the complex three-dimensional behavior of flow through heterogeneous porous and fractured media; (3) provide a means to account for the distribution of ground-water temperature measured within wells within the model area; (4) identify the potential role of fault as barriers or conduits to ground-water flow; and (5) provide a model of the flow system for subsequent flow, heat, and radionuclide-transport modeling.

Data used in the model were primarily developed from published sources or obtained from publicly available sources such as the USGS National Water Information System. Nearly all of these sources originated or were published before the implementation of the accepted Yucca Mountain Project (YMP) quality-assurance program in 1989. The only qualified hydrologic data used in the model analysis are hydraulic-test data from wells UE-25 WT#10, UE-25 WT#12, USW G-2 and USW SD-7 and permeability data. All other hydrologic data used in the model analysis are unqualified. No conclusions, based entirely on qualified data, can be drawn as a result of modeling, and all conclusions documented in this report are primarily based on unqualified data. Model construction and review, however, were performed in accordance with accepted YMP quality-assurance procedures and USGS policy.

The numerical model was developed by interfacing hydrogeologic-framework-model data directly into the construction of the numerical model of ground-water flow. The three-dimensional hydrogeologic framework model is developed using geologic maps, geologic cross sections and well data that

were gridded into structure contour maps. The structure contour maps were stacked to form a three dimensional solid using a 1.500 meters by 1.500 meters horizontal sampling interval and variable vertical thickness. As a result, the framework model has many simplifications that may or may not make it applicable for other uses.

The framework-model data were used to feed an automated mesh generator, which was designed to discretize irregular three-dimensional solids using tetrahedral elements, and to assign material properties from the hydrogeologic framework model to the nodes of the finite-element mesh. The mesh generator facilitated the addition of nodes to the finite-element mesh which correspond to the exact three-dimensional position of the potentiometric surface based on water-levels from wells, which were used for model calibration. Sixteen different hydrogeologic units were represented in the model mesh. The area of the flow model is larger than that of the three-dimensional site geologic framework model (ISM2.0) which was developed to support the Yucca Mountain site unsaturated zone model. The units identified in the geologic and hydrogeologic framework models can be correlated and are consistent.

The numerical model presented in this report is steady state and covers an area of approximately 1.350 km² over a saturated thickness of about 1.5 km, delimited by a rectangular box 45 km long and 30 km wide. The domain was selected to be: (1) coincident with grid cells in the regional ground-water flow model (D'Agnese and others, in press) such that the base of the site model was equivalent to the base of layer 2 of the regional model; (2) sufficiently large to minimize the effects of boundary conditions on estimating permeability values at Yucca Mountain; (3) sufficiently large to be able to assess ground-water flow at distances 30 km downgradient from the design repository area (a potential regulatory issue); (4) small enough to minimize the number of computational nodes used in the model; (5) thick enough to include part of the

regional Paleozoic carbonate aquifer; and (6) large enough to include well control in the Amargosa Desert at the southern end of the model.

Flow simulation was done using the FEHMN (Finite Element Heat Mass Nuclear) ground-water flow and transport computer code. For this report, only saturated ground-water flow was simulated and none of the transport options were used. Calibration of the model was facilitated using an automated parameter estimation routine (PEST) in conjunction with FEHMN which minimized the difference between 94 observed and simulated values of hydraulic head by adjusting selected permeability parameters. Optimal permeability estimates for the sixteen hydrogeologic units lie between high and low values for the same units reported in the literature.

The report also includes a discussion and analysis of the large hydraulic gradient to the north of Yucca Mountain. On a regional basis, other large hydraulic gradients are associated with a contact in the Paleozoic rocks between clastic rocks and regional carbonate aquifer; however, the cause and nature of the large hydraulic gradient near Yucca Mountain is not clear. Proposed explanations include: (1) fault that contain nontransmissive fault gouge; (2) faults that juxtapose transmissive tuff against nontransmissive tuff; (3) the presence of a different type of lithology that is less subject to fracturing; (4) a change in the direction of the regional stress field and a resultant change in the intensity, interconnectedness, and orientation of open fractures on either side of the area with the large hydraulic gradient; (5) the apparent large gradient actually represents a disconnected, perched or semi-perched water body so that the high water-level altitudes are caused by local hydraulic conditions and are not part of the saturated-zone flow system or (6) a highly permeable buried fault that drains water from tuff units into a deeper regional carbonate aquifer; or (7) a buried fault that forms a 'spillway' in the volcanic rocks.

For the model presented in this report, explanation (1) was used to represent the large hydraulic gradient by imposing a vertical barrier to horizontal ground-water flow. The sixth explanation was teste

in the model by specifying large permeability values in place of those used to define the vertical barrier to flow used in (1); however, this representation could not reproduce the large hydraulic gradient using reasonable permeability values. Explanation (2), which, in effect, is equivalent to the seventh explanation, has not been simulated with the model. A higher resolution mesh could be used to investigate this explanation in future models. Explanations (3) and (4) require lateral contrasts in permeability values within the same hydrogeologic unit to represent the large hydraulic gradient, but were not simulated with the model. Explanations (3) and (4) could be represented with the model by defining additional zones within the northern part of the upper volcanic confining unit and the middle volcanic aquifer, which then could be assigned small permeability values. This was not done in the present work. Explanation (5) differs from the others in that it does not require a permeability contrast to represent the large hydraulic gradient, because the large hydraulic gradient is absent, and actually represents a disconnected, perched or semi-perched water body.

If at least some of the water levels measured north of Yucca Mountain represent perched water conditions, the saturated zone potentiometric surface could be substantially different from those that show a large hydraulic gradient in that area. The wells for which perched conditions may be supported by available data are all located in the vicinity or upgradient of the large hydraulic gradient and include borehole USW UZ-14 on Yucca Mountain, and boreholes USW G-2, UE-25 WT#6, and UE-29 a#2.

The report includes a discussion of the ground-water chemistry as it relates to the saturated zone in the model area. The chemical characteristics of ground water in the Yucca Mountain area are a function of recharge-water chemistry and the materials with which the water interacts along the flow path. Preliminary analyses of geochemical and isotopic data from sat-

urated-zone water through February 1997 show little information that can support or refute any of these conceptual models. The chemistry of perched water appears to be different from water collected below the water table.

Hydraulic properties for each of the hydrogeologic units were obtained from previously published hydraulic analyses for wells at Yucca Mountain conducted during the 1980's, published hydraulic properties for hydrogeologic units obtained beyond the immediate Yucca Mountain area, and recent (1995-97) hydraulic analysis of wells USW WT-10, UE-25 WT#12, and USW SD-7, UE-25 c#1, UE-25 c#2, and UE-25 c#3, and USW G-2. A wide range of values are available for hydraulic conductivity and permeability for several hydrogeologic units such as the upper volcanic aquifer and the upper volcanic confining unit, among others. These large ranges likely reflect the presence or absence of permeable fractures, particularly for the carbonate and volcanic aquifers. They also reflect the scale of the test performed such as permeability determination done on core (which would tend to produce small values), as opposed to a long-term aquifer test using multiple wells (which would produce large values and likely be more suitable for use in a model).

Results from 40 model simulations are reported. The greatest improvements came when: (1) very low permeability barriers were added corresponding to the Solitario Canyon fault and the down gradient side of the large hydraulic gradient; and (2) the parameter for the permeability of the upper volcanic confining unit (Calico Hills Formation) was isolated and optimized. The largest class of hydraulic-head residuals (the difference between observed and simulated values) occurred between the range of -5 to +5 m.

Because the site model has lateral boundaries through which significant flow occurs, it was designed to be part of a larger integrated modeling effort in which fluxes would be derived from the USGS regional model. These fluxes could either be estimated, assigned directly within the site model,

used as a comparison with those from the site model. Comparisons of flux between the regional model and site models showed almost twice the amount discharging from the southern end of the site model, and substantially different amounts for the north and east sides. The major flux differences between the two models occur in the northeast corner where a large part of the recharge from the north is diverted east and discharges in part because of the interaction of the constant-head boundaries and the imposed east-west barrier used to represent the large-hydraulic gradient.

On initial inspection, model match to hydraulic-head data and the resulting distribution of residuals have some problems. Although permeability values for all of the hydrogeologic units used in the model lie within reported literature values, reported values for individual units have large ranges. Furthermore, in the case of the middle volcanic aquifer, values of permeability from large-scale hydraulic testing at the C-hole complex were 3 orders of magnitude larger than those used in the model. This discrepancy may be indicative of model error, or alternately, the possibility of a local, large-permeability zone not represented in the present model.

The model discussed in this report is preliminary, in that improvements are required to adequately calibrate the model. Therefore, uses of the current model are limited to the following: (1) provide description of the hydrogeologic framework of the site saturated zone flow system based on a sampling of 1.5 km by 1.5 km; (2) provide a mechanism to extend model calibration and sensitivity testing of parameters used in the model; (3) provide the flow field for doing preliminary transport simulations and estimates of ground-water travel time through the use of additional transport related capabilities within FEHMN; and (4) provide estimates of permeability for sixteen hydrogeologic units from the hydrogeologic framework model and two additional zones of small permeability and recharge at Fortymile Wash.

Limitations of the model include: (1) simulations are restricted to fully saturated conditions from the water table and below; (2) the model does not account for variations in temperature within the flow system; (3) it is likely that the flow model is non-unique; (4) the large hydraulic gradient is poorly understood and greatly affects model calibration, simulated permeability values, and flux; (5) flux into the site model domain is poorly defined and remains one of the most elusive of model variables; (6) limited hydraulic-test data exist for constraining permeability values used in the model; (7) definition of the hydrogeologic units within the model is limited by the sampling interval used (1.5 km). Improvements that could be incorporated to future iterations of the model that include (in no particular order): (1) conduct sensitivity analyses with regard to which model variables have the greatest effect when varied on the sum of squared residuals for hydraulic head; (2) refine the hydrogeologic framework model to better define the distribution of the hydrogeologic units; (3) use the higher resolution sampling of the hydrogeologic framework model to better delineate unit offsets caused by faulting; (4) add major faults explicitly as surfaces within the hydrogeologic framework model so that their potential as fast pathways to the accessible environment may be evaluated; (5) decouple permeability parameters for the upper and middle volcanic aquifers as practical during model calibration; (6) recalibrate the existing model with larger values of permeability in the upper and middle volcanic aquifers; (7) incorporate additional data, such as temperature, into the formal model calibration; (8) include lateral fluxes that are extracted from a refined, improved version of the regional ground-water flow model; (9) include vertical flux through the bottom of the model based on regional model values; and (10) use hydrochemical and isotopic data as a check against flow model result.

ABSTRACT

This report summarizes what is known of the hydrogeology in the saturated zone at Yucca Mountain, Nevada, the potential location for a high-level nuclear-waste repository. A preliminary three-dimensional model of the saturated zone is used to test a few concepts of the flow system, in particular, the large hydraulic gradient. The report presents an alternate concept to explain the apparent large hydraulic gradient, perched water, although the model is not used to test this concept. The development of the model advances the technology of interfacing: (1) complex three-dimensional hydrogeologic framework modeling; (2) fully three-dimensional, unstructured, finite-element mesh generation; and (3) ground-water flow simulation.

The three-dimensional hydrogeologic framework model is developed by using geologic maps, geologic sections, and well data that are converted to structure contour maps. The structure contour maps are stacked to form a three dimensional solid by using a 1,500 meters by 1,500 meters horizontal sampling area and a variable vertical thickness. The framework model consists of different hydrogeologic units that covering a 1,350 square-kilometer rectangular area, 45 kilometers long and 30 kilometers wide.

The framework-model data are used as direct input to an automated mesh generator, which is designed to discretize irregular three-dimensional solids by using tetrahedral elements, and to assign unit identifiers from the hydrogeologic framework model to the nodes within the mesh. The mesh generator was used to add nodes to the finite-element mesh to locate observed hydraulic-head values accurately. These nodes then are used as observation points for hydraulic head during model calibration. The resulting mesh consists of 9,279 nodes and 51,461 tetrahedral elements that represent 16 different hydrogeologic units.

The ground-water flow capabilities of a ground-water flow and heat-transport simulator

with variable saturation are used with the resulting finite-element mesh to simulate ground-water flow. Initial calibration of the model is facilitated by using an automated parameter-estimation routine, which minimizes the difference between 94 observed and simulated values of hydraulic head, by adjusting selected permeability and flow parameters. Optimal permeability estimates for 16 hydrogeologic units lie between high and low values for the units reported in the literature. Simulated hydraulic-head values agree closely with observed values, the majority of which have residuals of less than 5 meters. Results indicate that a more refined mesh and more detailed boundary conditions could be used to improve the model.

INTRODUCTION

Yucca Mountain, Nevada is being characterized by the U.S. Department of Energy and its contractors as to its suitability as a potential site for a repository for high-level nuclear waste. As part of this characterization, numerous studies of the ground-water flow system in the vicinity of Yucca Mountain have been done or are underway. Development of the modeling approach presented in this report represents a combined effort by personnel from the U.S. Geological Survey and Los Alamos National Laboratory. This report documents the progress of the understanding of the site saturated-zone ground-water flow system at Yucca Mountain on the basis of data analyses and ground-water flow-model simulations through September, 1997. The work is being done in cooperation with the U.S. Department of Energy under Interagency Agreement DE-AI08-92NV10874.

Purpose and scope

The purposes for developing this model of the saturated zone of Yucca Mountain and vicinity are to: (1) estimate ground-water flow direction and magnitude from beneath the design repository area to

the accessible environment: (2) characterize the complex three-dimensional behavior of flow through heterogeneous porous and fractured media; (3) provide a means to account for the distribution of ground-water temperature measured within wells within the model area; (4) identify the potential role of faults as barriers or conduits to ground-water flow; and (5) provide a model of the flow system for subsequent flow, heat, and radionuclide-transport modeling.

To accomplish these goals a hydrogeologic framework model was developed and used to construct a numerical ground-water flow model. In addition, optimal hydrologic-variable values used in the numerical model were obtained through non-linear regression techniques using PEST³ (Watermark Computing, 1994), a model-independent, parameter-estimation software package. The numerical flow model was developed by using the numerical code FEHMN (Finite Element Heat Mass Nuclear) (Zyvoloski and others, 1995). The resulting flow model will provide the basis for subsequent models of heat flow and radionuclide transport.

This report documents the understanding of the site saturated-zone ground-water flow system as of September, 1997, and discusses the development of a fully three-dimensional, finite-element model of the Yucca Mountain saturated-zone flow system. The following components are included: (1) description of the conceptual models of the flow system, which differ mainly in terms of the representation of a large hydraulic gradient; (2) description of the numerical code of ground-water flow and heat transport; (3) construction of a three-dimensional, hydrogeologic-framework model; (4) interfacing the framework model with a fully three-dimensional finite-element mesh; (5) hydrologic data and properties assigned within the model domain; (6) interfacing the finite-element numerical model with a parameter-estimation

³The use of brand, trade, or firm names in this report is for identification purposes only and does not constitute endorsement by the U.S. Geological Survey.

routine: (7) calibration of the model; and (8) uses, limitations and capabilities of the hydrogeologic framework and numerical models.

The numerical model presented in this report is steady state and covers an area of about 1,350 km² over a saturated thickness of about 1.5 km (fig. 1), delimited by a rectangular box 45 km long and 30 km wide. The domain was selected to be: (1) coincident with grid cells in the regional ground-water flow model (D'Agnesse and others, in press) such that the base of the site model was equivalent to the base of layer 2 of the regional model; (2) sufficiently large to minimize the effects of boundary conditions on estimating permeability values at Yucca Mountain; (3) sufficiently large to be able to assess ground-water flow at distances 30 km downgradient from the design repository area (a regulatory issue); (4) small enough to minimize the number of computational nodes used in the model; (5) thick enough to include part of the regional Paleozoic carbonate aquifer; and (6) large enough to include well control in the Amargosa Desert at the southern end of the modeled area.

Previous work

Several numerical models of ground-water flow have been developed at various scales to simulate ground-water flow in the vicinity of Yucca Mountain. Regional-scale modeling of the Nevada Test Site and vicinity was done by Waddell (1982), Rice (1984), and Sinton (1987). The areal domain of these models was virtually identical (about 18,000 km²). Waddell and Rice examined two-dimensional areal flow, whereas Sinton's model incorporated the third (depth) dimension in a quasi-three dimensional application of the MODFLOW (McDonald and Harbaugh, 1988) computer program. D'Agnesse (1994) modeled an even larger area (34,141 km²) of the Death Valley regional ground-water flow system in three dimensions, and used geoscientific information system (GIS) analyses to obtain estimates of recharge, discharge, and hydraulic conductivity. D'Agnesse and others (in press) advanced the original

model of D'Agnesse (1994) in a number of ways, including the application of non-linear regression techniques using MODFLOWP (Hill, 1992), in which observed values of hydraulic head and spring flows were used to estimate areal recharge rates, hydraulic conductivities, and other selected model parameters. A flow model of an area approximating that of Waddell (1982) has been developed for characterizing tritium migration and assessing risk subsequent to underground nuclear testing at the Nevada Test Site (U.S. Department of Energy, 1997).

Subregional modeling has included the two-dimensional model of Czarnecki and Waddell (1984) in which parameter estimation was used to estimate values of transmissivity through most of the model area. Czarnecki (1985) used the same finite-element mesh and a slightly modified distribution of transmissivity values to estimate the effect of increased recharge on water-table altitude and ground-water flow direction. A cross-sectional model was developed by Haws (1990) along a flow path constructed from the flow-field vectors of Czarnecki and Waddell (1984). Additional models by Czarnecki (1989a, 1991) examined the effects of abrupt changes in hydraulic conductivity in the vicinity of the large hydraulic gradient (LHG) on the north end of Yucca Mountain coupled with increases in recharge to the flow system. Modeling by Carrigan and others (1991) looked at potential changes of the water-table altitude at Yucca Mountain resulting from seismic events. Other modeling efforts by Dressel (1992) and Ahola and Sagar (1992) were used to examine the effects of changes in hydraulic properties and recharge on water-table altitude within the flow system. A model of ground-water flow in the immediate vicinity of Yucca Mountain was developed by Barr and Miller (1987). Buscheck and Nitao (1992) discuss the possible effects of heat from the design repository on ground-water flow in the unsaturated and saturated zones.

Acknowledgments

Lynn Trease (Los Alamos National Laboratory) maintains FEHMN and provided support for use on various platforms. Diana Perfect, Brandi Kirchoff, and William Oatfield (U.S. Geological Survey) compiled and input much of the data contained in the hydrogeologic framework model. Carma San Juan (Pacific Western Technologies, Ltd.) compiled potentiometric data from a variety of different sources. Shelley Piksa, Paul Denning, and G.M. O'Brien (U.S. Geological Survey) compiled the hydrogeologic properties for the hydrogeologic units represented in the model. John Doherty (Watermark Computing) provided prompt, expert guidance on the application of the PEST parameter-estimation software system. Wayne Belcher (U.S. Geological Survey) provided a careful comparison between the hydrogeologic framework model and the resulting finite-element mesh.

Quality Assurance Considerations

Because interpretations of model results may be used to assess the expected performance of a high-level nuclear-waste repository, confidence in the reliability of data used in model conceptualization, construction and evaluation is necessary. A quality-assurance program has been implemented by USGS for the Yucca Mountain Project (YMP) to support the reliability of the data and interpretations of data.

Data used by YMP are classified as either "qualified" or "unqualified". Qualified data are defined as "data acquired or developed for the YMP under a Nuclear Regulatory Commission accepted quality assurance plan or qualified in accordance with appropriate YMP procedures. Developed data cannot be classified as qualified if derived from unqualified data sources" (U.S. Department of Energy, written commun., 1993).

Data used in the construction of the hydrogeologic framework model and the ground-water flow model were primarily developed from published sources or obtained from publicly available sources.

such as the USGS National Water Information System. Nearly all of these sources originated or were published before the implementation of the accepted YMP quality-assurance program in 1989. Model construction and review, however, were performed in accordance with accepted YMP quality-assurance procedures and USGS policy.

The only qualified data used in the model analysis are hydraulic-test data from wells UE-25 WT#10, UE-25 WT#12, and USW SD-7 (O'Brien, 1997) and permeability data (Flint and Flint, 1990). All other data used in the model analysis are unqualified. Because of the preponderance of available unqualified hydraulic-head and hydraulic-test data, no saturated zone model of Yucca Mountain can be constructed using only qualified data.

CONCEPTUAL MODEL

Geologic Setting

The geologic setting, geologic history, stratigraphy, and structure of Yucca Mountain are reviewed in Luckey and others (1996, p. 7-13). Briefly, Yucca Mountain (fig. 2) is located in the Great Basin section of the Basin and Range physiographic province, and consists of a group of north-south-trending block-faulted ridges (fig. 3a,b) that are composed of volcanic rocks of Tertiary age that may be several kilometers thick. The basin to the west of Yucca Mountain is Crater Flat, which is composed of a thick sequence (about 2,000 m) of Tertiary volcanic rocks, Tertiary and Quaternary alluvium, and small basaltic lava flows of Quaternary age. Crater Flat is separated from Yucca Mountain by Solitario Canyon Fault (fig. 3b). West of Crater Flat is Bare Mountain (fig. 2), which is composed of Paleozoic and Precambrian rocks. Fortymile Wash (fig. 3b), a structural trough, delimits the eastern extent of Yucca Mountain. East of

Yucca Mountain are the Calico Hills, a mottled assemblage of Tertiary volcanic rocks and Paleozoic rocks. Yucca Mountain terminates to the south in the Amargosa Desert, which consists of interbedded Quaternary and Tertiary alluvial, paludal, and tuffaceous sediments.

These rocks and deposits in the vicinity of Yucca Mountain were classified into hydrogeologic units (fig. 3a). The hydrogeologic units were based on hydraulic properties. Where possible, hydrogeologic units identified by previous investigators (Luckey and others, 1996; Winograd and Thordarson, 1975) were used. Many of the units are not present in the model area and/or are not expressed at the land surface (fig. 3b). In all, 16 hydrogeologic units are present in the model area (fig. 4; table 1). Table 1 summarizes the 16 hydrogeologic units and how they correlate with the different geologic units in the model area. Figure 4 illustrates, by way of a fence diagram, the complex three-dimensional spatial relation among these units within the saturated zone of the model area. In general, the hydrogeologic units at Yucca Mountain form a series of alternating volcanic aquifers and confining units overlaying the regional carbonate aquifer. The volcanic aquifers and confining units interbed with undifferentiated valley-fill and the valley-fill aquifer to the south, while structural features delimit the eastern and western edges of Yucca Mountain (fig. 3b).

Table 1.--Hydrogeologic units, equivalent units, and associated lithologies in the vicinity of Yucca Mountain

[--, no units identified; hydrologic-unit names listed in parentheses; Q, Quaternary; T, Tertiary; Pz, Paleozoic; pC, Precambrian; data-availability rating (intended as a relative indicator of data availability, not to precisely estimate the knowledge of the spatial extent of each of the hydrogeologic units): 0.1, poor; 10.0, excellent]

Hydrogeologic Unit (Age)	Model Unit Number (Parameter Name)	Equivalent Unit			Lithology	Data-Availability Rating
		Winograd and Thordarson (1975)	Laczniak and others (1996)	Luckey and others (1996)		
Valley-fill aquifer (Q, T)	19 (qal)	Valley Fill (Valley-fill aquifer)	Alluvial deposits (Valley-fill aquifer)	Alluvium	Alluvial fan, fluvial, conglomerate, lakebed, collian and mudflow deposits	9.0
Valley-fill confining unit (Q, T)	18 (tpla)	Valley Fill (Valley-fill aquifer)	Alluvial deposits (Valley-fill aquifer)	Alluvium	Playa deposits	5.0
Limestone aquifer (T)	17 (tlm)	--	--	--	Lacustrine limestones, calcareous spring deposits	0.0
Lava-flow aquifer (Q, T)	16 (b)	Basalt of Kiwi Mesa Basalt of Skull Mountain (Lava-flow aquifer)	Basalt	--	Basalt flows, dikes and cinder cones, latite dikes	1.0
Upper volcanic aquifer (T)	15 (uva)	Timber Mountain Tuff Paintbrush Tuff (Welded-tuff aquifer)	Thirsty Canyon Group Timber Mountain Group Paintbrush Group (Welded-tuff and lava-flow aquifers)	Paintbrush Group (Upper volcanic aquifer)	Variably welded ash-flow tuffs and rhyolite lavas (non-welded tuffs)	6.0

Table 1.--Hydrogeologic units, equivalent units, and associated lithologies in the vicinity of Yucca Mountain (Continued)

[--, no units identified; hydrologic-unit names listed in parentheses; Q, Quaternary; T, Tertiary; Pz, Paleozoic; pC, Precambrian; data-availability rating (intended as a relative indicator of data availability, not to precisely estimate the knowledge of the spatial extent of each of the hydrogeologic units): 0.1, poor; 10.0, excellent]

Hydro-geologic Unit (Age)	Model Unit Number (Parameter Name)	Equivalent Unit			Lithology	Data-Availability Rating
		Winograd and Thordarson (1975)	Laczniak and others (1996)	Luckey and others (1996)		
Upper volcanic confining unit (T)	14 (uvcu)	Wahmonie Formation Salyer Formation Rhyolite flows and tuffaceous beds of Calico Hills (Lava-flow aquitard - Tuff aquitard)	Volcanics of Area 20 Wahmonie Formation (Lava-flow aquifers)	Calico Hills Formation (Upper Volcanic Confining Unit)	Rhyolite lavas, volcanic breccias, non-welded to welded tuffs, commonly argillaceous or zeolitic	10
Middle volcanic aquifer (T)	13 (mva)	Grouse Canyon Member Tuff of Crater Flat (Tuff aquitard)	Crater Flat Group Belled Range Group (Welded-tuff and lava-flow aquifers)	Crater Flat Group (Lower Volcanic Aquifer)	Variably welded ash-flow tuffs and rhyolite lavas	0.8
Middle volcanic confining unit (T)	12 (mvcu)	Local informal units of Indian Trail Formation (Tuff aquitard)	Tunnel Formation (Tuff confining unit)	Flow Breccia Lithic Ridge Tuff (Lower Volcanic Confining Unit)	Non-welded tuff, commonly zeolitized	0.8
Lower volcanic aquifer (T)	11 (lva)	Tub Spring Member (Tuff aquitard)	Volcanics of Big Dome (Lava-flow and welded-tuff aquifer)	--	Variably welded ash-flow tuffs, rhyolite lavas	0.1
Lower volcanic confining unit (T)	10 (lvcu)	? (Tuff aquitard)	Older Volcanics (Tuff confining unit)	--	Non-welded tuff, commonly zeolitized	0.1

Table 1.--Hydrogeologic units, equivalent units, and associated lithologies in the vicinity of Yucca Mountain (Continued)

[--, no units identified; hydrologic-unit names listed in parentheses; Q, Quaternary; T, Tertiary; Pz, Paleozoic; pC, Precambrian; data-availability rating (intended as a relative indicator of data availability, not to precisely estimate the knowledge of the spatial extent of each of the hydrogeologic units): 0.1, poor; 10.0, excellent]

Hydrogeologic Unit (Age)	Model Unit Number (Parameter Name)	Equivalent Unit			Lithology	Data-Availability Rating
		Winograd and Thordarson (1975)	Laczniak and others (1996)	Lucky and others (1996)		
Undifferentiated valley fill (T)	9 (lca)	Rocks of Pavits Spring Horse Spring Formation (Tuff aquitard)	Pavits Spring Formation Horse Spring Formation Paleocolloivium	--	Tuffaceous sandstone, tuff breccia, siltstone, claystone, conglomerate, lacustrine limestone, commonly argillaceous or calcareous. Sedimentary breccia.	5.0
Upper carbonate aquifer (Pz)	8 (uca)	Tippisah Limestone (Upper carbonate aquifer)	Bird Spring Formation (Upper carbonate aquifer)	--	Limestone	0.3
Upper clastic confining unit (Pz)	6 (ecu)	Eleana Formation (Upper clastic aquitard)	Eleana Formation (Eleana confining unit)	--	Siliceous siltstone, sandstone, quartzite, conglomerate, limestone	0.5
Lower carbonate aquifer (Pz)	3, 5, 7 (lca)	Devils Gate Limestone Nevada Formation Ely Springs Dolomite Eureka Quartzite Pogonip Group Nopah Formation Dunderberg Shale Bonanza King Upper Carrara Formation (Lower carbonate aquifer)	Guilmette Formation Simonson Dolomite Sevy, Laketown, and Lone Mountain Dolomite Roberts Mountain Formation Dolomite of the Spotted Range Ely Springs Dolomite Eureka Quartzite Pogonip Group Nopah Formation Bonanza King Formation Upper Carrara Formation (Lower carbonate aquifer)	Lone Mt. Dolomite Roberts Mt. Dolomite (Carbonate Aquifer)	Dolomite and limestone, locally cherty and silty	0.5

Table 1.--Hydrogeologic units, equivalent units, and associated lithologies in the vicinity of Yucca Mountain (Continued)

[--, no units identified; hydrologic-unit names listed in parentheses; Q, Quaternary; T, Tertiary; Pz, Paleozoic; pC, Precambrian; data-availability rating (intended as a relative indicator of data availability, not to precisely estimate the knowledge of the spatial extent of each of the hydrogeologic units): 0.1, poor; 10.0, excellent]

Hydrogeologic Unit (Age)	Model Unit Number (Parameter Name)	Equivalent Unit			Lithology	Data-Availability Rating
		Winograd and Thordarson (1975)	Laczniak and others (1996)	Luckey and others (1996)		
Lower clastic confining unit (Pz, pC)	4 (qcu)	Lower Carrara Formation Zabriskie Quartzite Wood Canyon Formation Stirling Quartzite Johnnie Formation (Lower clastic aquitard)	Lower Carrara Formation Zabriskie Quartzite Wood Canyon Formation Stirling Quartzite Johnnie Formation Noonday (?) Dolomite (Quartzite confining unit)	--	Quartzite, siltstone, shale, dolomite	0.8
Granitic confining unit (T)	2 (gran)	Granitic Stocks (A minor aquitard)	Granite	--	Granodiorite and quartz monzonite in stocks, dikes and sills	0.1

Hydrologic Setting

Luckey and others (1996, p. 13-28) provide a comprehensive review of the hydrologic setting of Yucca Mountain. Briefly, Yucca Mountain is centrally located within the Death Valley ground-water basin and also is centrally located within the Alkali Flat (Franklin Lake playa)-Furnace Creek subbasin (Luckey and others, 1996, p. 13). Neither of these basins is shown on the figures presented in this report, but Death Valley and Alkali Flat (Franklin Lake playa) are shown in figure 2. The subbasin is assumed to receive water from areal recharge within its boundaries and probably also receives water as underflow from adjoining subbasins. Depths to water range from about 3 m beneath Alkali Flat (Franklin Lake playa) to about 750 m beneath Yucca Mountain. Ground water beneath Yucca Mountain flows generally toward the south through fractured volcanic rocks which interfingers with Quaternary and Tertiary valley-fill in the Amargosa Desert.

The climate is arid to semiarid, with Yucca Mountain receiving annual precipitation between 150 mm to 200 mm (Hevesi and others, 1992, p. 683, fig. 3(a)). As a result, stream flow is infrequent and occurs following intense precipitation events which can be very localized. There are no perennial streams.

Potentiometric data

Hydraulic-head values from wells located within the model area that were used in model construction and calibration are listed in appendix A. All of the hydraulic-head values are unqualified data. The data (appendix A) include measurements from the WT holes (#3, 5, 7, 10, 11, 14, 15, 19, 20, 21, 24, 25, 27, 29, 30), C-holes (#16, 17, 18), and USW G-2 (#4). The data are from the USGS National Water Information System. Hydraulic-head data beyond the model area (fig. 1) are from Ciesnik (1995).

There are eighty boreholes located within the model area. Twelve of the boreholes (USW H-1, USW H-5, UE-25b 1, USW H-6, USW H-4, USW H-3, UE-25p 1, UE-25c 1, UE-25c 2, UE-25c 3, and two unnamed boreholes) have multiple piezometers. Forty-five of the boreholes are either uncased or have fifty percent or more perforated casing. Twelve boreholes are cased, while the presence or absence of casing is unknown for eleven of the boreholes.

Many of the boreholes are "dry" until a fracture zone is intercepted, at which point the water level in the borehole rises to a static level. Because of long open or perforated intervals, many boreholes intercept multiple permeable zones. As a result, the hydraulic head in many of the boreholes represents a composite head.

Vertical gradients

Luckey and others (1996, pp. 27-29) examined the vertical relationship of hydraulic head at Yucca Mountain, and found "no unambiguous areal patterns in the distribution of vertical hydraulic gradient around Yucca Mountain." However, they do make the following generalizations as to the distribution of potentiometric levels in the lower sections of the volcanic rocks. Potentiometric levels in the middle volcanic confining unit are relatively high (altitude greater than 750 m) in the western and northern parts of Yucca Mountain and are relatively low (altitude about 730 m) in the eastern part of Yucca Mountain. Based on potentiometric levels that were measured in borehole UE-25 p#1, the potentiometric levels in the middle volcanic confining unit in boreholes USW H-1, USW H-3, USW H-5, and USW H-6 may reflect the potentiometric level in the carbonate aquifer. Boreholes UE-25 b#1 and USW H-4 do not seem to fit the pattern established by the other boreholes. They report that potentiometric levels generally are higher in the lower intervals of the volcanic rocks than in the upper intervals, indicating a potential for upward ground-water movement. However, for unknown reasons, at four boreholes (USW G-4, USW H-1, USW H-6, and UE-25 b#1) potentiometric levels in the volcanic rocks are higher in the uppermost

intervals than in the next lower intervals.

The potentiometric levels in the Paleozoic carbonate aquifer at borehole UE-25 p#1 are about 21 m higher than in the overlying volcanics. Therefore, a potential for upward ground-water movement from the Paleozoic rocks to the volcanic rocks is indicated. However, upward ground-water flow from the Paleozoic rocks is considered to be minor. Because of the large difference in potentiometric levels in these two aquifers, Luckey and others (1996, pp. 27-29) conclude that they seem to be hydraulically separate. This conclusion appears to be supported by hydrochemical data. However, some of the analyses of hydraulic-test data at the C-hole complex indicate a possible hydraulic connection between the volcanics and the carbonate aquifer at the C-hole complex (Geldon, 1996). Hence, the vertical hydraulic gradients represent a complex three-dimensional flow system that is not completely understood. Little information is available for vertical gradients away from Yucca Mountain.

Steady-state conditions

A comprehensive analysis of water levels from all observation wells at Yucca Mountain (Graves and others, 1997) shows the fluctuations of water levels for the period 1985 to 1995. Generally, most wells at Yucca Mountain show less than 1 meter difference between the maximum and minimum values of water-level altitude during this period. Exceptions are listed in table 2. Even for these, the water level fluctuations are small relative to the total effective saturated thickness of the flow system. The preponderance of wells with small water level changes and the small fractional changes in saturated thickness at wells with greater changes indicates that assuming that the flow system is at steady state at Yucca Mountain is a reasonable approximation.

Table 2.--Largest water-level fluctuations in wells in the vicinity of Yucca Mountain

[+, indicates water-level rise, -, indicates water level decline]

Observation Well Name	Observation Number in Appendix A	Approximate Water Level Change During Hole History (meters)	Comment	References
USW G-2	4	-12	Water level has declined monotonically since hole construction in 1981 until present (1997); possibly related to perched water conditions. 1995 water level used in model.	Robison and others (1988, p. 86); Graves and others (1997, p. 36)
UE-25 WT#6	3	+4	Borehole was completed in June, 1983. Water levels rose from 1983 to 1988, then stabilized until the 1992 earthquake, after which erratic changes occurred. Water-levels stabilized within months. 1995 water level used in model.	Robison and others (1988, p. 36); Graves and others (1997, p.16)
USW H-3, Lower Interval	93	+9	Drilled 1982, packer initially installed in January 1983. Packer replaced in 1991; water-level change occurred between 1991-1995. 1995 water level used in model	Graves and others (1997, p.16)
UE-29 a#2	1	+4	Well completed December 1981. Water level oscillations observed between 1991 and 1995, and were temporally correlated with recharge from precipitation/run-off events in Fortymile Wash and its tributaries. 1984 water level used in model	C.S. Savard, U.S. Geological Survey, written commun., 1997
Wells in the Amargosa Farms area	45-79	-10	Water-level declines are attributable to irrigation. Dates of measurements range from 1958 through 1996.	Kilroy (1991, p. 14)

Kilroy (1991) discusses water-level changes in the Amargosa Desert between the 1950's and 1987.

Within the model area, water levels have declined by as much as about 10 m (Kilroy, 1991, p. 14) in the

Amargosa Farms area (southwest corner of the site model) resulting from ground-water withdrawals for irrigation. No attempt was made within this report to reconstruct the potentiometric surface for conditions prior to these ground-water withdrawals.

The potentiometric data dictate a complex three-dimensional flow system, but the following generalizations can be made. There appears to be a general upward gradient from the regional carbonate aquifer into the volcanic rocks. In general, this upward gradient persists in the volcanic rocks. Furthermore, the potentiometric data indicate that most of the flow system is essentially at steady state.

Potentiometric surface

Because the potentiometric data dictate a complex three-dimensional flow system, a number of different conceptual models of the flow system are possible. In particular, the different conceptual models may result in different potentiometric surfaces. Although the boreholes are open at different depths below the hydraulic head and are open to different geologic zones, water levels in most of the wells appear to represent a laterally continuous aquifer system. The well-connected system may result from the presence of many faults and fractures (Tucci and Burkhardt, 1995), and, at the scale of the site model, the ground-water flow system may behave as a porous medium. Flow in the volcanic rocks occurs primarily in fractures and secondarily in the matrix of the rock. Therefore, the uppermost aquifer may be unconfined or confined depending upon the areal location of the point being measured (Tucci and Burkhardt, 1995, p. 7).

Figure 5 shows a representation of a computer-generated potentiometric surface over the model area in which data from all available wells in and around the model area were used. The

well locations from which potentiometric data were used in contouring are shown on figures 1 and 5. Water-level altitude data outside the model domain, which were used for control at the map edges, were obtained from tables 1 and 2 in Ciesnik (1995); those within the model domain are listed in appendix A of this report. For the case of wells having multiple piezometers, only data from the upper-most completed borehole interval was used. Deep wells at Yucca Mountain are shown on figure 6.

Most of the wells are partially penetrating. No attempt was made to segregate and analyze water-level measurements associated with specific hydrogeologic units or fracture zones. Some water levels represent composite heads from multiple hydrogeologic units and fractures. In general, this portrayal of the potentiometric surface at Yucca Mountain (fig. 5) is consistent with those referenced consequent to and including Robison's 1984 work, which implies a hydraulically well-connected flow system within the saturated zone (that is, perched or semi-perched conditions are absent).

The potentiometric surface map presented in figure 5 does not strictly represent the water table, a concept reserved for the actual interface between the saturated and unsaturated zones. However, the potentiometric surface is probably a reasonable representation of the water table for the following reasons: (1) At Yucca Mountain, water levels at most wells were obtained from the uppermost part of the saturated zone (Graves and others, 1997). (2) South of Yucca Mountain, wells penetrate a significant thickness of the saturated zone, but in this area most ground-water flow is believed to be horizontal and all available data indicate that the vertical-head gradients are negligible. (3) For the case of wells having multiple piezometers, only water levels from the uppermost saturated interval were used in the construction of the potentiometric-surface map.

Large hydraulic gradient

Possible differences in conceptual models of the flow system pertain to the representation of an apparent large hydraulic gradient (LHG) on the north end of Yucca Mountain (fig. 5)--an area where the

altitude of the potentiometric surface appears to change by about 300 meters over a lateral distance of 2 kilometers (Czarnecki and others, 1994; Czarnecki and others, 1995). Prior to the construction of borehole USW G-2 in 1981, no water-level data existed at Yucca Mountain on which to base the LHG. As more boreholes were constructed at Yucca Mountain, particularly holes UE-25 WT#6 and UE-25 WT#16 (fig. 5), a somewhat better definition of the LHG developed.

On a regional basis, other large hydraulic gradients are associated with a contact in the Paleozoic rocks between clastic rocks and regional carbonate aquifer; however, the cause and nature of the LHG near Yucca Mountain is not clear. Proposed explanations include: (1) faults that contain nontransmissive fault gouge (Czarnecki and Waddell, 1984); (2) faults that juxtapose transmissive tuff against nontransmissive tuff (Czarnecki and Waddell, 1984); (3) the presence of a different type of lithology that is less subject to fracturing (Czarnecki and Waddell, 1984); (4) a change in the direction of the regional stress field and a resultant change in the intensity, interconnectedness, and orientation of open fractures on either side of the area with the LHG (Czarnecki and Waddell, 1984); or (5) the apparent large gradient actually represents a disconnected, perched or semi-perched water body so that the high water-level altitudes are caused by local hydraulic conditions and are not part of the saturated-zone flow system (Czarnecki and others, 1994; Ervin and others, 1994). Fridrich and others (1994) suggest two hydrogeologic explanations for the LHG: (1) a highly permeable buried fault that drains water from tuff units into a deeper regional carbonate aquifer or (2) a buried fault that forms a "spillway" in the volcanic rocks. Their second explanation, in effect, juxtaposes transmissive tuff against non-transmissive tuff, and is therefore the same as (2) above.

For the model presented in this report, explanation (1), was used successfully to represent

the LHG using reasonable permeability values by imposing a vertical barrier to horizontal ground-water flow. However, if the barrier is attributed to a fault, no through-going fault has been observed that is coincident with the strike of the large hydraulic gradient, although Fridrich and others (1994) argue for the presence of a buried graben with concomitant faults, based on interpretation of gravity and magnetic data. An alternate treatment of the fault as a vertical barrier is to consider it as a vertical drain as suggested in Fridrich and others' (1994). This alternate model was tested in the model by specifying large permeability values in place of those used to define the vertical barrier to flow used in (1); however, this representation could not reproduce the LHG using reasonable permeability values.

Explanation (2), which, in effect, is equivalent to Fridrich and others' (1994) second explanation (the 'spillway'), has not been simulated with the model. A higher resolution mesh could be used to investigate this explanation in future models. Indirect evidence supporting the possibility of the 'spillway' hypothesis is the observation of increased thermal alteration toward the north of the site model area that is expected to result in an overall decrease in permeability of the volcanic rocks (Broxton and others, 1987).

Explanations (3) and (4) require lateral contrasts in permeability values within the same hydrogeologic unit to represent the LHG, which may be supported by the concept of increased thermal alteration toward the north of the site model as a function of proximity to the Timber Mountain caldera. Both are similar from a permeability-distribution standpoint to the 'spillway' model. Neither explanation (3) or (4) were simulated with the model, but could be represented with the model by defining additional zones within the northern part of the upper volcanic confining unit and the middle volcanic aquifer, which then could be assigned small permeability values based on the alteration history. A smaller permeability may be warranted based on increased hydrothermal alteration in the northern part of the model area (Broxton and others, 1987) and an apparent reduction in permeability in the middle volcanic aquifer (this report,

based on the flow survey in borehole USW G-2 (Luckey and others, 1996, p. 38). However, this was not done in the present work. Explanation (5) differs from the others in that it does not require a permeability contrast to represent the large gradient, because the LHG is absent, and actually represents a disconnected, perched or semi-perched water body. The data relevant to potential perched water occurrence is discussed in the next section.

Potential perched water occurrence

If at least some of the water levels measured in the vicinity of Yucca Mountain represent perched-water conditions, the saturated zone potentiometric surface of figure 5 could be substantially different. The wells for which perched conditions are at least arguably supported by available data are all located in the vicinity or upgradient of the LHG and include borehole USW UZ-14 on Yucca Mountain, and boreholes USW G-2, UE-25 WT#6, and UE-29 a#2 (fig. 5).

To prove perched-water occurrence unequivocally requires demonstrating partial saturation beneath a suspected perched water body. Unfortunately, partial saturation cannot be proved or disproved unequivocally with the available data for the four boreholes in question. The data and possible consequences are reviewed in the following paragraphs.

USW UZ-14

Borehole USW UZ-14 was constructed, in part, to identify the occurrence of suspected perched water in nearby borehole USW UZ-1, located 26.2 m southeast of USW UZ-14. Land surface altitude at USW UZ-14 is about 1,349 m. During construction of USW UZ-14 in 1993, water was encountered at an altitude of 966 m. Drilling had stopped within the crystal-poor vitric member of the Topopah Spring tuff between altitudes of 940 m and 960 m

(sometimes referred to as the 'basal vitrophyre': the base of the upper volcanic aquifer, table 1). This member is considered to be capable of perching water because of its nearly impermeable character, which results from its dense, glassy composition. Water-transmitting fractures become clogged with clays and zeolites when the glass reacts with water (J. Rousseau, U.S. Geological Survey, written commun., 1996).

About 6,000 gallons of water was pumped from this interval during four different hydraulic tests for about 3 days, at rates ranging from 0.86 to 1.9 gallons per minute (Falah Thamir, U.S. Geological Survey, written commun., 1997). The water-level recovered fully after pumping was stopped. The water-producing zone was cased off, and coring continued. Drilling continued into the Bullfrog Member of the Crater Flat tuff (middle volcanic aquifer, table 1), in which water was ultimately encountered in an open fracture at an altitude of about 665 m. The water level associated with this water-producing fracture rose above the altitude of the fracture and stabilized at about 778 m, which was used in the construction of the potentiometric surface in figure 5.

Saturation values calculated from laboratory determinations on core for borehole USW UZ-14 show conditions at or near 100 percent saturation from core located between the reported perched-water level (966 m altitude) and the present water level (778 m altitude). The only exception to this trend occurs within a thin non-welded interval within the Prow Pass tuff (793 m altitude), which shows less than 50 percent saturation. Unfortunately, saturation measurements are unavailable below the 778 m altitude in spite of available core, which would provide confirmation of the laboratory measurement technique used to measure saturation.

USW G-2

USW G-2 is located on the upgradient side of the apparent LHG (fig. 5) and is one of two wells defining its northern extent. Land surface altitude at USW G-2 is about 1,554 m. The primary purpose

of this borehole was to obtain rock core in which to characterize the geology, rather than to characterize the occurrence of water in the borehole. Drilling to a depth of 534 m (or an altitude of 1020 m) is reported to have occurred on 4/25/81. The first reported depth-to-water measurement in USW G-2 at 534 m or an altitude of 1,020 m was made on 5/20/81 using geophysical logging equipment. The accuracy of this measurement is unknown. The substantial period of time between the drilling and the water level measurement allowed interborehole water flow to occur. The borehole was completed to a depth of 1,831 m (altitude of about -270 m) on October 24, 1981. Additional time passed prior to the first reported USGS water-level measurement: that measurement showed an altitude of 1,031.82 m (or a depth to water of about 522 m) on 11/10/81 (Robison and others, 1988, p. 86).

Because USW G-2 penetrated more than 1,300 meters of rock below the static water level (between altitudes of about +1,020 m to -270 m), the measured water level of 1,031.82 m was considered to reflect a composite water level of the saturated zone by Robison and others (1988, p. 86). More than 44,000 liters of water were air lifted out of the borehole during clean out efforts in July 1982, following which the water level was measured at a depth of 525 meters (or an altitude of 1,029 m).

Subsequent data have indicated potential complexities at USW G-2, as discussed in the following paragraphs. Present depth to water is about 533 meters below land surface (or an altitude of 1,021 m) indicating that water levels have declined almost 12 meters in USW G-2 since 1981 (table 2). Analyses of geophysical logs have indicated that an apparent partial saturation may exist in the rock mass above a depth of 825 m (altitude of 734 m), even though the water column is present within this interval. Calculation of saturation values required a correction which involved subtracting an estimated quantity of the structural water (computed from min-

eralogic data obtained from core) from the total water content derived from epithermal neutron and density logs (Phillip Nelson, U.S. Geological Survey, written commun., 1995). This correction is largest for rock containing clays and/or zeolites, but it is likely to be inexact, particularly in highly zeolitized sections, such as those that are present in USW G-2. The potential error is such that the rock may actually be saturated. (Note that the 734 m altitude is lower than expected based on the neighboring head of 751 m to the south in borehole USW G-1.) Unfortunately, side by side comparisons of laboratory- and geophysical-log derived values of saturation are unavailable for this borehole. Therefore, the degree of saturation is open to question.

Borehole USW G-2 was pumped for 408 hours, between April 8 and April 25, 1996, at a discharge rate of 3.6 liters per second, resulting in the removal of approximately 5.3 million liters of water. At the start of pumping water levels were approximately 0.2 meters below the undisturbed level due to previous pumping. Maximum drawdown was 37.9 m. The Calico Hills Formation (upper volcanic confining unit) was the only unit tested. After 186 days of recovery, residual drawdown was 0.5 m—an amount considered to be appreciably larger than what would be expected (that is, full recovery) based on the minimum estimated transmissivity from that test of $2.3 \text{ m}^2/\text{d}$ (G.M. O'Brien, U.S. Geological Survey, written commun., 1996).

Between late 1981, when USW G-2 was completed, and mid-1984, a number of thermal surveys were conducted at USW G-2 that indicate changes in the flow regime over time. Downward flow was indicated in USW G-2 by a persistent, nearly isothermal section of the borehole between the depths of 616 and 740 m (altitudes 938 and 814 m) (Sass and others, 1988, p. 70; 6 temperature profiles). A "stairstep" in the temperature log separates well-defined zones of conductive heat flow, 44 milliwatts per meter above and somewhat below the water level in the well (at approximately 1,025 m), and 71 milliwatts per meter below the step. Temperature profiles obtained during 1992-1995 show a collapse of t

stairstep shape of the temperature profile, and a slight increase of temperature at 740 meters (altitude of 814 m), the depth of the presumed outflow zone.

In summary, a number of complexities exist in the record of USW G-2: (1) twelve meter decline in head between 1981 and present, (2) geophysical logs may show partial saturation, (3) drawdown due to pumping in 1996 did not recover fully, and (4) change in borehole flow regime indicated by temperature logs. Other complexities have been indicated by flow surveys and visual logs of the borehole. Downward flows of between 0.3 to 0.6 liters per minute were observed within the topmost 300 meters of the water column (between altitudes of approximately 1,020 and 720 m) via a pulsed-heat flow survey (F. Paillet, U.S. Geological Survey, written communication, 1995). A combination downward-looking-fish-eye/sidescan camera was used to obtain a visual log of the borehole, and showed wet borehole walls extending about 40 meters above the top of the water column (an altitude of about 1,060 m). Capillary effects would probably be unable to produce wet borehole walls at a distance of more than a few meters above the water level (Weeks and Wilson, 1984).

Possible explanations for the continual decline in water level in the borehole include: (1) the dewatering of a perched-water body or (2) slow equilibration with lower potentiometric levels deep in the borehole, which would be expected in a recharge area (lower heads with depth). The slow water-level recovery in the borehole could result from the permanent dewatering of a perched-water body. Flow surveys may suggest a decrease in vertical flow velocity corresponding to local drainage of possible perched water into the borehole. The water-level decline may be the result of drainage from a perched or semi-perched water body in or above the Calico Hills Formation (upper volcanic confining unit), through the borehole, down to a receptive fracture or fracture zone. Although the evidence is not conclusive, taken together this informa-

tion suggests that the 1019.79 m water-level altitude (Appendix A) may represent perched or semi-perched conditions and may be higher than the top of the water table in this area.

UE-25 WT#6

UE-25 WT#6 is located just upgradient of the LHG (fig. 5) and is one of the wells defining the northern extent of the LHG. The open, water-filled interval within borehole UE-25 WT#6 is within the non- to partially welded section of the Calico Hills Formation (upper volcanic confining unit). Although no hydraulic testing has been conducted in UE-25 WT#6, inference can be made from its water-level history that the permeability is very small based on the gradual rise in water level between 1983 and 1986 of almost 4 meters (Robison and others, 1988, pp. 36-37) following its construction. A caliper log showing variation in the borehole diameter indicates few fractures or washouts within the water-filled part of the borehole. Because the more permeable rocks at Yucca Mountain generally are associated with fractured, welded volcanic units, this observation also supports the inference that permeability is very small.

If UE-25 WT#6 had been constructed into the underlying, presumably more transmissive Crater Flat Tuff (middle volcanic aquifer), the associated water level might be similar to that observed in boreholes located in the southern and eastern parts of Yucca Mountain (that is, less than 750 m altitude), particularly if the Crater Flat Tuff had been packed off and monitored. Although there is little information other than the water-level, the current state of understanding does not preclude the possibility that the 1.034.52 m water level observed in UE-25 WT#6 reflects a perched or semiperched water level. However, unlike other perched water locations, geophysical logs (Phillip Nelson, U.S. Geological Survey, written commun., 1995) for UE-25 WT#6 indicate fully saturated conditions below the water-level.

UE-29 a#2

UE-29a#2, which is located in Fortymile Canyon, has a hydraulic head (1.187 m) that is about 3

meters lower than nearby borehole UE-29 a#1 (not used in the construction of the potentiometric surface in fig. 5). Both holes terminate in the Calico Hills Formation (upper volcanic confining unit). Land surface altitude at both boreholes is 1,215.15 m (Waddell, 1984, p. 25). Drilling of UE-29 a#1 stopped at a total depth of 65.5 m (an altitude of 1,150 m) because of an irretrievable drill bit and collar down the hole (Waddell, 1984, p.1).

UE-29 a#2 was drilled 8.9 m from UE-29 a#1. UE-29 a#2 was drilled to a depth of 421.5 m (altitude of 793 m) before caving problems stopped the drilling. UE-29 a#2 was cased to a depth of 247.3 m (an altitude of 968 m). The casing was not cemented in place, nor was backfill material installed around it, allowing for the possibility of free water flow within the annular space. The casing was subsequently perforated within the interval of 86.9 to 213.4 m (an altitude of 1,128 m to 1,002 m) as part of hydraulic testing which provided communication over the entire water filled part of the borehole. The decreasing hydraulic head with depth between these two boreholes may be consistent with perched water occurrence. It is also consistent with downward vertical gradients in a recharge zone.

Hydrochemical samples taken at the end of hydraulic tests in both UE-29 a#1 and UE-29 a#2 indicate appreciably different water chemistries with depth (Waddell, 1984, table 4, p. 14). Based on tritium and carbon-14 analyses, shallower water obtained from UE-29 a#1 appears to be younger than the deeper water sampled in UE-29 a#2. This is consistent with both perched-water occurrence and/or localized recharge.

Water levels in UE-29 a#1 and UE-29 a#2 were affected periodically by streamflow events in Fortymile Wash and Pah Canyon Wash, as well as by earthquakes (Savard, 1995; Savard, 1996). Streamflow events caused abrupt rises in the water levels in both holes, which decline slowly over periods of years (Savard, 1995, pp. 25-26). The slow decline may indicate

a small permeability in each hole, which would be expected for holes completed in the Calico Hillis Formation (upper volcanic confining unit). Overall, these periodic changes in water levels may be important, particularly in the case of UE-29 a#2, because they could obscure any possible long-term monotonic decline in water levels which might be interpreted as being caused by perched-water draining down an open borehole, similar to conditions in USW G-2.

In summary, hydraulic-head and hydrochemical data for these two wells can be explained by the occurrence of localized recharge (that is, younger, more recently recharged water at the top of the flow system). However, these observations are not incompatible with potential perched water occurrence.

Hydraulic properties

Knowledge of hydraulic properties is critical to understanding the hydrogeology of Yucca Mountain and is required for numerical models (Luckey and others, 1996, p. 32). Hydraulic properties for each of the hydrogeologic units were obtained from available data sources listed in table 3. These sources include: (1) previously published hydraulic analyses for wells at Yucca Mountain conducted during the 1980's; (2) published hydraulic properties for hydrogeologic units obtained beyond the immediate Yucca Mountain area; and (3) recent (1995-97) hydraulic analysis of wells USW WT-10, UE-25 WT#12, and USW SD-7 (O'Brien, 1997), UE-25 c#1, UE-25 c#2, and UE-25 c#3 (Geldon, 1996; A.M.J. Umari, U.S. Geological Survey, written commun., 1997), and USW G-2 (G.M. O'Brien, U.S. Geological Survey, written commun., 1997). Table 3 lists the hydrogeologic units, and high and low values of hydraulic conductivity, permeability, and porosity. High and low values are either the literal reported value, or when sufficient data were not available for a particular unit, the 83.5 (high value) and 16.5 (low value) percentiles of the probability distribution of similar rock types (Bedinger and others, 1989, p. A18). Data from all sources are incorporated into table 3, however, analyses for individual wells or

hydrogeologic units may not be listed in the table.

Aquifer tests

Several aquifer tests were conducted in Yucca Mountain boreholes during 1995 and 1996. Single borehole, composite interval tests resulted in transmissivity estimates in boreholes USW WT#10, UE-25 WT#12, and USW G-2. The middle volcanic aquifer was the primary hydrogeologic unit tested in boreholes USW WT#10 and UE-25 WT#12. Transmissivity in these boreholes ranged from 7 to 1,800 m²/day (O'Brien, 1997). The upper volcanic confining unit was tested in USW G-2 and the mean transmissivity was 9.4 m²/day (Grady O'Brien, U.S. Geological Survey, written commun., 1997). Transmissivity was reported for these boreholes because composite intervals were tested and the thickness of water-producing intervals was unknown. Hydraulic-conductivity estimates obtained from these transmissivity estimates would probably underestimate the actual hydraulic conductivity because the entire interval thickness does not contribute water to the borehole. Hydraulic properties obtained from single-borehole aquifer tests generally represent flow conditions within tens of meters of the borehole. Given the large degree of heterogeneity in the Yucca Mountain area, individual single-borehole aquifer-test results are not directly appropriate for the scale represented by the site model (kilometers).

Preliminary aquifer tests were conducted at the C-hole complex during 1984. Horizontal hydraulic conductivity was about 0.15 m/d in the upper volcanic confining unit and ranged from 3 to 30 m/d within the middle volcanic aquifer (Geldon, 1996). Cross-hole aquifer tests during 1995-96 in the c-well complex also resulted in transmissivity and hydraulic-conductivity estimates. During these tests borehole UE-25 c#3 was pumped and boreholes UE-25 c#1, UE-25 c#2, UE-25 ONC-1, USW H-4, and UE-25 WT#3 were used as observation wells. The

lower Bullfrog Tuff is the most transmissive interval within the middle volcanic aquifer and hydraulic conductivity ranges from approximately 1×10^{-5} to 7×10^{-2} meters per second in the observation borehole (Geldon and others, 1997). This range is at the high end of values found in table 3.

Hydraulic properties obtained from the cross-borehole aquifer tests at the C-hole complex represent flow properties between the tested boreholes. The area affected by the C-hole hydraulic tests is about 21 km^2 and extends as far north as Yucca Wash. As such, these tests likely are more appropriate for the scale of the site model than those obtained from single-hole tests. There is evidence that this area has extensive fractures that enhance the transmissive properties of the aquifer system. Northerly and northwesterly trending high-angle faults such as the Paintbrush Canyon, Midway Valley, and Bow Ridge Faults have brecciated, offset, and tilted the tuffaceous rocks in the vicinity of the C-hole complex (Day and others, in press). Extensive tectonic and cooling fractures have been identified in the C-hole complex boreholes (Geldon, 1996). Furthermore, preferential flow paths are possible based on the response of water levels in observation wells during the pumping of well UE-25 C#3. However, because of concurrent rather than sequential scheduling of the C-hole hydraulic tests with respect to the development of the flow model in this report, results from the large-scale C-hole testing were unavailable but are expected to be incorporated into future revisions to the model.

Ranges of hydraulic properties

A feature of table 3 is the wide range of values available for hydraulic conductivity and permeability for several hydrogeologic units such as the upper volcanic aquifer (range of about 10^8 m^2) and the upper volcanic confining unit (range of about 10^7 m^2) among others. These large ranges reflect the scale of the test performed such as permeability determination done on core (which would tend to produce small values), as opposed to a long-term aquifer test using multiple wells (which would tend to produce large values and likely be more suitable for use in a model). Hydraulic-conductivity values listed in table

Table 3: Hydrologic properties of hydrogeologic units

[High and low values taken from 16.5 (low) and 83.5 (high) percentiles of probability distribution. References denoted by superscripts: a) Anderson, 1994; b) Bedinger and others, 1989; c) Blankennagel and Weir, 1973; d) Craig and Robison, 1984; e) Czarnecki, 1990; f) Flint and Flint, 1990; g) Geldon, 1993; h) Lahoud and others, 1984; i) Lohmeyer, 1986; j) Rush, 1984; k) Thordarson, 1983; l) Whitfield and others, 1985; m) Winograd and Thordarson, 1975; n) Luckey and others, 1996; o) Geldon and others, 1997. 1) Hydraulic properties compiled from laboratory and hydraulic testing data. 2) Anderson, 1981; Craig and Reed, 1991; Garber and Thordarson, 1962; Moore and Garber, 1962; Robison and Craig, 1991; Thordarson and others, 1985; Waddell and others, 1984; and Weeks and Wilson, 1984 were used to in the compilation of the table, but are not cited because values from these reports fall within the high and low values for respective units. 3) Permeability value obtained by converting reported hydraulic conductivity value if no explicit permeability value was available. 4) Only one value available.]

Hydrogeologic Unit	Model Unit Number	Model Variable Name	Hydraulic Conductivity (meters/second)		Permeability (meters ²)		Permeability Specified in Simulation 40 (meters ²)	Porosity (percent)	
			High	Low	High	Low		High	Low
Valley-fill aquifer	19	qal	6.0x10 ⁻⁰⁵ m	9.2x10 ⁻⁰⁷ m	6.0x10 ⁻¹² m ³	9.2x10 ⁻¹⁴ m ³	8.8x10 ⁻¹⁴	23 ^h	12 ^h
Valley-fill confining unit	18	apla	3.9x10 ⁻⁰⁵ c	1.2x10 ⁻¹⁰ h	3.9x10 ⁻¹² c ³	1.2x10 ⁻¹⁷ h ³	3.0x10 ⁻¹⁶	66 ^c	29 ^h
Lava-flow aquifer	16	b	1.2x10 ⁻⁰⁶ h	5.8x10 ⁻¹⁰ b	1.2x10 ⁻¹³ h ³	1.1x10 ⁻¹⁸ b ⁴	4.5x10 ⁻¹⁴	19 ^h	0.1 ^h
Upper volcanic aquifer	15	uva	3.2x10 ⁻⁰⁴ m	9.6x10 ⁻¹² h	1.8x10 ⁻¹³ f	0.0x10 ⁻⁰⁰ a	1.6x10 ⁻¹⁴	54.4 ^h	1.4 ^f
Upper volcanic confining unit	14	uycu	4.6x10 ⁻⁰⁵ m	2.9x10 ⁻¹¹ f	3.9x10 ⁻¹⁴ a	3.0x10 ⁻¹⁸ f	1.0x10 ⁻¹⁸	50.3 ^c	12.3 ^f
Middle volcanic aquifer	13	mva	7x10 ⁻⁴ o	9.6x10 ⁻¹² h	4.5x10 ⁻¹⁴ a	0.0x10 ⁻⁰⁰ a	1.6x10 ⁻¹⁴	43.6 ^f	1.8 ^f
Middle volcanic confining unit	12	mvcu	1.3x10 ⁻⁰⁶ la	6.4x10 ⁻¹¹ ja	2.6x10 ⁻¹⁶ a	0.0x10 ⁻⁰⁰ a	1.9x10 ⁻¹⁶	27.4 ^a	9.3 ^f
Lower volcanic aquifer	11	lva	no data available	no data available	no data available	no data available	5.0x10 ⁻¹³	38.4 ^c	8.1 ^f
Lower volcanic confining unit	10	lvcu	1.7x10 ⁻⁰⁸ d,4	1.7x10 ⁻⁰⁸ d,4	4.0x10 ⁻¹⁶ b	8.3x10 ⁻¹⁸ a	1.0x10 ⁻¹⁶	17 ^f	8.8 ^h
Undifferentiated valley fill	9	lcu	3.5x10 ⁻⁰⁶ b	3.5x10 ⁻¹³ b	3.5x10 ⁻¹³ h,3	3.5x10 ⁻²⁰ h,3	2.9x10 ⁻¹⁴	30 ^h	10 ^h
Limestone aquifer	17	tlim	no data available	no data available	no data available	no data available	1.0x10 ⁻¹⁴	no data available	no data available
Granitic confining unit	2	gran	4.6x10 ⁻⁰⁶ b	2.3x10 ⁻¹³ b	4.6x10 ⁻¹³ h,3	2.3x10 ⁻²⁰ h,3	3.5x10 ⁻¹⁴	7 ^h	0.001 ^h
Upper carbonate aquifer	8	uca	4.6x10 ⁻⁰⁵ h	5.8x10 ⁻⁰⁹ b	4.6x10 ⁻¹² h,3	5.8x10 ⁻¹⁶ h,3	6.7x10 ⁻¹³	16 ^h	0.5 ^h
Upper elastic confining unit	6	ecu	no data available	no data available	no data available	no data available	5.5x10 ⁻¹⁹	15.1 ^f	0.6 ^f
Lower carbonate aquifer	3, 5, 7	lca	2.6x10 ⁻⁰³ m	5.8x10 ⁻⁰⁹ b	5.4x10 ⁻¹⁵ b	1.1x10 ⁻¹⁸ b	4.4x10 ⁻¹²	16 ^h	0 ^h
Lower elastic confining unit	4	qcu	4.6x10 ⁻⁰⁶ h	2.3x10 ⁻¹³ b	5.5x10 ⁻¹⁹ b	3.9x10 ⁻²⁰ b	2.0x10 ⁻¹⁵	7 ^h	0.001 ^h

3 tend to reflect results from hydraulic testing in wells, whereas, the permeability values tend to reflect results from laboratory tests on core, except those that were converted from hydraulic conductivity values.

The large ranges of hydraulic conductivity values likely reflect the presence or absence of permeable fractures, particularly for the carbonate and volcanic aquifers. Hydraulic conductivity values are affected by depth and by the degree and type of faulting. Intergranular flow is not significant in carbonate rocks; the large transmissivity is primarily due to fractures and solution channels (Winograd and Thordarson, 1975). Hydraulic tests of carbonate-rock aquifers throughout eastern and southern Nevada indicate that faults can increase their transmissivity by factors of 25 times or more (Dettinger, 1989).

Welded ash-flow tuffs, representative of the volcanic aquifers, characteristically have an interstitial porosity of about 5 percent or less (Bedinger and others, 1989); thus, the commonly moderate to large hydraulic conductivity of welded ash-flow tuffs is largely a function of secondary openings along joints, bedding planes, and partings within the flows. Where these welded tuffs are not fractured or jointed, they tend to form confining beds; thus, welded tuffs can only transmit significant quantities of water where they are fractured or faulted.

In contrast, non-welded ash-flow tuffs may have a large interstitial porosity, but low hydraulic conductivity, and function as confining beds. Fractures and joints are virtually absent in non-welded ash-flow tuffs (I.J. Winograd, U.S. Geological Survey, written commun., 1971). Hence, the non-welded tuffs generally act as confining units.

Currently, the hydrogeologic units are not separated as to their presence or absence of permeable fractures or faults. In general, the aquifers are composed of welded tuffs that, because of fracturing, have a higher permeability. Hydraulic tests of faults within the saturated zone are not available; therefore, data are not available on hydraulic properties of faults within the saturated zone. Small permeability

ues are believed to be associated with the Solitario Canyon Fault, because of the apparent 50-m difference in potentiometric levels on either side of the fault.

In the regional flow model, D'Agnese and others (in press) do incorporate some structures explicitly. In the regional model (D'Agnese and others, in press), northeast-southwest trending regional structures are identified as zones of large permeability and northwest-southeast trending regional structures are identified as zones of small permeability. Because of the large-scale of the regional model, hydraulic properties of such features used in that model may not be appropriate at the scale of the site model. The area underlying Fortymile Wash was also identified as a zone of large permeability in the regional model. Because the site model does not explicitly consider many structural features, the hydraulic conductivity ranges for these hydrogeologic units are much larger than those defined for the regional flow model (D'Agnese and others, in press, table 16).

Specification of permeability, rather than hydraulic conductivity, is required in the FEHMN application. Therefore, to fill in data gaps, several values of permeability were calculated in table 3 by converting reported values of hydraulic conductivity to permeability by multiplying by 10^{-7} . Porosity values (table 3) are not used in the current model because only flow simulations are considered, which are invariant to specified values of porosity.

Recharge

Recharge to the model area is assumed to be from the following sources: (1) downward and possible lateral recharge from episodic flooding of Fortymile Wash; (2) throughflow from Pahute and Rainier Mesas, which is hypothesized to result in recharge along the northern border of the study area; (3) throughflow from the northwestern part of the Amargosa Desert; (4) minor recharge from episodic flooding of the Amargosa River channel; and (5) net infiltration

from precipitation events. Fortymile Wash is a major southward-draining ephemeral channel located adjacent to Yucca Mountain (fig. 5) and it is thought to contribute intermittent recharge to the saturated zone. Water levels in UE-29 a#1 and UE-29 a#2 are affected periodically by streamflow events in Fortymile Wash and Pah Canyon Wash. In various numerical ground-water flow models (Czarnecki and Waddell, 1984; Rice, 1984; Czarnecki, 1985; Sinton, 1987), recharge had to be specified in Fortymile Wash to replicate potentiometric levels. Czarnecki and Waddell (1984) simulated a flux in Fortymile Wash of $22,140 \text{ m}^3/\text{d}$ or 256 kg/s . Based on geomorphic/distributed-parameter simulations, Osterkamp and others (1994) estimated recharge along the entire 95-km length of Fortymile Wash to be about $4.22 \times 10^6 \text{ m}^3/\text{year}$ or 134 kg/s . Based on field studies of stream loss (C.S. Savard, U.S. Geological Survey, written commun., 1997), the total recharge in Fortymile Wash is estimated as 0.86 kg/s . Savard acknowledges that this estimate would represent a minimum value based on the inability to account for all reaches of Fortymile Wash, which may have received unobserved runoff and recharge, coupled with the minimum period of streamflow observations.

Throughflow from the northwestern part of the Amargosa Desert and Pahute and Rainier Mesas is difficult to quantify. As a result, these fluxes are calculated in the model. Estimates for these fluxes could be obtained from the regional flow model (D'Agnesse and others, in press). The regional model employs the concept that some of the recharge waters from Pahute and Rainier Mesas likely flow to Yucca Mountain. In contrast, Czarnecki and others (1990) developed alternative conceptual models of flow toward Yucca Mountain that include the possibility of either: (1) a ground-water divide between the Crater Flat/Yucca Mountain area and Beatty Wash; or (2) a westward extension of an inferred hydrogeologic barrier (which may cause the LHG north of Yucca Mountain) into northern Crater Flat. Both possibilities would result in diversion of more of the water from Pahute Mesa into the Oasis Valley subbasin, although the second case would permit some flow into Crater Flat. Because of differences in the distri-

bution of hydrogeologic units between the site and regional models. simulated fluxes from the regional model are not specified directly into the site model. but are used as a "reasonableness check" on fluxes calculated by the site model.

The Amargosa River is an intermittent stream in the southwestern portion of the model area, where channelized flow ceases to exist. Streamflow in the Amargosa Farms area is generally very limited (Osterkamp and others, 1994). Based on channel-morphology measurements, the composite average recharge is estimated to be $0.2 \times 10^6 \text{ m}^3/\text{year}$ or 6 kg/s along the 15.9-km length Amargosa River from Ashton to Big Dune, an area proximate to the model area (Osterkamp and others, 1994). Hence, recharge is assumed to be negligible along the few kilometers of the Amargosa River in the southwestern portion of the model.

A detailed description of net infiltration to the water table in the vicinity of Yucca Mountain has been developed (A. L. Flint, U.S. Geological Survey, written communication, 1997) that shows recharge increases on the northern end of Yucca Mountain (relative to the central and southern end) and below some of the major surface water drainages. Flint showed that for an average precipitation year (approximately 170 mm of precipitation), recharge at Yucca Mountain ranges from zero, for a soil thickness of 6 meters or more, to over 80 mm/yr for a thin soil on north-facing slopes and at high elevations that overlies highly-permeable bedrock. Recharge (net infiltration) averages 4.5 mm/yr, but on a year-to-year basis, ranges from zero in dry years to over 20 mm/yr when average precipitation exceeds 300 mm (A. L. Flint, U.S. Geological Survey, written communication, 1997). Direct mapping of these infiltration flux values onto the top nodes of a finite-element mesh in an areally weighted fashion has been used for mapping precipitation values onto an unsaturated-zone model of the site (A. Wolfsberg, Los Alamos National Laboratory, written commun., 1996).

In summary, recharge from episodic flooding of Fortymile Wash and throughflow from Panute and Rainier Mesas is thought to be the dominant source of recharge to the model area. In the model area, episodic flooding of the Amargosa River channel is thought to result in negligible recharge. Recharge from net infiltration, although relatively small, may play an important part in the distribution of heads at Yucca Mountain. This was not incorporated into this version of the model.

Discharge

No natural discharge occurs within the model domain. The nearest natural discharge areas connected to the saturated-zone flow system beneath Yucca Mountain are Franklin Lake playa (also known as Alkali Flat) and possibly the major springs at Furnace Creek Ranch and the valley floor of Death Valley. Although most models of the region (D'Agnese and others, in press, Rice (1984), Czarnecki and Waddell (1984)) require a ground-water flow path from Yucca Mountain to Death Valley, Czarnecki and Wilson (1991) postulate that a ground-water flow path from Yucca Mountain to Death Valley (by way of the Amargosa Desert and the Funeral Mountains) was unsubstantiated (but not inconsistent with) with available data. They suggest that ground water from Yucca Mountain ultimately discharges at Franklin Lake playa through evapotranspiration (Czarnecki, 1990).

Discharge through ground-water withdrawals occurs within the model domain in the Amargosa Desert for agricultural and domestic use. This discharge, which was estimated in the USGS regional flow model at about $6,300 \text{ m}^3/\text{d}$ (Patrick Tucci, U.S. Geological Survey, written commun., 1997), occurs mostly in the southwestern corner of the model domain. This discharge may be responsible for the southwestwardly oriented gradient which appears to have persisted since the 1950's (Kilroy, 1991, p. 12).

Hydrochemistry

The chemical characteristics of ground water in the Yucca Mountain area are a function of recharge water chemistry and the materials with which the water interacts along the flow path (Luckey and others, 1996, p.44). As such, the chemical characteristics of ground water can be used to trace ground water movement and help interpret possible conceptual models of ground-water flow. Major-ion data for Yucca Mountain may be subject to question because of the presence of tracer chemicals that were added to drilling fluids in water samples, which indicate incomplete removal of drilling fluid prior to sample collection in many of the wells (Luckey and others, 1996, p.44). Despite this possible contamination some conclusions can be drawn regarding ground-water movement based on hydrochemical data.

Ground water at Yucca Mountain has a Na-K-HCO₃ signature that reflects contact primarily with volcanic rocks (Chapman and Lyles, 1993). Hydrochemical data (Benson and McKinley, 1985; Matuska, 1989) indicate that the calcium/sodium ratio in the water increased by an order of magnitude from west to east at Yucca Mountain, the lowest values being west of and near Solitario Canyon Fault. This increase may indicate that water to the west has been in contact with the rock for a longer time. Further, carbon-14 (¹⁴C) apparent ages from Benson and McKinley (1985) indicate the oldest water occurs beneath the crest of Yucca Mountain and the youngest water occurs beneath Fortymile Wash. These young waters may indicate recharge along Fortymile Wash. In addition, the lower salinity of downgradient wells in Fortymile Wash may also reflect the diluting effect of infiltrating recharge along the length of the wash (Chapman and Lyles, 1993). These observations support the concepts that (1) the Solitario Canyon fault acts as a barrier to east-west ground-water flow, an observation that is consistent with the moderate hydraulic gradient (fig. 5) (Ervin and others, 1994) which occurs there; and (2) that

recharge occurs along Fortymile Wash.

The volcanic rocks at Yucca Mountain overlie the regional Paleozoic carbonate aquifer. The interaction of ground water between the Paleozoic carbonate and the Tertiary rocks is poorly understood. Using carbon isotope data, Stuckless and others (1991) identified three sources for water mixing under the mountain: (1) lateral flow from the volcanics to the north that had a long residence time in the volcanic rocks; (2) local recharge in areas such as Fortymile Wash; and (3) water that upwells from the carbonate aquifer into the volcanics south of the large gradient. The latter is based on a mixing line of ^{14}C versus Cl^- between water from J-13 and UE25 p#1, and cannot be substantiated using ^{13}C versus Cl^- (stable, conservative constituents) or any other relation.

Fridrich and others (1994) state that definitive evidence of interaction between the carbonate and volcanic aquifers under Yucca Mountain is provided by ground-water isotopic data. They interpret the generally southward increase in $\delta^{13}\text{C}$ values in the volcanics as indicating a southward-increasing contribution of flow from the carbonate aquifer into the volcanics. In addition, Fridrich and others (1994) proposed that the pattern of $\delta^{13}\text{C}$ within the volcanic units is the result of upwelling ground water along faults, derived from the underlying Paleozoic carbonate aquifer. Although this interpretation appears to be supported by the heat flux pattern (Fridrich and others, 1994), upwelling along faults is still controversial because of the ambiguity in the chemical data.

Only one borehole at Yucca Mountain, UE-25 p#1, penetrates the Paleozoic rocks. The hydrochemical characteristics of UE-25 p#1 reflect the carbonate aquifer and are significantly different from the other boreholes at Yucca Mountain that penetrate only the Tertiary volcanic rocks (Chapman and Lyles, 1993). The relatively high chloride and sodium concentrations at UE-25 p#1 has been interpreted as a contribution of volcanic water to the carbonate aquifer in the Fortymile Wash area (Chapman and Lyles, 1993). Although this interpretation is consistent with recharge in Fortymile Wash, it is inconsis-

tent with the observed 20-m higher hydraulic head within the Paleozoic carbonate rocks tapped by UE-25 p#1, which would indicate the potential for upward flow into the Tertiary rocks. Furthermore, recharge within Fortymile Wash at the latitude of UE-25 p#1 is estimated to be minor (C.S. Savard, U.S. Geological Survey, written commun., 1997).

Geldon (1993, p. 75) hypothesized that water from the C-hole complex likely originates from upward flow transmitted from underlying Paleozoic rocks along a low angle fault at the base of the Tertiary rocks which was observed in borehole UE-25 p#1. UE-25 p#1 is about 600 m east of the C-holes and has a 50-m thick interval of tuffaceous and sedimentary rocks above the fault which is postulated to provide upward flow from the carbonate rocks. An increase in hydraulic head with increasing depth is also observed within Tertiary rocks at Yucca Mountain (see section on "Vertical Hydraulic Head", this report). In spite of the observed increase in hydraulic head with increasing depth, no systematic change in hydrochemistry with depth within any individual borehole completed in the Tertiary volcanic rocks at Yucca Mountain has indicated a trend toward or evidence of volcanic to carbonate-type water.

Therefore, based on the hydrochemical data, this report assumes that the contribution of ground-water by upward flow from the Paleozoic rocks is negligible within the study area. Furthermore, the conceptual model includes lateral flow from the tuff aquifer to the north, suggested by the chemical data reported by Stuckless and others (1991) and previous numerical flow models, does occur. In addition, the conceptual model includes Solitario Canyon fault as a barrier to east-west ground-water flow and recharge along Fortymile Wash.

Luckey and others (1996, p. 44) state that hydrochemical and isotopic data, where adequate data are available, can provide information for checking results from numerical flow models. Numerical models can be used to identify potential flow paths through and between

the volcanic and carbonate flow systems. Hydrochemical data can then be used to support or refute the potential flow paths by analyzing the evolution of the water along the potential flow path. These checks were not done; however, these types of flow path analyses could be performed to check the numerical model.

Temperature

Temperature data are available for the saturated zone from temperature logs obtained in 30 wells in the vicinity of Yucca Mountain (Sass and others, 1988). These data are summarized in table 4. For the "WT-series" wells, which are completed only a short distance into the saturated zone, bottom-hole temperature data are not included in table 4. Average temperature at the water table is 30.8°C; however, water-table temperatures range from 18.2°C in well UE-29 a#2 (depth to water about 29 m) to 38.8°C in well USW WT-10 (depth to water about 347 m). Temperature profiles within the saturated zone are available for 16 wells (table 4). Bottom-hole (deepest depth logged) temperatures range from 18.8°C in well UE-29 a#2 (logged maximum depth about 170 m) to 63°C in well USW G-1 (logged maximum depth about 1,800 m). Average water temperatures for the saturated interval logged in each of the 16 wells is about 37.3°C, and average saturated-zone temperatures range from 18.5°C in well UE-29 a#2 to 46.2°C in well USW G-1. Borehole temperature gradients within the saturated zone are very irregular (Sass and others, 1988, p. 2) due to water entering or leaving the boreholes through discrete fractures or fracture zones.

Table 4 -- Summary of saturated-zone temperature data available for wells near Yucca Mountain .

[m = meters; °C = degrees Celsius; n/a = not available; superscripts denote the following: 1, depth to water table is 1985-95 average (from Graves and others, 1997) or from temperature log (from Sass and others, 1988); 2, From temperature log (Sass and others, 1988); 3, Bottom of volcanic rocks penetrated in well UE-25 p#1. Average temperature in carbonate interval below the volcanic section is about 55.5 °C]

Well Number	Hydraulic Head at Time of Temperature Log (m)	Depth to water in borehole at time of temperature log ¹ (m)	Water-Table Temperature ² (°C)	Bottom of Logged Interval (m)	Bottom-Hole Temperature ² (°C)	Average Saturated-Zone Temperature (°C)
UE-25 n#1	729	470	31.5	750	35.0	33.2
UE-25 b#1	731	470	32.0	1,220	42.0	37.0
UE-29 n#2	1186	29	18.2	170	18.8	18.5
USW G-1	751	575	29.5	1,800	63.0	46.2
USW G-2	1029	525	29.5	1,350	57.0	43.2
USW G-3	731	750	32.5	1,370	43.5	38.0
USW G-4	729	540	30.5	920	35.0	32.8
USW H-1	731	572	23.0	1,200	53.0	38.0
USW H-3	731	752	34.0	1,200	42.0	38.0
USW H-4	730	518	31.0	1,200	40.5	35.8
USW H-5	776	703	35.0	1,200	42.5	37.5
USW H-6	776	526	54.0	1,200	54.0	44.0
J-13	728	283	31.0	1,040	38.0	34.5
UE-25 p#1	714	400	34.5	1,244 ³	57.0 ³	45.8
USW VH-1	780	184	27.0	762	41.5	34.2
USW VH-2	814	160	26.5	1,200	54.5	40.5

Table 4 -- Summary of saturated-zone temperature data available for wells near Yucca Mountain (Continued).

[m = meters; °C = degrees Celsius; n/a = not available; superscripts denote the following: 1, depth to water table is 1985-95 average (from Graves and others, 1997) or from temperature log (from Sass and others, 1988); 2, From temperature log (Sass and others, 1988); 3, Bottom of volcanic rocks penetrated in well UE-25 p#1. Average temperature in carbonate interval below the volcanic section is about 55.5 °C]

USW WT-1	730	471	30.6	n/a	n/a	n/a
USW WT-2	731	570	31.6	n/a	n/a	n/a
UE-25 WT#3	730	300	33.0	n/a	n/a	n/a
UE-25 WT#4	731	438	31.4	n/a	n/a	n/a
UE-25 WT#6	1035	280	27.6	n/a	n/a	n/a
USW WT-7	776	421	33.8	n/a	n/a	n/a
USW WT-10	776	347	38.8	n/a	n/a	n/a
USW WT-11	731	363	35.4	n/a	n/a	n/a
UE-25 WT#12	730	349	33.0	n/a	n/a	n/a
UE-25 WT#13	730	303	28.6	n/a	n/a	n/a
UE-25 WT#14	730	346	29.9	n/a	n/a	n/a
UE-25 WT#15	729	354	27.5	n/a	n/a	n/a
UE-25 WT#16	739	472	32.3	n/a	n/a	n/a
UE-25 WT#17	730	394	31.1	n/a	n/a	n/a

The approximate average ground-water temperature beneath Yucca Mountain may be 44°C (B.W. Arnold, Sandia National Laboratory, written commun., 1997). However, temperatures at the southern end of the model domain are about 20°C at a depth below land surface of about 80 m, which is the top of the saturated zone (John Sass, U.S. Geological Survey, written commun., 1991). An average temperature for the entire saturated zone contained within the site model has not been calculated. Simulations were done at uniform system temperatures of 20°C and 44°C to assess the effect on ground-water flux (see section entitled "Simulated Fluxes" later in this report).

The different specifications of average ground-water temperature have an appreciable effect on viscosity (1.002 centipoise for fresh water at 20°C; 0.6067 centipoise for fresh water at 44°C). The effect on hydraulic conductivity would be an overall increase of about 65 percent for this temperature change. Hence, the ground-water temperature may have an appreciable effect on the flow system. In addition, the ground-water temperature may be indicative of ground-water flow patterns.

Another feature in the temperature data is the occurrence of a large area of anomalously low heat flow under central Yucca Mountain (Sass and others, 1988, fig. 7). Fridrich and others (1994) state that this anomaly is most clearly defined in the unsaturated zone, because of the large number of drill holes. They also suggest that the heat flow is very low in the saturated zone. Sass and others (1988) conclude that at least 80 percent of the heat-flow anomaly is attributable to the saturated zone. Fridrich and others (1994) feel that because the data indicate that the zone of decreased heat flow extends to at least 2 km in depth, the regional carbonate aquifer must be involved. Fridrich and others (1994, pp. 154-155) suggest two related interpretations to explain the heat flow anomaly. First, part of the anomaly results from the cool under-

flow in the deep carbonate aquifer. Second, because the northern limit of the heat-flow anomaly corresponds to the location of the LHG, it may indicate the northern limit of the carbonate aquifer.

Fridrich and others (1994, pp. 155-157) describe another feature of interest: the occurrence of linear zones of elevated temperature at the water table south of the LHG. The thermal highs correspond with major north-trending fault zones. They suggest that these hydrostructural units form the pathways (volcanic rocks in the fault zones are significantly more permeable than unfaulted rock) for upwelling water from the carbonate aquifer under Yucca Mountain. They further note that the thermal highs could also be explained by unsaturated-zone processes or upward gradients in the volcanic rocks, or both.

HYDROGEOLOGIC FRAMEWORK MODEL

To characterize the complex 3D, heterogeneous, porous, and fractured media beneath Yucca Mountain, a detailed 3D hydrogeologic framework model (HFM) was developed. The framework model was developed so that it could be converted into a tetrahedral mesh, using GEOMESH (Gable and others, 1996), for use in the FEHMN ground-water flow modeling code. As a result, the framework model has many simplifications that may limit its use for other applications.

The HFM used in this model (sampled at 1,500 m) is only suitable for initial calibration of a preliminary flow model using a very coarse resolution. For example, the upper volcanic confining unit is much more extensive in the coarse HFM than in reality. Because of the coarse grid increment (1,500 m), offsets across faults are much less abrupt than in reality. Hence, this coarse HFM should only be used to depict the extent or the boundaries of the hydrogeologic units in a very general sense. However, the underlying HFM can be constructed at a much greater resolution to give a more accurate depiction of the hydrogeologic units.

Initially, the HFM was developed for the area bounded by latitude 35°N and 38°N and longitude

115°W and 118°W, that encompasses the Death Valley regional ground-water flow system. This regional HFM represents approximately 100,000 km² and extends from land surface to depths of 10 km, incorporating ten hydrogeologic units. Additional subdivision of hydrogeologic units was done on an area bounded by latitude 36°N and 37°15'N and longitude 116°W and 117°W resulting in the identification of 18 hydrogeologic units (fig. 3a). A subarea of this refined HFM used in the site model is 1,350 km² and extends from 533,340 meters to 563,340 meters (30 km west to east) and 4,046,782 meters to 4,091,782 meters (45 km south to north), UTM Zone 11 (fig. 3b). The subarea grid was chosen to be coincident with the Death Valley regional flow model (D'Agnese and others, in press).

The area of the site-scale flow model is larger than that of the three-dimensional site geologic framework model (Clayton and others, 1997) which was developed to support the Yucca Mountain site unsaturated zone model, but extends into the saturated zone as well. Due to simplifications necessary for conceptualization and modeling of the flow system, the geologic units are lumped into hydrogeologic units. The geologic units used in the site geologic framework model can be correlated with the hydrogeologic units used in the HFM. The data sets for the site geologic framework model were received on April 28, 1997, too late to be incorporated into the hydrogeologic framework model used for this version of the flow model. These data sets have been incorporated subsequently into a higher resolution hydrogeologic framework model which has been sampled over a 250-m by 250-m grid.

Development of an HFM begins with the assembly of primary data: geologic maps and cross sections, lithologic logs, and topography (digital elevation model (DEM)). Each of these primary data can be manipulated by standard Geographic Information Systems (GIS); however the merging of these diverse data types to form a single coherent 3D digital model requires

more specialized geologic modeling software.

Construction of a 3D framework model involves seven steps: (1) geologic units are classified into hydrogeologic units based on their hydraulic properties and lateral extent; (2) DEM data are combined with hydrogeologic maps to provide a series of points in 3D space locating outcrops of individual hydrogeologic units; (3) cross sections and lithologic logs are used to locate hydrogeologic units in the subsurface; (4) maps and cross sections are used to locate faults; (5) structure contour maps for each hydrogeologic unit are developed by interpolating both surface and subsurface positions with gridding software which incorporates unit offsets across faults; (6) an HFM is developed when the structure contour maps for the individual hydrogeologic units are combined, utilizing appropriate stratigraphic principles to control their sequence, thickness, and lateral extent; and (7) the potentiometric surface is used to clip the framework model. The first step is discussed in the Conceptual Model Section, while the last 6 steps are discussed in the following sections.

Surface Information

A surface hydrogeology map (fig. 3) provided the "ground truth" for other model-building data and was the foundation upon which the rest of the HFM was constructed. To define the 3D extent of units exposed on the ground surface, the hydrogeologic map (fig. 3a) and the digital elevation model (DEM) were integrated. The digital elevation data is from 1:250,000 scale maps with a grid spacing of approximately 90 m (U.S. Geological Survey, 1987). The DEM defined an array of points in which each point was located by its x,y and altitude (z) coordinates. Points falling within each outcrop area were tagged with the corresponding hydrogeologic unit code.

Subsurface Information

The cross sections (fig. 2) used to construct the HFM were all at a scale of 1:100,000 or larger. The detailed stratigraphy was simplified into the appropriate hydrogeologic unit (table 1). The simplified cross sections were then digitized, merged, scaled, warped to fit their digitized traces, and accurately placed in 3D space. A data-base was populated with the different hydrogeologic units. This data base was then linked to the sections by pointing to each hydrogeologic unit top and keying in the appropriate hydrogeologic unit.

Records for wells in the area contain lithologic data that were used to help correlate between the cross sections. The lithologic units shown in the well records were reclassified into the appropriate hydrogeologic units. In order to be consistent with the other altitude data being used, the altitude of the top of each hydrogeologic unit was determined by subtracting its depth from the DEM at the well location.

Representation of Faults

Information on faults include: (a) fault trace maps that show where faults intersect land surface; and (b) faults shown on cross sections. All of the faults with surface traces (1:100,000 scale), regardless of length, are included (fig. 3b) in the HFM. The fault traces were compared with the faults shown on the cross sections. Some fault traces were extended horizontally to connect the cross section faults. Some of the faults shown on the cross sections were provided with an interpreted fault trace when they were not represented by existing mapped surface traces.

Faults in the model area can dip at almost any angle, but most are high angle faults. Given software constraints and the flow model resolution, the faulting in the area is greatly

simplified. The major simplification is that nearly all faults are treated as vertical features. Where it was thought to be hydrologically important, thrust faults were represented by repeating hydrogeologic units. Because of the relatively large grid spacing (1,500 m), these simplifications are assumed to have minimal effect on flow model results; however, no sensitivity analyses regarding these simplifications were performed.

Structure Contour Maps

To construct the 3D HFM, the different hydrogeologic unit tops must be interpolated and extrapolated from available land-surface and throughout the subsurface between the cross sections and wells. The emphasis in this step was to create structure contour maps in a consistent manner by interpolating and extrapolating from available data points. These data points included: (1) topographic elevations derived from DEM data within the outcrop areas of each hydrogeologic unit; (2) separate files defining the tops of each hydrogeologic unit supplied from the cross sections; (3) elevations of hydrogeologic unit tops from well logs, and 4) geophysical evidence of unit tops from published sources. Distribution of geologic, geophysical, and well-data locations are shown on figure 2. The structure contour maps were created by interpolating between data points. A grid increment of 1,500 m coincident with the regional ground-water flow model of D'Agnesse and others (in press) was used; this resulted in grids with 21 columns and 31 rows. This coarse grid increment greatly simplifies the available data.

A hybrid gridding technique was used to construct a continuous grid or surface for each unit utilizing a set of points in x,y,z space. Using a fault-handling package built into the gridding software, the fault traces were used during the gridding procedure so that the elevation of a unit was not translated across a fault. Hence, the resulting structure contour maps contain a series of undulating surfaces, broken by faults.

Thrust faults occur in the model area, but are difficult to represent because geologic, structural, or stratigraphic surfaces stored as grids, cannot have multiple z values. Simplifying techniques were used to handle this limitation. Where units were repeated by thrust faults, two different grids were created for the same hydrogeologic unit. Repeating hydrogeologic structural unit altitude values were treated as defining unique additional hydrogeologic unit(s).

The quality of individual structure contour maps depends on the density of the data points used to define them. Some of these surfaces, such as the upper volcanic aquifer, were relatively well defined by more than one data set (derived from surface information, lithologic logs, and cross sections). Others, especially the units that outcrop less frequently, were less well defined and were extrapolated from sparser data and published geophysical interpretations. A relative rating of data availability for each of the hydrogeologic units appears in table 1; the rating does not imply accuracy regarding the extent and location of each unit. Although the rating is subjective, it is partially based on the number of data points used to define each hydrogeologic unit.

Assembling the Framework Model

The 3D HFM was constructed using the set of interpolated structure contour maps of individual hydrogeologic units. These structure contour maps were stacked in stratigraphic order to build the 3D HFM. Landmark's Stratamodel SGM (Stratigraphic Geocellular Modeling) is a geologic modeling software product that uses "geologic rules" to help define the geographic extent and intersection of surfaces. The SGM software was developed for modeling sedimentary basin environments. It allows for the specification of sedimentary depositional units, as well as the truncation of units and faulting.

SGM has not been designed to handle the time stratigraphic emplacement of intrusions. To include intrusions, they must be inserted into the SGM model out of their correct stratigraphic order. Therefore, the youngest intrusion is the first surface included in the SGM model.

The following sequence was used to build the 3D HFM:

1) The base of the HFM was set to an independent surface located at the boundary between the second and third layer of Death Valley regional ground-water flow model (D'Agnese and others, in press).

Hence, the hydrogeologic units and structures occurring above the third layer of the Death Valley regional ground-water flow model are modeled.

2) The granitic intrusions were input as the first geologic unit.

3) The lower clastic confining unit was input. Where the granites extend through this grid, the unit was truncated (or "clipped").

4) The remaining units (lower carbonate aquifer, upper clastic confining unit, upper carbonate aquifer, lower valley-fill confining unit, volcanic aquifers and confining units, basalt flows, and limestone aquifer) were deposited in sequential order onto the lower clastic confining unit and intrusions.

5) The valley-fill aquifer and confining units were deposited in the valleys.

6) Finally, the top of the HFM was clipped by one of the potentiometric surfaces considered for the flow model.

The HFM has volumetric units defined by the structure contour maps of individual hydrogeologic units (such as the upper volcanic aquifer). The hydrogeologic units are numbered consecutively in stratigraphic order from bottom to top (table 1) beginning with sequence number 2 (the SGM requires the specification of an arbitrary base unit, or sequence number 1, which is not used in the actual model). Although the cells have uniform horizontal dimensions throughout the HFM, the geoscientist controls the number of cell layers. In many locations these hydrogeologic units have large thickness. To

improve the vertical resolution, the units were subdivided into "layers", each with a maximum thickness of 125 m to minimize gridding and computational problems.

The SGM software allows each cell to reflect multiple attributes. The software automatically assigns some attributes to each cell, including row number, column number, sequence number, layer number, and elevation. The cells were further attributed to reflect the hydrogeologic units. For ground-water flow modeling, the HFM can be used to assign appropriate hydraulic property values. The available hydraulic property data which were used to assign hydraulic properties to each cell are summarized later in this report.

The geology and structure represented in the HFM is shown in a fence diagram through the site model (fig. 4). Surficial views in the region surrounding the area of the site model and within the site model area that were constructed using higher resolution surface data are shown in figures 3a and 3b, respectively.

The resulting HFM omits many small and even intermediate-scale features within the subsurface. It does, however, represent the large-scale features as accurately as possible given the grid resolution, and, therefore provides substantial constraints for model development. For the initial simulation of ground-water flow, this resolution is probably adequate. For future flow and transport, the effect of the small-scale variations will need to be considered. For example, the HFM with 250-m grid spacing much more accurately represents the offsets across faults and a change in the geometry of the units which corresponds with the LHG.

Incorporation of Potentiometric Surface

Gridded values from the potentiometric surface were used in the construction of the hydrogeologic framework model (HFM). The potentiometric surface was used to clip the top

of the HFM. The HFM was then translated into a finite-element mesh through the use of automated gridding software (discussed later in this report).

MODELING APPROACH

To model the saturated-zone flow system at the site scale at Yucca Mountain several simulation capabilities were considered important, including the ability to: (1) simulate 3D transient ground-water flow and heat transport, including 3D representation of spatially variable permeability, porosity, and thermal conductivity; (2) allow specification of constant pressure, constant hydraulic head, constant fluid and heat flux boundary conditions; (3) represent discontinuous, irregularly shaped 3D hydrogeologic units; (4) permit specification of dual permeability and porosity representing both fracture and matrix flow; (5) represent hydraulic-head and temperature observation points where they occur in 3D space; (6) calibrate the model with respect to observations of hydraulic head and temperature through the use of automated parameter estimation techniques; and (7) directly interface the resulting flow model with radionuclide transport models used in Performance Assessment of the Yucca Mountain site. This list includes features of the model not used in the present report, but important for anticipated modeling efforts. The FEHMN simulation code was selected because it possessed these capabilities when coupled with the mesh generation software, GEOMESH (described later in this report), and with the model-independent parameter estimation software, PEST (also described later in this report). The following section discusses the theory for many aspects of FEHMN.

Description of FEHMN Computer Code

The FEHMN (Finite Element Heat Mass Nuclear) computer code is capable of simulating flow and transport through both the unsaturated and saturated zones. FEHMN is a nonisothermal, multiphase flow

and transport code. It can simulate the flow of water and air, and the transport of heat and contaminants, in 2- and 3D saturated or partially saturated, heterogeneous porous media. The code includes comprehensive reactive geochemistry and transport modules and a particle tracking capability. Fractured media can be simulated using an equivalent continuum, discrete fracture, dual porosity or dual permeability approach. The basic conservation equations, constitutive relations and numerical methods are described in Zyvoloski (1983), Zyvoloski (1986), Zyvoloski and Dash (1990), Reeves (1994), and Zyvoloski and others (1995).

Conservation Equations

FEHMN solves three conservation equations: conservation of total fluid mass (air and water), conservation of air, and conservation of solute (contaminant). The mass of the solute is assumed to be small enough not to affect the total fluid mass balance. When energy transport mechanisms are considered, such as evaporative processes, conservation of energy is also considered.

Detailed derivations of the governing equations for two-phase flow including heat transfer have been presented by several investigators (Mercer and Faust, 1975; Brownell and others, 1975). Therefore, only a brief development will be presented here.

Conservation of total fluid mass (air and water) is expressed by the equation

$$\frac{\partial A_m}{\partial t} + \nabla \cdot f_m + q_m = 0 \quad (1)$$

where the mass per unit volume, A_m , is given by

$$A_m = \phi(S_v \rho_v + S_l \rho_l) \quad (2)$$

and the mass flux, f_m , is given by

$$f_m = \rho_v v_v + \rho_l v_l \quad (3)$$

where

ϕ is the porosity of the matrix;

S_v, S_l is the saturation for vapor and liquid phases, respectively;

ρ_v, ρ_l is the density for vapor and liquid phases, respectively;

v_v, v_l is the velocity for vapor and liquid phases, respectively; and

q_m is a source and sink term (such as flow from or to wellbores).

Note that the liquid phase includes liquid water and air dissolved in liquid water, and the vapor phase includes both air and water vapor. Also, the subscript m denotes mass, as opposed to the subscript e , which denotes energy.

Conservation of energy is expressed by the equation

$$\frac{\partial A_e}{\partial t} + \nabla \cdot f_e + q_e = 0 \quad (4)$$

where the energy per unit volume, A_e , is given by

$$A_e = (1 - \phi)\rho_r u_r + \phi(S_v \rho_v u_v + S_l \rho_l u_l) \quad (5)$$

where $u_r = c_p T$, and the energy flux f_e is given by

$$f_e = \rho_v h_v v_v + \rho_l h_l v_l - K \nabla T \quad (6)$$

where:

u_r, u_v, u_l is the internal energy of the rock matrix, vapor and liquid phases, respectively;

ρ_r, ρ_v, ρ_l is the density for the rock matrix, vapor and liquid phases, respectively;

c_p is specific heat at constant pressure;

h_v, h_l is the specific enthalpy for vapor and liquid phases, respectively;

K is the effective thermal conductivity of the saturated rock matrix;

T is temperature; and

q_e is energy contributed from sources and sinks.

It is assumed that Darcy's Law applies to the movement of each phase. The equations are:

$$v_v = -\frac{k_s k_{rv}}{\mu_v} (\nabla P_v - \rho_v g) \quad (7)$$

and

$$v_l = -\frac{k_s k_{rl}}{\mu_l} (\nabla P_l - \rho_l g) \quad (8)$$

where

k_s is the saturated permeability;

k_{rv}, k_{rl} is the relative permeability for vapor and liquid phases, respectively;

μ_v, μ_l is the viscosity for vapor and liquid phases respectively;

P_v, P_l is the phase pressure for vapor and liquid phases, respectively; and

g is the acceleration due to gravity.

The phase pressures are related by $P_v = P_l + P_{cap}$, where P_{cap} represents capillary pressure. For simplicity, the equations are shown for an isotropic medium, although this restriction does not exist in the FEHMN computer code. Using Darcy's Law the basic conservation of mass and energy equations can be rewritten as

$$-\nabla \cdot (D_{mv} \nabla P_v) - \nabla \cdot (D_{ml} \nabla P_l) + q_m + \frac{\partial}{\partial z} g (D_{mv} \rho_v + D_{ml} \rho_l) + \frac{\partial A_m}{\partial t} = 0 \quad (9)$$

and

$$-\nabla \cdot (D_{ev} \nabla P_v) - \nabla \cdot (D_{el} \nabla P_l) - \nabla \cdot (K \nabla T) + q_e + \frac{\partial}{\partial z} g (D_{ev} \rho_v + D_{el} \rho_l) + \frac{\partial A_e}{\partial t} = 0 \quad (10)$$

where z is oriented in the direction of gravity. The coefficients in equations 9 and 10 are defined as

$$D_{mv} = \frac{k_s k_{rv} \rho_v}{\mu_v} \quad (11a)$$

$$D_{ml} = \frac{k_s k_{rl} \rho_l}{\mu_l} \quad (11b)$$

$$D_{ev} = h_v D_{mv} \quad (12a)$$

and

$$D_{el} = h_l D_{ml} \quad (12b)$$

The conservation of mass equation for air is

$$-\nabla \cdot (\eta_v D_{mv} \nabla P_v) - \nabla \cdot (\eta_l D_{ml} \nabla P_l) - \nabla \cdot (D_{va} \nabla \eta_v) + q_\eta + \frac{\partial}{\partial t} (\eta_v D_{mv} \rho_v + \eta_l D_{ml} \rho_l) + \frac{\partial A_\eta}{\partial t} = 0 \quad (13)$$

where the source or sink strength, q_η , and accumulation term, A_η , are defined as

$$q_\eta = \eta_v q_v + \eta_l q_l \quad (14)$$

and

$$A_{\eta} = \phi(\eta_v S_v \rho_v + \eta_l S_l \rho_l) \quad (15)$$

Here η is the ratio of the mass of air to the total fluid mass (water and air). D_{va} , the diffusivity of water vapor in air, is given by a function of tortuosity, porosity, vapor phase saturation, vapor phase density, temperature and pressure. All other terms have been defined previously.

The FEHMN code has the capability of handling solute transport. The conservation of solute equation is not directly coupled to the flow (pressure) field, and is, therefore, density independent. The source or sink strength, q_c , and accumulation term, A_c , are defined for the solute conservation equation as

$$q_c = C_v q_v + C_l q_l \quad (16a)$$

$$A_c = \phi(C_v S_v \rho_v + C_l S_l \rho_l) \quad (16b)$$

The conservation equation for a given solute is given by

$$\begin{aligned} & -\nabla \cdot (C_v D_{mv} \nabla P_v) - \nabla \cdot (C_l D_{ml} \nabla P_l) - \nabla \cdot (D_{cv} \nabla C_v) - \nabla \cdot (D_{cl} \nabla C_l) + \\ & q_c + \frac{\partial}{\partial t} \phi(C_v D_{mv} \rho_v + C_l D_{ml} \rho_l) + \rho_r \frac{\partial C_r}{\partial t} + \frac{\partial A_c}{\partial t} = 0 \end{aligned} \quad (17)$$

Here C is the concentration of the solute (contaminant). $\nabla \cdot (D_c \nabla C_i)$ and $\nabla \cdot (D_v \nabla C_v)$ are the dispersion terms and $\rho_s \partial C_s / \partial t$ is the adsorption term. C_s represents the adsorption of a solute onto the porous media. FEHMN supports several adsorption models, including a simple linear model: $C_s = K_D C_i$ where K_D is the distribution coefficient. q_c is the source or sink term. All other terms have been defined previously.

Constitutive Relations

FEHMN requires information about air and water properties (including density, viscosity, enthalpy, and their derivatives) as functions of temperature (T) and pressure (P). Rational function approximations are used to estimate these variables in FEHMN, where the rational functions are a ratio of polynomials. For water, polynomial coefficients were obtained by fitting data from the National Bureau of Standards/Nuclear Regulatory Commission Steam Tables (Harr and others, 1984). The density of air is assumed to obey the ideal gas law.

FEHMN also has the capability of simulating flow in partially saturated conditions. FEHMN also requires information about the relation between values of relative permeability, capillary pressures and air-water saturations. Several well known functions (for example, Brooks-Corey; van Genuchten) are available to the user. Only the van Genuchten functions (van Genuchten, 1980) are described here. The van Genuchten relative permeability function is described by the following formulae:

$$k_{rl} = \sqrt{\hat{S}} \left[1.0 - (1.0 - \hat{S}^m)^n \right] \quad (18)$$

where

$$\hat{S} = \frac{S - S_r}{S_s - S_r} \quad (19)$$

$$m = 1 - \frac{1}{n} \quad (20)$$

and n is an experimentally fitted parameter; S is saturation; S_r is residual liquid saturation; and S_s is the maximum liquid saturation.

The van Genuchten function for capillary pressure is described by the following equation

$$\hat{S} = \left[\frac{1}{1 + (\alpha h)^n} \right]^m \quad (21)$$

and

$$\dot{h} = P_{can}/\rho g$$

(22)

where α is an experimentally fitted parameter.

Numerical Methods

FEHMN uses a finite-element/finite-volume method to discretize the conservation equations to be solved. Newton-Raphson iteration is applied to the fully coupled system of equations. This system of equations is solved with multi-degree of freedom preconditioned conjugate gradient methods, using generalized minimum residual (GMRES) acceleration techniques (Zyvoloski, 1986).

Features Used in Current Model

For the current model, the following FEHMN macros were invoked:

FEHMN Macro Used	Description
sol	defines solver, in this case water and saturation
head	allows specification of pressure in terms of hydraulic head
cond	specifies thermal conductivity
node	specifies output request for hydraulic head, flux, and saturation for specific nodes
pest	specifies output in a form that can be read conveniently by PEST
air	specifies air/water solution; as used, full degree of freedom (fully two-phase solution) is specified along with reference temperature for properties and reference pressure for properties
perm	specifies permeability values of different hydrogeologic units and zones
zone	used to specify nodes contained in individual zones or geometries of prisms which contain nodes; nodes identified within zone lists or zone geometries are then used in perm, rock, flow, and node macros
flow	used to specify constant hydraulic head conditions and specified flux
iter	specifies iteration parameters which are needed for the nonlinear equation solver
ctrl	specifies simulation control variables (for example, minimum and maximum time steps)
rock	specifies rock density, specific heat, and porosity
time	specifies initial time step, final time step, maximum number of time steps, and starting date
cont	specifies file output for graphical postprocessing
stop	ends list of input commands

All of the above macros were tested and verified in the process of assigning the version number of the software (accession no. MOL.19970610.0204). Validation and verification of the FEHMN code was done according to the plan of Dash and others (1995). If changes are made to the code, verification testing is done, such that the code remains qualified.

Parameter Estimation

The parameter estimation component of the model was achieved through the use of the model independent parameter estimation software, PEST (Watermark Computing, 1994). PEST uses nonlinear least-squares regression to estimate parameters. The benefits of using nonlinear regression include: (1) expedited determination of best-fit parameter values; (2) quantification of the quality of the calibration; (3) estimates of the confidence limits on parameter estimates; and (4) identification of the correlation among parameters (Poeter and Hill, 1997, p. 250).

PEST was selected because of the ability to couple it with FEHMN without significantly changing the FEHMN software. PEST is designed to be used with virtually any model, provided that one can identify: a) model input files; b) model output files; c) commands that invoke the model; d) observation data; and e) model parameters. Each of the required input and output files need to be in ASCII format.

PEST was used to run FEHMN and to vary user-specified model parameters prior to each run such that the weighted sum of the differences between observed and simulated values of pressure, hydraulic head, or temperature is minimized using nonlinear regression. The optimization is accomplished using the Gauss-Marquardt-Levenberg method. The strength of this method lies in the fact that it can generally estimate parameters using fewer model runs than any other estimation method, a definite advantage for large models whose run times may be considerable (Watermark Computing, 1994, p. 1-4).

SATURATED-ZONE FLOW-MODEL CONSTRUCTION

3D Finite-Element Mesh

After constructing the 3D hydrogeologic framework model (HFM), an automated finite-element mesh-generation computer program, GEOMESH (Gable and others, 1995), is used to construct a computational grid of tetrahedral elements in three dimensions. The HFM is converted automatically for direct input into GEOMESH. There are three basic criteria to ensure grid integrity and quality in translating from an HFM to a finite-element grid. First, the final grid must preserve the geometry of the HFM input. All material interfaces, layer truncations, external boundaries and model geometry must be preserved. Second, grid quality is ensured by always producing a Delaunay grid (Gable and others, 1995). In two dimensions, a Delaunay triangulation of a point set produces a grid where the circumscribed circle of every triangle will not have any points in its interior. This has desirable qualities when implementing finite-element equation solvers. The third criterion is that the grid is designed such that the geometric coupling coefficients of the finite-element mesh are all positive and form a semi-positive coefficient matrix (Trease and Dean, 1990). The second and third criteria involve creating a grid with advantageous numerical properties.

GEOMESH can be used to construct structured or unstructured grids. A structured grid consists of regularly shaped elements, such as rectangular prisms, in which changes in horizontal elevations along the tops of geologic units are approximated by placement of these elements in a stair-step fashion. An unstructured grid consists of tetrahedral elements that can more closely represent irregular geometries associated with geologic units with varying thickness and areal extent.

In the generation of a computational grid from an HFM, care must be taken near pinchouts or other regions where extremely thin cells can occur. The HFM consists of an ordered array of hexahedral (8 node, 6 face) elements, whose array of $I \times J \times K$ elements has $(I+1) \times (J+1) \times (K+1)$ nodes. However, a large

number of these elements may have to be eliminated. The reason for this is that if a hydrogeologic layer pinches out to zero thickness, the HFM does not eliminate the layer from the data structure, it simply continues the layer with zero thickness. This can produce zero-volume elements that must be removed. Also, because the HFM representation must have a rectangular shape in map view, irregular areas are modeled by assigning null values to cells outside the area of interest. These null elements also must be eliminated. When this process is finished, the model is an unstructured, hexahedral, finite-element representation of the hydrogeologic model.

Hexahedral elements are then converted to tetrahedral elements. Each hexahedra can be broken into five, six or twenty-four tetrahedra, the later being used for this model. Delaunay criteria are enforced without allowing any connections to cross material interfaces by adding nodes on interfaces when a connection crosses an interface, thereby increasing the number of nodes and elements. The final step is to ensure that there are no negative-coupling coefficients. This is done by calculating the area vectors associated with all elements, and if any are negative, the element is divided until the coupling coefficients are positive. This step also adds nodes and elements to the mesh.

Finally, hydraulic-head observation nodal points are added to the mesh for spatially correct calibration points. Because the altitude at which the hydraulic head measurement applies is uncertain, the nodal points are located at the midpoint of either the water column for uncased boreholes or the midpoint of a screened or packed-off interval within the borehole. Figure 7 shows a sketch of these locations. Figure 8 shows the areal distribution of the nodes and the hydrologic unit in which the node is located.

The resulting finite-element mesh appears in figure 9. Figure 10 shows north-to-south

and west-to-east exploded views of the different 3D units as captured with the resulting 3D finite-element mesh.

A comparison of the finite-element mesh and the hydrogeologic framework model was made to check for inconsistencies in representing material interfaces, layer truncations, external boundaries and model geometry. The top of the model (coincident with the potentiometric surface), sides, and bottom were represented correctly. Overall the geometries of the hydrogeologic units appeared to be adequately represented; however, some of the hydrogeologic unit geometries appeared to be inconsistent between the HFM and the finite-element mesh. A summary of the comparison is presented in table 5.

Table 5.--Results of comparing hydrogeologic framework model unit geometries with 3D finite-element tetrahedral mesh

Errors in Framework in Simulations 1-39

[HFM, hydrogeologic framework model; gran, Granitic Confining Unit; qcu, Lower Clastic Confining Unit; lca, Lower Carbonate Aquifer; ecu, Upper Clastic Confining Unit; uca, Upper Carbonate Aquifer; lcu, Lower Valley-Fill Confining Unit; lvcu, Lower Volcanic Confining Unit; lva, Lower Volcanic Aquifer; mvcu, Middle Volcanic Confining Unit; mva, Middle Volcanic Aquifer; uvcu, Upper Volcanic Confining Unit; uva, Upper Volcanic Aquifer; b, Lava-Flow Aquifer; llim, Limestone Aquifer; tpla, Valley-Fill Confining Unit; qal, Valley-Fill Aquifer]

HFM Sequence Numbers (from Table 1)	Comparison Result
2 (gran)	Two model nodes lie outside the HFM sequence and appear to be part of the model base southwest of the HFM unit extent.
3 (lca)	Six model nodes lie outside the HFM sequence and appear to be part of the model base.
4, 5, 6 (qcu, lca, ecu)	All the model nodes appear to conform to the HFM sequence. Parts of these units appear to be missing. For example, unit number 6 is missing where unit number 7 exists in error.
7 (lca)	All the model nodes lie outside the HFM sequence and appear to be part of model unit number 6.
8 (uca)	Six model nodes lie outside the HFM sequence and appear to be part of the model base.
9, 10 (lcu, lvcu)	All the model nodes appear to conform to the HFM sequence.
11 (lva)	Only two nodes exist in the model. One of these two lies outside the HFM sequence. The HFM sequence shows that more nodes are required to define the geometry of this unit.
12 (mvcu)	Three model nodes lie outside the HFM sequence and appear to be part of the model base.
13 (mva)	One model node lies outside the HFM sequence.
14, 15 (uvcu, uva)	All the model nodes appear to conform to the HFM sequence.
16 (b)	One model node lies outside the HFM sequence
17 (llim)	Two model nodes lie outside the HFM sequence.
18 (tpla)	Four model nodes lie outside the HFM sequence.
19 (qal)	All the model nodes appear to conform to the HFM sequence

The finite-element mesh on which the present calibration was done consisted of 9,279 nodes. From the comparison presented in table 5, 40 nodes were identified as being assigned to a hydrogeologic unit incorrectly. To assess the error, the nodes were corrected to reflect the appropriate permeability values and the model simulation performed again. In some instances, the nodes of the correct hydrogeologic unit could not be identified. As a result, at least one of the hydrogeologic units is still under-represented. The maximum difference in observation well heads in model simulation 40, made with the partially corrected and uncorrected finite-element meshes, was three meters and the average difference was much less than one meter. The mesh errors, therefore, probably did not substantially affect the calibration process, which is documented in this report. The first 39 simulations listed in appendix C used the uncorrected mesh; simulation 40 (the final simulation) used the corrected mesh. A 250-m sampled mesh is planned with improved error checking, which will improve the quality of both the framework model and the numerical grid based on the framework model.

Assumptions

In the model presented in this report, the following assumptions are applicable:

1. The hydrogeologic framework is an appropriate description of the principal hydrogeologic units and faults.
2. Permeability is invariant within each hydrogeologic unit
3. Ground-water flow occurs in three dimensions and within the rock mass (which includes both rock matrix and fractures).
4. Ground-water flow system is isothermal at 44°C (the effect of this assumption was tested by simulating system at 20°C).
5. Hydraulic heads of the potentiometric surface (fig. 5) along the north, south, east, and west edges of

the modeled area are an appropriate data set for specifying boundary conditions along the sides of the model.

6. The system is at steady state so that ground-water flow into and out of the flow domain is invariant with time.
7. Volumes associated with the finite-element mesh are sufficiently large so as to exceed the representative elementary volume necessary to simulate fracture flow as porous-media flow.
8. A no-flow boundary at the base of the model approximates hydrologic conditions.
9. The large hydraulic gradient is part of the saturated zone and not an artifact of perched-water occurrence.
10. Recharge is assumed to occur only at the top of the model along upper Fortymile Wash; all other nodes on the top of the model are specified as a no-flow boundary.

Assumptions 5 and 8 are not and have not been supported. Areally-distributed recharge likely occurs in the vicinity of Yucca Mountain, in contrast to assumption 10. All three of these assumptions represent an expedient means to assign boundary conditions, which may affect model calibration.

Description of numerical flow model

Several different conceptual models were tested as part of the present work. Simulation 40 (Appendix C) is thought to be most probable and is the model primarily described in this report. Sixteen permeability zones are defined by the hydrogeologic units of the HFM. Two additions were made to this framework: (1) inclusion of an east-west barrier representing a possible buried fault of small permeability in the vicinity of the LHG; and (2) inclusion of a

north-south barrier of small permeability along the Solitario Canyon fault zone. The framework additions and recharge parameters are summarized in the "Zonal Definitions" section.

Specified-head boundaries were used around the vertical sides of the model (see section entitled "Specified-head boundary conditions" later in this report). Specified-head boundaries are used around the model sides to allow flow in or out of the model. Implicit within the specified head boundaries is the conceptual model of recharge or throughflow occurring in the north and discharge out the south of the model domain. No pumping wells, evapotranspiration, or springs are included in the model. As a result, the only discharge from the model is along the specified head boundaries.

Observations in this application are hydraulic-head values. In the present study, estimated parameters are either permeability, specified flux values, or the length associated with a zone of low permeability. The model was then calibrated to 94 hydraulic-head measurements. The only flux observations available are from a regional flow model of the area (D'Agnese and others, in press). Flux along the specified-head boundaries calculated by the site model is compared to the flux from the regional model.

Although the simulator (FEHMN) is required to be used in a transient mode, the simulations presented in this report assume a steady-state flow system. Steady-state conditions are achieved by using large values of storage (porosity values of 0.3) coupled with a large simulation period (1×10^{10} days). Steady-state conditions are attained when the difference between the total mass flux into the system and the total mass flux out of the system, divided by the total mass of the system, is small (1×10^{-3} was used).

In addition, a number of problems were identified during the calibration process (see Appendix B). The mesh problem (discussed in Appendix B) and problems with incorporation of the HFM into the flow model have been corrected. Likewise, the recharge distribution at Fortymile Wash was corrected to be only at the top most nodes.

Permeability

Values of permeability for the 16 hydrogeologic units used in the model that is thought to represent the system realistically (simulation 40) are listed in table 3. Permeability values used in the model are considered preliminary. All of these permeability values fall within the ranges cited for either hydraulic conductivity or permeability in table 3. The spatial distribution of permeability used in the model is shown through the use of block and fence diagrams in figures 11a and 11b. Only the nodes closest to Fortymile Wash and Solitario Canyon Fault are represented explicitly as fault or fracture zones. In the numerical model, Solitario Canyon is a separate permeability zone and forms a barrier to flow.

The permeability values used in the model are derived partly from a sequence of parameter-estimation simulations discussed in appendix B. Not all permeability values were estimated as parameters, and those that were not estimated are listed in appendix D. Note that in runs with parameter estimation, only 1 or 2 parameters typically were estimated.

Permeability specified for the middle volcanic aquifer ($1.6 \times 10^{-14} \text{ m}^2$) is about three orders of magnitude less than values reported by Geldon (1996, p. 70) for tests at the C-holes. A possible explanation for this discrepancy is that the C-hole tests reflect hydraulic conditions in locally faulted and intensely fractured rock. The possibility of such a condition was tested to a limited extent by specifying a vertical zone, extending approximately 5 km southeast from the C-holes, with a larger permeability of $1 \times 10^{-11} \text{ m}^2$. The small increase in the resultant sum of squared residuals ($23,262 \text{ m}^2$) over that of simulation 40 ($23,163 \text{ m}^2$) indicates that the model was insensitive to such a zone and that such a zone might be possible. This zone would be consistent with northwest-southeast oriented faults in the area. The small change could also be an artifact of the density of observation points near this zone of large permeability coupled

with the small horizontal hydraulic gradient. However, because of the non-unique nature of the model, an overall large permeability ($1 \times 10^{-11} \text{ m}^2$) for the entire middle volcanic aquifer also is possible, but would require a considerably different combination of permeability values for the other hydrogeologic units to achieve calibration. Investigating the possibility of a zone of large permeability would be more appropriate using a more finely sampled hydrogeologic framework model and associated finite-element mesh.

Model Zonal Definitions and Variable Values Used in Final Simulation

In FEHMN, nodes are grouped into zones in which rock and hydraulic properties, and boundary conditions may be specified. There are several zones used in the model that define nodes pertaining to hydrogeologic units with specific permeability and porosity values. Zones 00002 through 00019 correspond to material properties of the units which are listed in tables 1 and 3. These zones and the permeability values used in the final model simulation are listed in table 6.

Additional zone lists were used to specify boundary conditions and special permeability zones where abrupt changes in the potentiometric surface occur in the vicinity of Solitario Canyon fault zone and the LHG. These zones and their associated values are listed in table 6.

Table 6.--Zone descriptions and values used in the final model simulation.

[Table lists values used in simulation 40, appendix C; permeability values in meters²; mass flux values in kilograms/second; model parameter abbreviations: gran, Granitic Confining Unit; qcu, Lower Clastic Confining Unit; lca, Lower Carbonate Aquifer; ecu, Upper Clastic Confining Unit; uca, Upper Carbonate Aquifer; lcu, Undifferentiated Valley Fill; lvcu, Lower Volcanic Confining Unit; lva, Lower Volcanic Aquifer; mvcu, Middle Volcanic Confining Unit; mva, Middle Volcanic Aquifer; uvcu, Upper Volcanic Confining Unit; uva, Upper Volcanic Aquifer; b, Lava-Flow Aquifer; tlim, Limestone Aquifer; tpla, Valley-Fill Confining Unit; qal, Valley-Fill Aquifer; lkns, zone of low permeability associated with Solitario Canyon Fault oriented north to south; lkew, zone of low permeability oriented east to west located at approximate southern end of large hydraulic gradient]

Zone Number	Parameter Name	Description and Purpose	Value Used in Model
00002	gran	Used to identify nodes for specifying permeability	3.5×10^{-14}
00003	lca	do.	4.4×10^{-12}
00004	qcu	do.	2.0×10^{-15}
00005	lca	do.	4.4×10^{-12}
00006	ecu	do.	5.5×10^{-15}
00007	lca	do.	4.4×10^{-12}
00008	uca	do.	6.7×10^{-13}
00009	lcu	do.	2.9×10^{-14}
00010	lvcu	do.	1.0×10^{-16}
00011	lva	do.	5.0×10^{-13}
00012	mvcu	do.	1.9×10^{-16}
00013	mva	do.	1.6×10^{-14}
00014	uvcu	do.	1.0×10^{-18}
00015	uva	do.	1.6×10^{-14}
00016	b	do.	4.5×10^{-14}
00017	tlim	do.	1.0×10^{-14}
00018	tpla	do.	3.0×10^{-16}
00019	qal	do.	8.8×10^{-14}
00061	lkew	do.	1.6×10^{-17}
00062	lkns	do.	1.15×10^{-15}

Table 6.--Zone descriptions and values used in the final model simulation.

[Table lists values used in simulation 40, appendix C; permeability values in meters²; mass flux values in kilograms/second; model parameter abbreviations: gran, Granitic Confining Unit; qcu, Lower Clastic Confining Unit; lca, Lower Carbonate Aquifer; ecu, Upper Clastic Confining Unit; uca, Upper Carbonate Aquifer; lcu, Undifferentiated Valley Fill; lvcu, Lower Volcanic Confining Unit; lva, Lower Volcanic Aquifer; mvcu, Middle Volcanic Confining Unit; mva, Middle Volcanic Aquifer; uvcu, Upper Volcanic Confining Unit; uva, Upper Volcanic Aquifer; b, Lava-Flow Aquifer; llim, Limestone Aquifer; tpla, Valley-Fill Confining Unit; qal, Valley-Fill Aquifer; lkns, zone of low permeability associated with Solitario Canyon Fault oriented north to south; lkew, zone of low permeability oriented east to west located at approximate southern end of large hydraulic gradient]

Zone Number	Parameter Name	Description and Purpose	Value Used in Model
00073	--	All west nodes; used to specify fixed hydraulic head	Hydraulic head distribution shown on figure 13
00074	--	All south nodes; used to specify fixed hydraulic head	Hydraulic head distribution shown on figure 14
00075	--	All east nodes; used to specify fixed hydraulic head	Hydraulic head distribution shown on figure 15
00076	--	All north nodes; used to specify fixed hydraulic head	Hydraulic head distribution shown on figure 16
00079	fm	Nodes along the top of Fortymile Wash used to specify mass flux as recharge	-0.22

Large Hydraulic Gradient Zone

To reproduce the LHG on the north end of Yucca Mountain, where the apparent water-table altitude changes about 300 meters in a distance of less than 2 km, an additional zone (zone 00061) was defined within the model as an east-west barrier to flow. Large head residuals had occurred at the wells defining the LHG prior to the definition of this zone. Because no independent geologic evidence for a structure exists, and because the length of such a structure is in question, the coordinate defining the eastern extent of this zone was selected as a parameter and allowed to vary from the western limit (fig. 12) of zone 00061 to the eastern edge of the model during earlier scoping simulations. Model fit was best when zone 00061 extended to the eastern edge.

Zone 00061 extends from the top of the water table to the bottom of the model, and is one node thick forming a 2D plane shown on figure 12. The present model zonation results in uniform permeability changes over the entirety of the upper volcanic aquifer, the upper volcanic confining unit, and the middle volcanic aquifer wherever they occur within the model. Zone 00061 was estimated to have a permeability of $1.6 \times 10^{-17} \text{ m}^2$. This planar feature appears as a blue east-west cutting plane in figure 11a. This interpretation implies the presence of a buried fault of low permeability, which is consistent with one of the hypotheses suggested by Fridrich and others (1994) to explain the LHG. Specifying larger permeability values (1×10^{-14} to $1 \times 10^{-11} \text{ m}^2$) to test the 'drain' conceptual model of Fridrich and others (1994) resulted in a poor match to observed hydraulic head.

An alternate approach to representing the LHG would be to further subdivide the zones defining the upper volcanic aquifer, the upper volcanic confining unit, and the middle volcanic confining unit along the east-west occurrence of the LHG. This subdivision would then allow

reduction of the permeability of these units where they occur to the north of the gradient, producing a 'spillway' model (Fridrich and others, 1994). Such a model, if successful in representing the LHG, would not require zone 00061 to produce a permeability contrast. Further refinement of the HFM may also help to better represent the LHG. A 250-m resolution mesh better represents the fault and the hydro-geologic unit distribution, coincident with the LHG as portrayed by Fridrich and others (1994).

Solitario Canyon Fault Zone

Based on hydrologic and hydrochemical data, the Solitario Canyon fault appears to act as at least a partial barrier to ground-water flow. Currently, Solitario Canyon fault is not specifically identified in the HFM. Therefore, zone 00062 (fig. 12) was included to better reproduce the approximately 50 meter change in hydraulic head across the Solitario Canyon fault system. Like zone 00061, zone 00062 extends the full thickness of the model, is one node thick, and represents a vertical plane. Its exact correlation with Solitario Canyon fault is approximate owing to the coarseness of the grid. This zone was introduced after initial attempts to simulate the 50-m change in head resulted in large hydraulic-head residual values.

Zone 00062 was estimated to have a small permeability of $1.15 \times 10^{-15} \text{ m}^2$. This permeability value is consistent with that expected for a barrier to ground-water flow, and is somewhat larger than the value estimated for zone 00061—a relation which is also consistent with the different hydraulic gradients observed across these two zones. No hydraulic-test data exist to provide information about the permeability of the Solitario Canyon fault zone.

Fortymile Wash Recharge Zone

Many lines of evidence indicate recharge occurs in upper Fortymile Wash. Zone 00079 was used

to specify recharge in upper Fortymile Wash. The zone consists of seven nodes located at the top of the model (fig.12). Recharge is assigned as a uniform mass rate at each of these nodes, and was defined as a parameter (fm). The estimated recharge was 0.22 kg/s applied over this zone. The zone over which this recharge is specified is smaller than that used to obtain the 0.86 kg/s estimate, which was based on field studies of stream loss (C.S. Savard, U.S. Geological Survey, written commun., 1997).

Specified-Head Boundary Conditions

Because the site model has lateral boundaries through which significant flow occurs, it was designed to be part of a larger integrated modeling effort in which fluxes would be derived from the regional model of D'Agnese and others (in press). These fluxes could either be estimated, assigned directly within the site model, or used as a comparison with those from the site model. The latter approach was taken and is discussed in the section entitled "Simulated Fluxes" which appears later in this report.

Hydraulic-head data are considered to be more accurate than flux data within the site model, and for that reason were chosen for specifying boundary conditions for the model despite the influence that such a constant-head boundary is likely to have on a model being calibrated to hydraulic-head observations. Specified-head boundary conditions are based on the potentiometric surface that includes the LHG as represented in figure 5. However, no measured vertical head distributions at the boundaries of the model exist. The regional model (D'Agnese and others, in press) does provide coarse estimates of vertical hydraulic head, but were not used in assigning the boundaries at the site model. An appropriate set of hydraulic-head values on the outside nodes of the model consistent with the potentiometric-surface

data was computed for use in specifying constant hydraulic-head boundary conditions by using the model as described in the following paragraph.

The basic concept used in calculating the boundary hydraulic-head values is that the sides of the constructed model can be thought of as cross-sections through the ground-water system connected at the corners. The hydraulic heads of the cross sections need to be consistent, in some manner, with the potentiometric surface they intersect. For the present version of the model, this consistency is attained as follows. Very small permeability values ($1 \times 10^{-29} \text{ m}^2$) are specified within the model interior, and nodes on the outside faces of the model are assigned large permeability values of $1 \times 10^{-14} \text{ m}^2$. The nodes along the top edges of the model were specified with the hydraulic-head values from the potentiometric surface and the underlying side nodes allowed to equilibrate to achieve a vertical head distribution. Equilibrium head distributions for the four vertical sides of the model are shown in figures 13 through 16. Although there are no corroborative data, head distribution on the west (fig. 13) and east (fig. 15) are consistent with recharge or throughflow from the north and potential for upward flow in the south. The northern boundary (fig. 16) shows the potential for flow away from a mound which is located under Fortymile Wash and upward flow north of Crater Flat. The southern boundary (fig. 14) shows the potential for upward flow toward the west, which is consistent with observed increasing head with depth.

Using these constant-head boundaries (fig. 13 to 16), simulations are performed by setting all node permeability values according to the distributions of the various hydrogeologic units (removing the $1 \times 10^{-29} \text{ m}^2$ permeability specification at nodes internal to the model). By using specified-head conditions, flow into or out of the nodes on the outside faces can be calculated by the model.

The method of assigning hydraulic heads for the lateral constant-head boundaries described above has the advantage of producing a continuous head distribution, but the distribution produced may not be representative of the hydraulic-head values that actually occur along these cross-sections for the follow

ing reasons: (1) the hydraulic-conductivity distribution along the sides is not homogeneous, as implied by this method of generating head values; and (2) flow through all four sides, and especially the north and south sides, is significant but is implicitly assumed to be negligible in the calculation of heads along the sides.

Alternate methods to estimate specified head could have been used. Specifying permeability values along the vertical sides using values appropriate for individual hydrogeologic units where they intersect the model boundaries would have addressed the first problem. However, the model failed to converge to a solution when this approach was tried. Incorporating boundary fluxes from the regional model into the analysis could address the second problem, but this was not attempted in the present work. The original intent during the construction of the site model was to assign fluxes extracted from the regional model of ground-water flow and assign them uniformly along the outside nodes of the site model (figures 13 through 16). The regional model fluxes for the site model boundaries are listed in table 7 (which appears later in this report). Specifying fluxes from the regional model directly onto the side nodes of the site model was considered, but was recognized to be a complex task, and one likely to cause inconsistent hydraulic head distributions adjacent to zones of contrasting permeability between the regional and site models, resulting from the different resolution of the two models.

Improving the representation of the lateral boundary conditions is considered to be of primary concern for future modeling efforts. Alternate ways to specify boundary conditions within the site model exist. These include but are not limited to: (1) specifying constant heads only along the top edge of the model (this was not done because no flow would be allowed at the remaining nodes along the sides); (2) specifying flux explicitly (this was not done because of the difficulties in redistributing flux from the regional model onto the sides of the site

model): or (3) projecting hydrostatic head from the top edge down the outside faces of the model (this was not selected because it forces flow to be horizontal).

As noted previously, one concern with specifying hydraulic heads on all model sides, while calibrating using hydraulic heads within the model, is that the specified heads are likely to dominate the simulated heads at the observation locations. The severity of this problem was tested in independent numerical experiments using a model developed by Sandia National Laboratory of a subdomain that included Yucca Mountain. The results indicated that specified pressure (constant head) boundary conditions could be applied while still observing changes in model simulated pressures as a result of changes in model permeability values (B.W. Arnold, Sandia National Laboratory, written communication, 1997). Because the site model covers a substantially larger area than that of the Sandia model, application of specified head boundary conditions was considered to be less of a constraint. However, the use of any specified-head boundary condition will have some constraint on model calibration. As a result, the fluxes in and out of the model will have to be checked against any available data.

Model calibration procedure

Model calibration was attempted using nonlinear least-squares regression to estimate parameter values. Permeability values were modified to achieve a close match to 94 measured hydraulic heads, all of which were equally weighted. Fluxes at the specified-head nodes for the outside nodes were summed for each side of the model for comparison against regional model values. It may be advantageous to compare flows for smaller parts of each side, but this was not done in the present work.

Several simulations using a pressure-based configuration instead of hydraulic heads, provided experience regarding which parameters tended to be highly correlated, a condition which indicates that

the available data are not sufficient to estimate all parameters individually. Hydrogeologic units with similar permeabilities were combined or "lumped" as parameters to gain some insight about the hydrologic importance of areas of large and small permeability. For example, the permeability parameter of the middle volcanic aquifer (mva) was observed to be correlated to the upper volcanic aquifer (uva). Experience has shown that spatially connected hydrogeologic units with similar permeability which are oriented approximately parallel to the direction of ground-water flow tend to be highly correlated, preventing independent estimates of their associated permeability values. An initial strategy focused on optimizing permeability in those units that appeared to have sufficient information provided by hydraulic-head observation points (see "Simulated Hydraulic Head"). In addition, a determination of which potential model parameters were highly correlated was done using PEST by assigning as many model variables of permeability and flux as possible so that correlation among parameters could be evaluated. From these correlations, parameters either could be lumped with other correlated parameters, or set so that parameter estimation could be achieved.

Forty PEST parameter estimation runs were done for various combinations of fixed and estimated parameters (appendix C). Fixed parameter values are not modified during a run; estimated parameter values are adjusted using nonlinear regression. In most of the runs, one or two parameter values are estimated; at most, 5 are estimated. Because so few parameters are estimated without a thorough evaluation showing that the other parameters are unimportant, the regression runs presented here need to be considered as very preliminary. The results of the PEST simulations include 95% confidence intervals for the adjustable parameters, which may or may not be meaningful, depending on many factors in the model construction and parameter estimation processes. A large range in the 95% confidence interval generally indicates that the

data contain little information about the parameter. In many instances, minimum values of 95% confidence intervals were estimated as negative values (appendix C). Use of a log transformation of such a parameter typically would result in a minimum value with a large negative exponent (or essentially a minimum value of zero), indicating that insufficient information was available to provide a good estimate of the parameter.

Appendix C lists values for the adjustable parameters for each simulation, and the resulting estimates and objective function, phi (sum of squared residuals for hydraulic head). Appendix D lists parameters that were fixed at specific values for all or most of the simulation runs. Rationale for fixing these parameters at specified values include: (a) the parameter was found to be highly correlated to other parameters in the model; (b) few or no hydraulic-head observation data exist for the unit to permit optimization of its permeability; (c) the spatial location of the unit placed it out of the main flow within the system; (d) the volume or areal extent of the unit was very small (particularly true for granitic confining unit and lower volcanic confining unit); or (e) the regression would not converge if many parameter values were estimated simultaneously. In general, as modeling progresses and closer hydraulic head matches are achieved, phi should decrease. An overall decrease in phi occurred through the first 30 simulations and for the 40th simulation. Table 8 (listed in Appendix B) lists the most substantial changes in the objective function resulting from adjustments in particular model parameters.

MODEL EVALUATION

Simulated Hydraulic Head

Figure 8 shows the areal distribution of hydraulic-head observation nodes and the associated hydrogeologic unit in which each node is located. The observation nodes were positioned within the

finite-element mesh at an altitude corresponding to either the midpoint of the water column in the well or, if data were available, the midpoint of the packed off interval (fig. 7). The best represented hydrogeologic unit in the model is the valley-fill aquifer (unit 19) with 40 wells, the majority of these wells occur in the southwest corner of the model domain. The next best representations are for the upper volcanic aquifer (unit 15), with 20 wells, the upper volcanic confining unit (unit 14), with 12 wells, and the middle volcanic aquifer (unit 13), with 9 wells.

Simulated hydraulic head for simulation 40 (fig. 17) within the flow domain is consistent with the expected distribution of hydraulic head (fig. 5). In figure 17, the LHG is evident at the sharply contrasting east-west oriented green color band. Figure 17 also shows the distribution of hydraulic-head residuals at the observation wells, which show overall agreement between simulated and observed hydraulic head. Tabulated residual values for each observation point are listed in Appendix D. Negative residuals indicate that the simulated hydraulic head was too high; positive values indicate the converse. Forty five percent of the residuals lie between -5 and +5 m. The range in observed hydraulic head over the model area is about 500 m.

The largest residuals occur at observation points 5 (UE-25 WT#16; residual of -95.0 m), 80 (USW H-1, tube 1; residual of +62.7 m), and 2 (GEXA Well 4; residual of -36.6 m). The sum of squared residuals for these three points is $14,295 \text{ m}^2$, which represents greater than half of the total sum of squared residuals of $23,163 \text{ m}^2$ for all 94 observations.

Hydraulic head at observation point 5 (UE-25 WT#16) was simulated too high as a result of the placement of zone 00061 (zone of small permeability) at a position south of UE-25 WT#16 in the model, causing water levels to rise north of it. The coarse mesh in this area of the model restricted the choices for the placement of the barrier. Future simulations using a refined mesh will help in positioning and representing the LHG. Nonetheless, the LHG was

mostly reproducible with reasonable values of permeability for the barrier and adjacent units. The barrier provides a feasible conceptual model to explain the LHG, which indicates that the calibration effort does not contradict its existence.

The simulated hydraulic head at observation 80, which represents the deepest observation point in USW H-1, was lower than the observed values, probably because of the no-flow boundary specified at the bottom of the model. The no-flow boundary also may cause the lower simulated heads at observation points 94 (USW p#1; residual of +29.9 m), 85 (USW H-5, lower tube; residual of +25.4), and 93 (USW H-3, lower tube; residual of +11.6 m). A more appropriate boundary condition might have been to specify incoming mass flux or an elevated hydraulic head at the bottom of the model, or to couple the bottom of the model with the sides when establishing the constant head boundaries. These will be considered in future simulations.

Large discrepancies between observed and simulated vertical gradients occur in USW H-1, USW H-3, USW H-4, USW-H-5, UE25 b#1, and USW p#1. Simulated flow is either largely horizontal or downward at Yucca Mountain, in contrast to the conceptual model, which indicates the potential for upward flow. These discrepancies may have important ramifications should the model be used for transport simulations, and indicates the need for additional model calibration.

Observed head values indicate a horizontal hydraulic gradient of about 0.07 exists between GEXA Well 3 (located just west of the western model boundary with a hydraulic head of 1,192 m) and GEXA Well 4 (just inside that boundary with a hydraulic head of 1,010 m). The large residual at observation 2 (GEXA Well 4) is a result of a specified-head boundary condition defined by interpolating between these two hydraulic-head values, coupled with the occurrence of a large hydraulic gradient across the model boundary. It is possible that the water level in GEXA Well 3 is perched, but supporting data is lacking. If so, the gradient would be smaller, making it easier to match observation 2. Figure 13 illustrates the

complex flow condition that results at this location.

Additional discrepancies between specified head and simulated head occur along the southern boundary of the model. Variations in the vertical head distributions at the southern boundary (fig. 14) show considerable differences from the head values along the top. These discrepancies may result from positioning the observation node at the midpoint of the water column within the well and using an observed hydraulic head equal to that at the potentiometric surface.

In general, the model fits the observations well in small gradient areas, but fits less well in larger gradient areas. A plot of simulated against measured hydraulic head is shown in figure 18, which shows a high correlation coefficient ($R^2 = 0.979$) between the simulated and observed values. The high correlation is largely caused by the spread of the data. If all but data points greater than 1,000 m are considered, the resulting correlation coefficient is reduced significantly ($R^2 = 0.853$). A histogram of the distribution of hydraulic-head residuals is shown in figure 19. The largest classes of residuals occur between the range of -5 to +5 m. Residuals are well distributed about zero. The sum of squared residuals for the model is 23,163 m² resulting in a standard error of 15.7 m for the 94 observations, which when divided by the range in measured head values (500 m) is 3×10^{-2} .

Simulated Fluxes

Currently, the best independent estimates of flux into and out of the domain of the site model come from the regional model (D'Agnese and others, in press). A comparison of fluxes from the site model from simulation 40 and those associated with the regional model is given in table 7. The site-model boundaries were selected to be coincident with the finite-difference

grid cell boundaries in the regional ground-water flow model (D'Agnese and others, in press). Fluxes normal to the site-model boundaries on the sides of regional-model layers 1 and 2 and the bottom of regional model layer 2 were based on the fluxes calculated in the regional model (Patrick Tucci, U.S. Geological Survey, written commun., 1997). Because the specified system temperature affects the overall flux through the system, specified flux at Fortymile Wash (fig. 12) was estimated using PEST for each of the site model runs in table 7.

Values of the total mass fluxes on the eastern half of the northern boundary and northern third of eastern boundary are listed in table 7. A comparison of these fluxes shows that most of the incoming flux from the northern boundary ends up leaving the model through the northern third of the eastern boundary. This is illustrated through a planar projection of normalized 3D vectors of ground-water mass flux (fig. 20), whose tails lie on a horizontal plane cutting approximately midway through the model. This flux pattern occurs, in part, because of the specification of the zone of small permeability (zone 00061) which diverts water to the east. It also occurs as an artifact of the specified head boundary conditions. There is no evidence to support either the magnitude or pattern of such flow. Because most of this water leaves the model north of Yucca Mountain, flux vectors near Yucca Mountain are of substantially smaller magnitude. This helps explain the large discrepancy between the flux values from regional and site models at these boundaries. This condition likely would be corrected by specifying flux derived from the regional model at the northern boundary explicitly, rather than specifying head.

Table 7.--Comparison of ground-water fluxes derived from the regional and site flow models

[negative values indicate injection into the rock mass; *, areal recharge, some of which occurs in upper Fortymile Wash. Values of flux do not account for the spatial distribution of flux either into or out of a specific side of the model, but rather the net sum of all the fluxes for a side. Superscript designation: 1, results from magnitude of mass balance errors being comparable to flux magnitude; 2, difference based on remaining flux from western half of northern boundary; 3, difference based on remaining flux from southern two-thirds of eastern boundary.]

Flux Location	Net Flux from Regional Model (D'Agnes and others, in press) [kg/s]	Flux Total From Site Model (kg/s)		Percent Increase in Flux Between 20°C and 44°C Simulations	Percent Difference in Flux Between Regional and Site Model (Simulation 40)
		At 20°C (Simulation 40 with temperature modified)	At 44°C (Simulation 40)		
North	-174.0	-4235.7	-6946.9	64	
North (eastern half)	--	--	-6826.6	--	31 ²
West	-90.7	-18.3	10.7	159 ¹	-112
East	-167.1	3643.7	6056.5	60	
East (northern third)	--	--	6807.3	--	340 ³
South	323.38	610.5	879.9	44	172
Bottom	57.85	0	0	0	--
Wells	73.1	0	0	0	--
Fortymile Wash	-22.4*	-0.13	-0.22	69	99

The comparison of the fluxes for the regional and site models listed in table 7 shows flux discharging from the southern end of the site model to be about 172 percent greater for the site model simulation at 44°C than that from the regional model. No temperature was specified in the regional model so that a direct comparison is not possible. In addition, no flux was simulated in or out of the base of the site model. Hence, some substantial differences between fluxes from the regional and site models are expected.

The regional model used specified ground-water discharge from wells in the Amargosa Desert. If pumpage from wells (73.1 kg/s) is subtracted from the flux value for the site model then the difference is 150 percent. The pumping would account for about 22 percent of the differences in flux out the southern boundary. The large differences between the fluxes for the north and east boundaries likely results from the different gradients represented by each model, the boundary conditions specified, the permeability distributions, different conceptual models (for example, inclusion of barrier for representing the LHG in the site model) and the greater vertical resolution of the hydrogeologic units in the site model. If the flux from the eastern-half of the northern boundary is removed from the total flux from the northern boundary, the remaining flux (-120.3 kg/s) is about 31 percent less than that for the regional model. Likewise, if the flux from the northern third of the eastern boundary of the site model is removed from the total flux from the eastern boundary, the remaining flux (-741 kg/s) is about 340 percent larger than that for the regional model.

SOURCES OF ERROR

Model discretization is coarse, and as a result causes incomplete definition of hydrogeologic units. The flexibility of the tetrahedral elements used to construct the finite-element computational grid provides greater accuracy in representing the individual hydrogeologic units than would be available at the

resolution with less flexible gridding techniques, but problems still remain. For example, many of the faults are implicit in the grid through offset of units, hence the exact location for faults will always be approximate, regardless of grid spacing. However, explicit representation of selected faults could be achieved through explicit specification of the fault as a surface within the HFM, which would cause it to be defined as a set of nodes within the subsequent finite-element mesh, complete with its own set of hydraulic properties. Larger problems are identifying those faults (a) for which hydraulic properties are available or could be anticipated (very little is known); and (b) that are most important to represent explicitly within the flow and transport model.

Permeability is known to vary spatially within individual hydrogeologic units. The assumption of uniform permeability within each unit is a simplification of a complex system. Small scale variations in hydraulic head likely cannot be represented, without greater resolution. Even with a more refined model, permeability data to support spatial variation of permeability would be lacking. Local areas of large permeability may exist that would explain very large estimates of permeability based on hydraulic tests (for example, within the middle volcanic aquifer), that are not represented in the final model. Specification of fault and fracture zones from independent geologic information may be the only way to incorporate spatial variations of permeability.

An average temperature for the entire saturated zone contained within the site model has not been calculated. Different specifications of average ground-water temperature (20°C and 44°C) have an appreciable effect on viscosity (1.002 centipoise for fresh water at 20°C; 0.6067 centipoise for fresh water at 44°C). Table 7 illustrates that this temperature has about a 60 percent effect on simulated flux as expected. A more appropriate way to address the issue of tem-

perature effects on flow is to simulate coupled ground-water flow and heat transport with appropriate temperature and heat-flow boundary conditions. Temperature data collected from wells throughout the model area are available for use in calibration. Using temperature and hydraulic-head data in model calibration likely would better constrain simulated results.

Hydraulic-head boundary conditions are based on a process of extrapolation and interpolation of extant data. An artifact of that process is the resultant large fluxes that occur in the northeast part of the model. Furthermore, no vertical hydraulic-head data exist at the model boundaries making it difficult to verify the resulting hydraulic-head distribution. Possible inaccuracies of assigned hydraulic-head values at the side model boundaries are an important potential source of model error.

The steady-state assumption may be invalid in areas in which ground-water withdrawals are occurring. The hydraulic-head observation data span almost 50 years of record, which results in irregularities in the potentiometric surface. The slope of the potentiometric surface toward the southwest may be indicative of ground-water withdrawal which were not specified in the model. About 73.1 kg/s of discharge by pumping wells occurs in the Amargosa Desert in the southwest part of the model, but was not represented in the model.

No flow is specified along the base of the model. This omission may explain the error in simulating lower hydraulic head values than those observed in the deeper observation points within the model. This error results in horizontal to vertically-downward flow within the model, a condition unsupported by the hydraulic-head observations. However, observed upward flow cannot be confirmed with existing data.

Finally, the representation of the large hydraulic gradient remains inconclusive. By specifying an east-west oriented barrier to flow, the observed hydraulic-head data may be better matched, but the resulting flow field is difficult to reconcile. If a buried fault does exist and is a barrier to flow, no data are available to prove or disprove its existence. Furthermore, if the large hydraulic gradient is actually an

artifact of perched-water occurrence, then the resulting flow field would be considerably different.

USES AND LIMITATIONS OF THE MODEL

Uses of the current model include the following:

1. Provide a large-scale description of the hydrogeologic framework of the site saturated zone flow system based on a sampling of 1.5-km by 1.5-km mesh;
2. Provide a mechanism to extend model calibration and sensitivity testing of parameters used in the model;
3. Provide the flow field for doing preliminary transport simulations and estimates of ground-water travel time through the use of additional transport related capabilities within FEHMN; and
4. Provide initial estimates of permeability for 16 hydrogeologic units from the HFM and 2 additional zones of small permeability and recharge at Fortymile Wash.

Limitations of the model include:

1. Simulations are restricted to fully saturated conditions from the water table and below. Although the model was built by use of a framework model that extended to land surface, the unsaturated zone was not included as part of the flow model. The unsaturated zone was omitted because of time constraints and the long execution times for forward simulation runs associated with two-phase flow problems.
2. The model does not account for variations in temperature within the flow system. Temperature varies within the ground-water flow system and may be a useful constraint in identifying acceptable model representations of both temperature and hydraulic head. The

preliminary status of the model limited the extent to which temperature could be evaluated. Furthermore, the temperature of the system was specified at a uniform 44°C, which may be too high to represent the average temperature.

3. **It is likely that the flow model is non-unique. Coordinated adjustments in permeability values (either higher or lower by some multiplier) might lead to similar hydraulic head distribution and calibration. Because fluxes were not specified explicitly at either the upgradient or downgradient ends of the model, the model is less constrained as it would be with fluxes included in the calibration. However, because some permeability values (of admittedly minimal accuracy) were specified explicitly throughout the parameter estimation, the model was partially constrained, which likely caused the parameter estimation process to converge in many instances.**
4. **The large hydraulic gradient is poorly understood and greatly affects model calibration, simulated permeability values, and flux. Additional data and testing are required to adequately characterize this feature. Testing and reconfiguration of monitoring intervals within borehole USW G-2 could be done to provide permeability, flow-survey, temperature, and hydraulic-head data at different depths, particularly for the middle volcanic aquifer. Construction of additional boreholes in the large hydraulic gradient area, such as a corehole into the middle volcanic aquifer adjacent to drill-hole WT-6, could provide useful vertical gradient, hydraulic-head, saturation, and permeability data. The model contained in this report was successful in representing the large hydraulic gradient through the incorporation of a vertical barrier to flow, but other representations are possible.**
5. **Flux into the site model domain is poorly defined and remains one of the most elusive of model variables. The quality of the model is in part a measure of the understanding of the distribution and amount of recharge within the model domain. Comparison of fluxes into and out of the model is dependent on available flux data, which although greatly lacking will not likely be improved sub-**

stantially through additional field studies because of the large uncertainty associated with the techniques used to estimate recharge. Water levels within the flow system could still be adjusting to recharge supplied during climatically wetter conditions. If such a condition exists, the effect may be too subtle to observe with the available hydraulic data. Adjusting water-level conditions could be evaluated using the regional model to replicate conditions necessary to observe the effect of increased recharge under past wetter climates.

6. **Limited hydraulic-test data exist for constraining permeability values used in the model. Few hydraulic-test data are available that involve multiple observation wells within the model domain from which large-scale transmissivity or hydraulic conductivity values can be derived. The exception to this condition is the C-hole-complex hydraulic testing, which is optimally located for conditions at Yucca Mountain and provides a test involving a large volume of the middle volcanic aquifer. In general, the model does not distinguish between the permeability of the rock matrix, fractures, or faults. Two zones of small permeability were added at Solitario Canyon and the LHG. It is possible to add large-scale features such as faults explicitly within the model by regriding, but hydraulic characteristics for faults in the saturated zone are not presently available.**
7. **Definition of the hydrogeologic units within the model is limited by the sampling interval used (1.5 km). By sampling the framework model at a smaller interval (for example, 250 m) better resolution of the hydrogeologic units could be obtained, but resulting in a larger computation mesh. Experience from the current modeling exercise sug-**

gests that this approach is warranted and likely would succeed. However, higher resolution sampling alone may be insufficient to explicitly represent faults.

SUMMARY AND CONCLUSIONS

A preliminary model of the saturated zone ground-water flow system in the vicinity of Yucca Mountain, Nevada was developed and calibrated. Development of the model began with the construction of a digital hydrogeologic framework model that, when developed, was sampled at a plan-view spacing of 1,500 m by 1,500 m with variable thickness. This sampling resulted in a gridded data set that was used as input data for the automated generation of a fully three-dimensional tetrahedral finite-element mesh, which consists of 9,279 nodes and 51,461 tetrahedral elements that represent 16 different hydrogeologic units. The mesh generator was designed to discretize irregular three-dimensional solids, and to assign material properties from the hydrogeologic framework model to the tetrahedral elements. The mesh generator facilitated the addition of nodes to the finite-element mesh, which correspond to the exact three-dimensional position of the potentiometric surface based on water-levels from wells, which were used for model calibration.

The conceptual model represented within the numerical model of ground-water flow is based on the assumption that recharge occurs as throughflow from the northern, eastern, and western boundary of the modeled area, and by minor recharge in upper Fortymile Wash. Discharge occurs mainly out the southern end of the model. No flow is assumed through the bottom. A large hydraulic gradient (300-m change in hydraulic head over about 2 km) is assumed to be part of the saturated zone (as opposed to being an artifact of the occurrence of perched water) and caused by buried fault of small permeability. A 50-m change in hydraulic head across Solitario Canyon fault zone is assumed to result from a fault of small permeability.

A ground-water flow simulator was run with the resulting finite-element mesh and resulted in a reasonably accurate mass balance. The model used an automated parameter estimation routine to minimize the difference between 94 observations of hydraulic head and those simulated by the flow simulator by adjusting selected permeability and flux parameters. Results from 40 simulations are reported. The greatest improvements resulted when: (1) vertical low permeability barriers that correspond to the Solitario Canyon fault and the downgradient side of the large hydraulic gradient were added; and (2) the parameter for the permeability of the upper volcanic confining unit (Calico Hills Formation) was isolated and optimized. Optimal permeability estimates for the sixteen hydrogeologic units generally lie between high and low values for the same units reported in the literature. The largest class of hydraulic-head residuals (the difference between observed and simulated values) occurred between the range of -5 to +5 m. The least accurately fitting hydraulic-head observation resulted from the inability to locate accurately the low permeability barrier used to produce the large hydraulic gradient accurately because of the existing node density in the finite-element mesh.

Comparisons of flux from the regional model showed almost twice the amount discharging from the southern end of the site model, and substantially different amounts for the northern and eastern sides. The major flux differences between the two models occur in the northeast corner where a large part of the recharge from the north is diverted east and discharges in part because of the interaction of the constant-head boundaries and the imposed east-west barrier needed to represent the large-hydraulic gradient.

On initial inspection, model match to hydraulic-head data and the resulting distribution of residuals have some problems. Although permeability values for all of the hydrogeologic units used in the model lie within reported literature values, reported values for individual units have

large ranges. Furthermore, in the case of the middle volcanic aquifer, values of permeability from large-scale hydraulic testing at the C-hole complex were 3 orders of magnitude larger than those used in the model. This discrepancy may be indicative of model error, or alternately, the possibility of a local, large-permeability zone not represented in the present model. Finally, any model calibrated by using hydraulic heads alone is subject to error in simulated flux.

Improvements for future model developments include (in no particular order):

- Conduct sensitivity analyses with regard to which model variables have the greatest effect when varied on the sum of squared residuals for hydraulic head. This would provide a guide for additional field studies to reduce uncertainty in the model.
- Refine hydrogeologic framework model to better define the distribution of the hydrogeologic units. In particular, the upper volcanic confining unit is currently over-represented. This discrepancy substantially influences simulated flow and transport simulations.
- Use higher resolution sampling of the hydrogeologic framework model to better delineate unit offset caused by faulting. This would result in a denser finite-element mesh, resulting in longer execution times, but would provide a more realistic portrayal of the flow system than is available in the model presented in this report.
- Add major faults explicitly as surfaces within a refined version of the hydrogeologic framework model, so that their potential as barriers to flow or as fast pathways to the accessible environment may be evaluated.
- Decouple permeability parameters for the upper and middle volcanic aquifers as practical during model calibration. This separation of the two primary volcanic aquifers at Yucca Mountain within the model would better represent the permeability distribution.
- Recalibrate the existing model with larger values of permeability in the middle volcanic aquifer (mv

and the upper volcanic aquifer (uva).

- Incorporate additional data into the formal model calibration. This could include flux data from the regional model for at least one face of the model and borehole-temperature data to better constrain the solution.
- Fluxes should be extracted from a refined, improved existing version of a regional model of ground-water flow in which the topmost layer has been subdivided to better represent the hydrogeologic units at Yucca Mountain and in the Amargosa Desert.
- Include vertical flux through the bottom of the model based on regional model values.
- Use hydrochemical and isotopic data as a check against flow model results.

REFERENCES

- Ahola, M., and Sagar, B., 1992. Regional ground-water modeling of the saturated zone in the vicinity of Yucca Mountain, Nevada: U.S. Nuclear Regulatory Commission, NUREG/CR-5890.
- Anderson, L.A., 1981, Rock property analysis of core samples from the Yucca Mountain UE25a-1 borehole, Nevada Test Site, Nevada: U.S. Geological Survey Open-File Report 81-1338, 36 p.
- Anderson, L.A., 1994, Water permeability and related rock properties measured on core samples from the Yucca Mountain USW GU-3/G-3 and USW G-4 boreholes, Nevada Test Site, Nevada: U.S. Geological Survey Open-File Report 92-201, 36 p.
- Barr, G.E., and Miller, W.B., 1987. Simple models of the saturated zone at Yucca Mountain: Sandia National Laboratories SAND87-0112, 90 p.
- Bedinger, M.S., Sargent, K.A., Langer, L.H., Sherman, F.B., Reed, J.E., and Brady, B.T., 1989, Studies of geology and hydrology in the Basin and Range Province, Southwestern United States, for isolation of high-level radioactive waste- Basis of characterization and evaluation: U.S. Geological Survey Professional Paper 1370-A, 41 p.
- Benson, L.V., and McKinley, P.W., 1985. Chemical composition of ground water in the Yucca Mountain area, Nevada, 1971-1984; U.S. Geological Survey Open-File Report 85-484, 10 p.

- Blankennagel, R.K., and Weir, J.E., 1973, Geohydrology of the Eastern part of the Pahute Mesa, Nevada Test Site, Nye County, Nevada: U.S. Geological Survey Professional Paper 712-B, 35 p.
- Brownell, D.H., Garg, S.K., and Pritchett, J.W., 1975, Computer simulation of geothermal reservoirs: Proc. of the 45th California Regional Meeting of the Soc. Pet.Eng. of AIME, Ventura California, Paper SPE 5381.
- Broxton, D.E., Bish, D.L., and Warren, R.G., 1987, Distribution and chemistry of diagenetic minerals at Yucca Mountain, Nye County, Nevada: *Clays and Clay Minerals*, v. 35, no. 2, p. 89-110.
- Buscheck, T.A., and Nitao, J.J., 1992, The impact of thermal loading on repository performance at Yucca Mountain: American Nuclear Society, 1992 International High Level Radioactive Waste Management Conference, Proceedings of the Third Annual International Conference, Las Vegas, Nevada, April 12-16, 1992: La Grange Park, Ill., American Nuclear Society, p. 1003-1017.
- Carrigan, C.R., King, G.C.P., Barr, G.E., and Bixler N.E., 1991, Potential for water-table excursions induced by seismic events at Yucca Mountain, Nevada: *Geology*, v. 19, p. 1157-1160.
- Chapman, J.B., and Lyles, B.F., 1993, Groundwater chemistry at the Nevada Test Site: data and preliminary interpretations: Desert Research Institute Publication No. 45100, 45 p.
- Ciesnik, M.S., 1995, Ground-water altitudes and well data, Nye County, Nevada, and Inyo County, California: U.S. Geological Survey Open-File Report 93-89, 27 p.
- Claassen, H.C., 1985, Sources and mechanisms of recharge for ground water in the West-Central Amargosa Desert, Nevada--A geochemical interpretation: U.S. Geological Survey Professional Paper 712-F, 31 p.
- Clayton, R.W., Zelinski, W.P., and Rautmann, C.A., 1997, ISM2.0: A 3D geologic framework and integrated site model of Yucca Mountain: Civilian Radioactive Waste Management System, Management and Operating Contractor, Las Vegas, Nevada, 86 p., 72 plates.
- Craig, R.W., and Reed, R.L., 1991, Geohydrology of rocks penetrated by test well USW H-6, Yucca Mountain, Nye County, Nevada: U.S. Geological Survey Water Resources Investigations Report 89-4025, 40 p.
- Craig, R.W., and Robison, J.H., 1984, Geohydrology of rocks penetrated by test well UE-25p No. 1, Yucca Mountain Area, Nye County, Nevada: U.S. Geological Survey Water Resources Investigations Report 84-4248, 62 p.
- Czarnecki, J.B., 1985, Simulated effects of increased recharge on the ground-water flow system of Yucca Mountain and vicinity, Nevada-California: U.S. Geological Survey Water-Resources Investigations Report 84-4344, 33 p.
- Czarnecki, J.B., 1989a, Preliminary simulations related to a large horizontal hydraulic gradient at the north end of Yucca Mountain, Nevada: *Transactions, American Geophysical Union*, v. 70, no. 1.

- _____. 1989b, Characterization of the subregional ground-water flow system at Yucca Mountain and vicinity, Nevada-California: Radioactive Waste Management and the Nuclear Fuel Cycle, v. 13 (1-4), pp. 51-61.
- Czarnecki, J.B., 1990, Geohydrology and evapotranspiration at Franklin Lake playa, Inyo County, California: U.S. Geological Survey Open-File Report 90-356, 96 p.
- Czarnecki, J.B., 1991, Preliminary simulations showing potential effects of a wetter future climate coupled with a localized increase in hydraulic conductivity on the ground-water flow system of Yucca Mountain and vicinity, Nevada-California: Trans. American Geophysical Union, EOS, no. 17, v. 72, p. 121.
- Czarnecki, J.B., and Waddell, R.K., 1984, Finite-element simulation of ground-water flow in the vicinity of Yucca Mountain, Nevada-California: U.S. Geological Survey Water-Resources Investigations Report 84-4349, 38 p.
- Czarnecki, J.B., Steinkampf, W.C., and Kroitoru, L., 1990, From where and by what flow paths does ground water beneath Yucca Mountain, Nevada originate? [abs.]: Trans. American Geophysical Union, EOS, no. 43, v. 71, p. 1299.
- Czarnecki, J.B., and Wilson, W.E., 1991, Conceptual models of the regional ground-water flow system, and planned site-characterization studies, Yucca Mountain and vicinity, Nevada-California: Hydrological Science and Technology, v. 7, no. 1-4, pp. 15-25.
- Czarnecki, J.B., O'Brien, G.M., Nelson, P.H., Sass, J.H., Nelson, P.H., Bullard, J.W., and Flint, A.L., 1994, Is there perched water under Yucca Mountain in borehole USW G-2?: Trans. American Geophysical Union, EOS, v. 75, no. 44, pp. 249-250.
- Czarnecki, J.B., Nelson, P.H., O'Brien, G.M., Sass, J.H., Thapa, Bhaskar, Matsumoto, Yoshitaka, and Murakami, Osamu, 1995, Testing in borehole USW G-2 at Yucca Mountain: The saga continues: Trans. American Geophysical Union, EOS, v. 76, no. 7, p. F190.
- D'Agnesse, F.A., 1994, Using geoscientific information systems for three-dimensional modeling of regional ground-water flow systems, Death Valley region, Nevada and California: unpublished Ph.D. Dissertation, Dept. of Geology and Geological Engineering, Colorado School of Mines, Golden, Colorado, 331 p.
- D'Agnesse, F.A., Faunt, C.C., Turner, A.K., and Hill, M.C., in press, Hydrogeologic evaluation and numerical simulation of the Death Valley regional ground-water flow system, Nevada and California: U.S. Geological Survey Water-Resources Investigations Report 96-4300.
- Dash, Z.V., Robinson, B.A., and Zyvoloski, G.A., 1995, V&V plan and procedures for the

- Day, W.C., Potter, C.J., Sweetkind, D.S., Dickerson, R.P., and San Juan, C.A., in press. Bedrock geologic map of the central block area, Yucca Mountain, Nye County, Nevada: U.S. Geological Survey Miscellaneous Investigations Series I-2601, 1:6,000-scale, 2 plates with text. DTN GS96-708314221.001.
- Dettinger, M.D., 1989, Distribution of carbonate-rock aquifers in southern Nevada and the potential for their development, Summary of findings, 1985-88, Program for the study and testing of carbonate-rock aquifers in eastern and southern Nevada, Summary Report No. 1: State of Nevada, Carson City, Nevada, 37 p.
- Dressel, B.W., 1992, A hydro-seismic model of the Yucca Mountain waste repository site: unpublished Master's thesis, Ohio University, 111 p. plus appendices.
- Ervin, E.M., Luckey, R.R., and Burkhardt, D.J., 1994, Revised potentiometric-surface map, Yucca Mountain and vicinity, Nevada: U.S. Geological Survey Water Resources Investigations Report 93-4000, 17 p.
- Flint, L.E., and Flint, A.L., 1990, Preliminary permeability and water-retention data for nonwelded and bedded tuff samples, Yucca Mountain area, Nye County, Nevada: U.S. Geological Survey Open-File Report 90-569, 57 p.
- Fridrich, C.J., Dudley, W.W., Jr., and Stuckless, J.S., 1994, Hydrogeologic analysis of the saturated-zone ground-water system, under Yucca Mountain, Nevada: *Journal of Hydrology*, v. 154, pp. 133-168.
- Gable, C.W., Trease, H.E., and Cherry, T.A., 1996, Automated grid generation from models of complex geologic structure and stratigraphy in Third international conference/workshop on integrating GIS and environmental modeling: National Center for Geographic Information and Analysis, Santa Barbara, California (Accessed on January 15, 1996, on the World Wide Web at URL http://www.ncgia.ucsb.edu/conf/SANTA_FE_CD-ROM/main.html)
- Gable, C.W., Cherry, T.A., Trease, H.E., and Zvoloski, G.A., 1995, Geomesh Grid Generation: Yucca Mountain Project Letter Report LA-UR-95-4143.
- Garber, M.S., and Thordarson, W., 1962, Ground water Test Well C, Nevada Test Site, Nye County, Nevada: U.S. Geological Survey TEI-818, 79 p.
- Geldon, A.L., 1993, Preliminary hydrogeologic assessment of boreholes UE-25c#1, UE-25c#2, and UE-25c#3, Yucca Mountain, Nye County, Nevada: U.S. Geological Survey Water Resources Investigations Report 92-4016, 176 p.
- Geldon, A.L., 1996, Results and interpretation of preliminary aquifer tests in boreholes UE-25 c#1, UE-25 c#2, and UE-25 c#3, Yucca Mountain, Nye County, Nevada: U.S. Geological Survey Water-Resources Investigations Report 94-4177, 119 p.

- Geldon, A.L., Umari, A.M.A., Fahy, M.F., Earle, J.D., Gemmell, J.M., and Darnel, J., 1997, Results of hydraulic and conservative tracer tests in Miocene tuffaceous rocks at the C-hole complex, 1995 to 1997, Yucca Mountain, Nye County, Nevada: U.S. Geological Survey Milestone Report SP23PM3
- Graves, R.P., Tucci, Patrick, and O'Brien, G.M., 1997, Analysis of water-level data in the Yucca Mountain area, Nevada, 1985-95: U.S. Geological Survey Water-Resources Investigations Report 96-4256, 140 p.
- Harr, L., Gallagher, J., and Kell, G.S., 1984, NBS/NRC Steam Tables, Thermodynamics, and Transport Properties and Computer Programs for Vapor and Liquid States of Water, Hemisphere Press.
- Haws, S.J., 1990, The distribution of vertical groundwater flow in the saturated zone of the Yucca Mountain area: A cross-sectional finite element model: University of Nevada, Las Vegas, unpublished Master's thesis, 120 p.
- Hevesi, J.A., Flint, A.L., and Istok, J.D., 1992, Precipitation estimation in mountainous terrain using multivariate geostatistics: Part II: Isohyetal Maps: *J. Applied Meteorology*, v. 31, no. 7, p. 677-688.
- Hill, M.C., 1992, A computer program (MODFLOWP) for estimating parameters of a transient three-dimensional, ground-water flow model using nonlinear regression: U.S. Geological Survey Open-File Report 91-484, 358 p.
- Kilroy, K.C., 1991, Ground-water conditions in Amargosa Desert, Nevada-California, 1952-87: U.S. Geological Survey Water Resources Investigations Report 89-4101, 93 p.
- Laczniak, R.J., Cole, J.C., Sawyer, D.A., and Trudeau, D.A., 1996, Summary of hydrogeologic controls on ground-water flow at the Nevada Test Site, Nye County, Nevada: U.S. Geological Survey Water-Resources Investigations Report 96-4109, 59 p., 4 plates.
- Lahoud, R.R., Lobmeyer, D.H., and Whitfield, M.S., Jr., 1984, Geohydrology of volcanic tuff penetrated by test well UE-25b#1, Yucca Mountain, Nevada: U.S. Geological Survey Water Resources Investigation 84-4253, 48 p.
- Lobmeyer, D.H., 1986, Geohydrology of rocks penetrated by test well USW G-4, Yucca Mountain, Nye County, Nevada: U.S. Geological Survey Water Resources Investigations Report 86-4015, 42 p.
- Luckey, R.R., and Tucci, Patrick, Faunt, C.C., Ervin, E.M., Steinkampf, W.C., D'Agnesse, F.A., and Patterson, G.L., 1996, Status of understanding of the saturated-zone ground-water flow system at Yucca Mountain, Nevada as of 1995: U.S. Geological Survey Water-Resources Investigations Report 96-4077, 71 p.

- Matuska, N.A., 1989. The relationship of the Yucca Mountain repository block to the regional groundwater system--A geochemical model: Las Vegas. University of Nevada at Las Vegas. Master's thesis, 199 p.
- McDonald, M.G., and Harbaugh, A.W., 1988, A modular three dimensional finite-difference ground-water flow model: U.S. Geological Survey Techniques of Water-Resources Investigations, book 6, chap. A1, 576 p.
- Mercer, J.W., and Faust, C.R., 1975, Simulation of water- and vapor-dominated hydrothermal reservoirs: Proc. of the 50th Annual Meeting of the Soc. Pet.Eng. of AIME, Paper SPE 5520.
- Moore, J.E. and Garber, M.S., 1962, Ground water test well B, Nevada Test Site, Nye County, Nevada: U.S. Geological Survey TEI-808, 39 p.
- O'Brien, G.M., 1997, Analysis of aquifer tests conducted in boreholes USW WT-10, UE-25 WT#12, and USW SD-7, 1995-96, Yucca Mountain, Nevada: U.S. Geological Survey Water-Resources Investigations Report 96-4293, 36 p.
- Osterkamp, W.R., Lane, L.J., and Savard, C.S., 1994, Recharge estimates using a geomorphic/ distributed-parameter simulation approach, Amargosa River Basin: Water Resources Bulletin, V. 30, no. 3, p. 493-507.
- Poeter, E.P., and Hill, M.C., 1997, Inverse models: A necessary next step in ground-water modeling: Groundwater, v. 35, no. 2, p. 250-260.
- Rice, W.A., 1984, Preliminary two-dimensional regional hydrologic model of the Nevada Test Site and vicinity: SAND83-7466, Sandia National Laboratories, Albuquerque, New Mexico, 89 p.
- Reeves, M., 1994, Review and Selection of Unsaturated Flow Models, Intera Document B00000000-01 425-2200-00001.
- Robison, J.H., 1984, Ground-water level data and preliminary potentiometric-surface maps, Yucca Mountain and vicinity, Nye County, Nevada: U.S. Geological Survey Water Resources Investigations Report 84-4197, 11 p.
- Robison, J.H., Stephens, D.M., Luckey, R.R., and Baldwin, D.A., 1988, Water levels in periodically measured wells in the Yucca Mountain area, Nevada, 1981-87: U.S. Geological Survey Open-File Report 88-468, 132 p.
- Robison, J.H., and Craig, R.W., 1991, Geohydrology of rocks penetrated by test well USW H-5, Yucca Mountain, Nye County, Nevada: U.S. Geological Survey Water Resources Investigations Report 88-4168, 44 p.
- Robison, J.H., Stephens, D.M., Luckey, R.R., and Baldwin, D.A., 1988, Water levels in periodically measured wells in the Yucca Mountain area, Nevada, 1981-1987: U.S. Geological Survey Open-File Report 88-468, 136 p.

- Rush, F.E., 1984, Geohydrology of test well USW H-1, Yucca Mountain, Nye County, Nevada: U.S. Geological Survey Water Resources Investigations Report 84-4032, 62 p.
- Sass, J.H., Lachenbruch, A.H., Dudley, W.W. Jr., Priest, S.S., and Munroe, R.J., 1988, Temperature, thermal conductivity, and heat flow near Yucca Mountain, Nevada: Some tectonic and hydrologic implication: U.S. Geological Survey Open-File Report 87-649, 118 p.
- Savard, C.S., 1995, Selected hydrologic data from Fortymile Wash in the Yucca Mountain area, Nevada, water year 1992: U.S. Geological Survey Open-File Report 94-317, 38 p.
- Savard, C.S., 1996, Selected hydrologic data from Fortymile Wash in the Yucca Mountain area, Nevada, water years 1993-94: U.S. Geological Survey Open-File Report 95-709, 30 p.
- Sinton, P.O., 1987, Three-dimensional, steady-state, finite-difference model of the ground-water flow system in the Death Valley ground-water basin, Nevada-California: Golden, Colo., Colorado School of Mines, unpublished Master's Thesis, 145 p.
- Stuckless, J.S., Whelan, J.F., and Steinkampf, W.C., 1991, Isotopic discontinuities in ground water beneath Yucca Mountain, Nevada: American Nuclear Society
- Thordarson, W., 1983, Geohydrologic data and test results from Well J-13, Nevada Test Site, Nye County, Nevada: U.S. Geological Survey Water Resources Investigations Report 83-4171, 63 p.
- Thordarson, W., Rush, F.E., and Waddell, S.J., 1985, Geohydrology of Test Well USW H-3, Yucca Mountain, Nye County, Nevada: U.S. Geological Survey Water Resources Investigations Report 84-4272, 44 p.
- Trease, H.E. and Dean, S.H., 1990, Thermal diffusion in the X-7 three-dimensional code in Proc. of the Next Free-Lagrange Conference, Jackson Lake Lodge, Wyoming, June 3-7, 1990, Springer-Verlag Press, v. 395, pp. 193-202.
- Tucci, Patrick, and Burkhardt, D.J., 1995, Potentiometric-surface map, 1993, Yucca Mountain and vicinity, Nevada: U.S. Geological Survey Water Resources Investigations Report 95-4149, 15 p.
- U.S. Department of Energy, 1997, Regional groundwater flow and tritium transport modeling and risk assessment of the underground test area, Nevada Test Site, Nevada: U.S. Department of Energy Nevada Operations Office DOE/NV-UC-700, 12 chaps., 4 plates.
- U.S. Geological Survey, 1987, Digital elevation models: Data Users Guide 5, 38 p.
- Van Genuchten, M.T., 1980, A closed form equation for predicting hydraulic conductivity of unsaturated soils: Soil Sci. Soc. Am. J., v. 44, pp. 892-898.

- Waddell, R.K., 1982, Two-dimensional, steady-state model of ground-water flow, Nevada Test Site and vicinity, Nevada-California: U.S. Geological Survey Water-Resources Investigations Report 82-4085, 72 p.
- Waddell, R.K., 1984, Hydrologic and drill-hole data for test wells UE-29a#1 and UE-29a#2, Fortymile Canyon, Nevada Test Site: U. S. Geological Survey Open-File Report 84-142, 25 p.
- Waddell, R.K., Robison, J.H., Blankennagel, R.K., 1984, Hydrology of Yucca Mountain and vicinity, Nevada-California: investigative results through mid-1983: U.S. Geological Survey Water Resources Investigations Report 84-4267, 134 p.
- Watermark Computing, 1994, PEST Model-Independent Parameter Estimation: User's Manual, Watermark Computing, Oxley, Australia.
- Weeks, E.P., and Wilson, W.E., 1984, Preliminary evaluation of hydrologic properties of cores of unsaturated tuff, test well USW H-1, Yucca Mountain, Nevada: U.S. Geological Survey Water-Resources Investigations Report 84-4193, 30 p.
- Winograd, I.J., and Thordarson, William, 1975, Hydrogeologic and hydrochemical framework, south-central Great Basin, Nevada-California, with special reference to the Nevada Test Site: U.S. Geological Survey Professional Paper 712-C, 126 p.
- Whitfield, M.S. Jr., Eshom, E.P., Thordarson, W., 1985, Geohydrology of rocks penetrated by test well USW H-4, Yucca Mountain, Nye County, Nevada: U.S. Geological Survey Water Resources Investigations Report 85-4030, 37 p.
- Zyvoloski, G.A., 1983, Finite element methods for geothermal reservoir simulation, *Int J. Numer. Anal. Meth. Geomech.*, v. 7, pp. 75-86.
- Zyvoloski, G.A., 1986, Incomplete factorization for finite element methods: *Int. J. for Numerical Methods in Engineering*, v. 23, pp. 1101-1109.
- Zyvoloski, G. A. and Z. V. Dash, 1990, Software Verification Report FEHMN Version 1.0, Los Alamos National Laboratory document TWS-EES-5/5-90-3.
- Zyvoloski, G.A., Robinson, B.A., Dash, Z.V., and Trease, L.L., 1995, Models and methods summary for the FEHMN application: Los Alamos National Laboratory LA-UR-94-3787, 69 p.

FIGURES

1-3. Maps showing:

1. The study area, associated geographic features, and hydraulic-head observation wells.

2. Geologic, geophysical, and well-data locations used in the construction of the hydrostratigraphic framework model

3a. Generalized hydrogeologic units with major structural features for region surrounding the area of the site model

3b. Generalized hydrogeologic units with major structural features and lines of section specific to site model area

4. Fence diagram showing geologic cross sections indicated on figure 2(b).

5. Map showing the potentiometric surface that includes the large hydraulic gradient. Water-level altitude data outside the model domain, which were used for control, were obtained from tables 1 and 2 in Ciesnik (1995) (shown on fig. 1); those within the model domain are listed in appendix A.

6. Locations of deep boreholes in the vicinity of Yucca Mountain (after Luckey and others, 1996).

7. Location of hydraulic-head observation nodal points for (a) uncased or profusely perforated casing (or unknown casing/perforation) of boreholes; (b) packed-off borehole

8. Observation node numbers and associated hydrogeologic units

9. Three-dimensional finite-element mesh. Top of mesh is the conventional representation of the potentiometric surface shown in figure 5. Value adjacent to color bar represents the hydrogeologic unit number from Table 1 used in the model.

10. Exploded view of hydrogeologic units as captured with the finite-element model mesh oriented (a) north to south; and (b) west to east. The dark areas of the individual units result from the simulated light angle hitting the faces of the tetrahedral elements comprising each of the hydrogeologic units. The hydrogeologic units are represented as discontinuous, irregularly shaped objects, which interlock with their adjacent units in a 3D jig-saw puzzle fashion. The rendered objects appear where they would in the horizontal dimension, and are depicted with shading, which emphasizes the faces of individual tetrahedral elements.

11. Permeability values used in the model. (a) block perspective; (b) fence diagram.

12. Locations of nodes for recharge in upper Fortymile Wash (zone 00079), the north-south

barrier in Solitario Canyon (zone 00062), and the east-west barrier (zone 00061)

13 - 16 . Specified head boundary conditions and nodal distributions for:

13. West face of model (zone 00073)
14. South face of model (zone 00074)
15. East face of model (zone 00075)
16. North face of model (zone 00076)

17. Simulated hydraulic head and residuals. Residuals pertain to simulation sequence number 40 in Appendix B.

18. Simulated hydraulic head compared to measured hydraulic head.

19. Histogram of hydraulic-head residuals

20. Ground-water flow for normalized vectors

LIST OF TABLES

1. Hydrogeologic units, equivalent units, and associated lithologies in the vicinity of Yucca Mountain

2. Largest water-level fluctuations in wells in the vicinity of Yucca Mountain.

3. Hydrologic properties of hydrogeologic unit

4. Summary of saturated-zone temperature data available for wells near Yucca Mountain

5. Results of comparing hydrogeologic framework model unit geometries with 3D finite-element tetrahedral mesh

6. Additional zones defined in the site model.

7. Comparison of ground-water fluxes derived from the regional and site flow model

8. Key model parameters affecting model calibration

APPENDICES

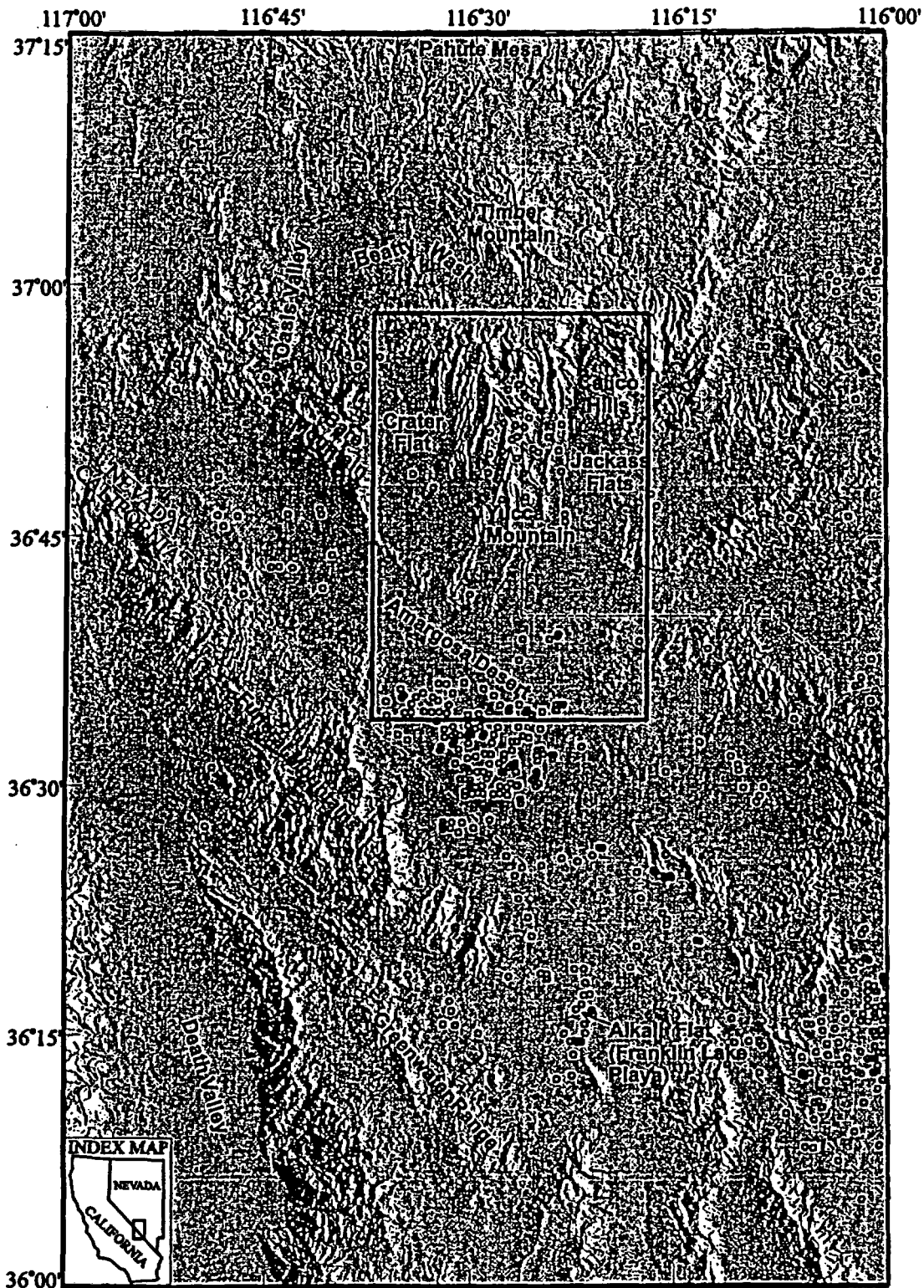
A. Observation-well data used in the construction of the Yucca Mountain site saturated-zone model

B. Supporting information regarding parameter estimation sequence

C. Model-calibration parameter estimates

D. Fixed parameter values used in parameter-estimation runs

E. Comparison between simulated and observed values of hydraulic head



EXPLANATION

- Nevada Test Site Boundary
- . - State-line Boundary
- Model Boundary
- Hydraulic-head observation well

Universal Transverse Mercator projection, Zone 11.
 Shaded-relief base from 1:250,000-scale Digital Elevation Model;
 sun illumination from southeast at 30 degrees above horizon

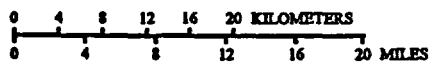
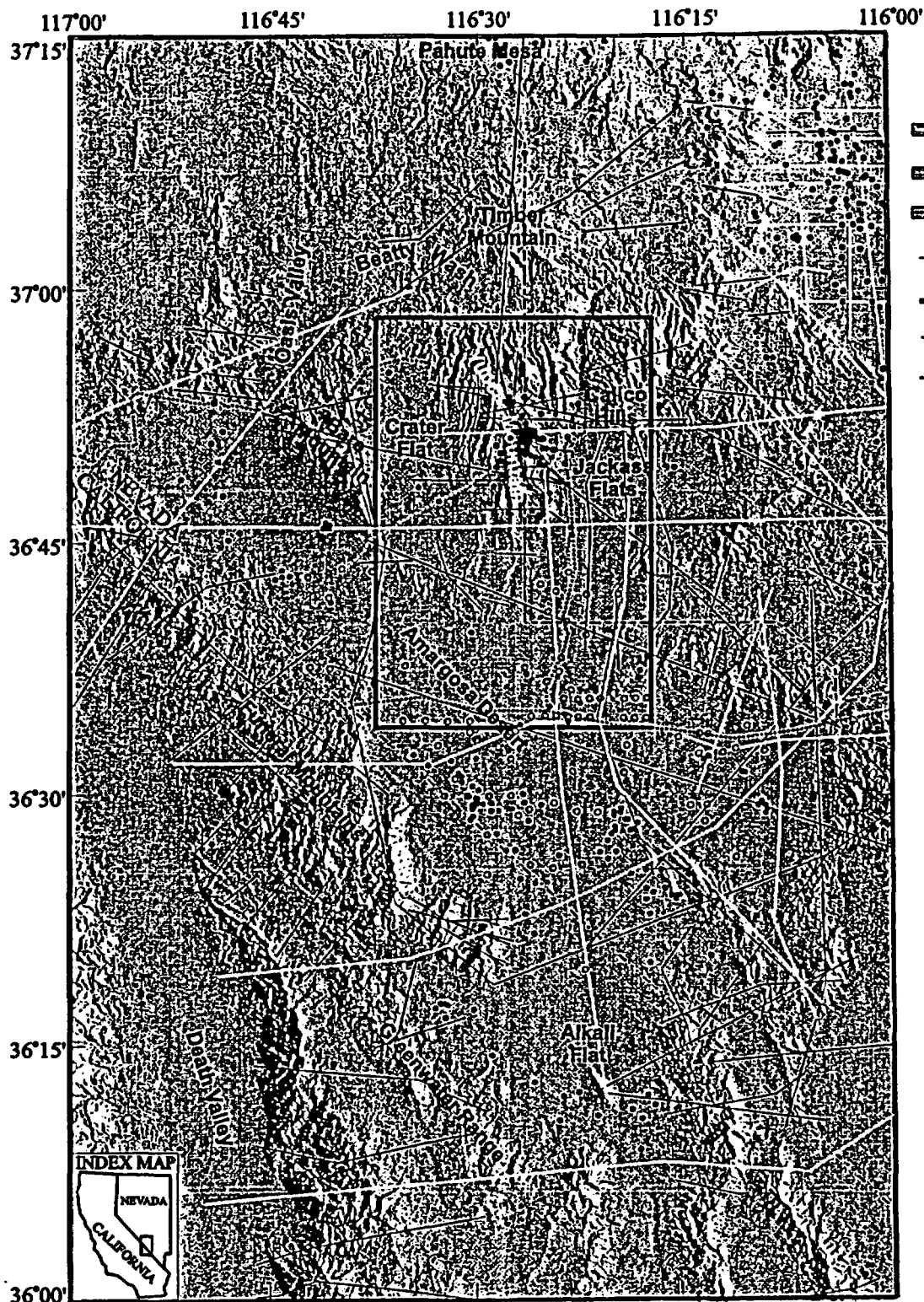


Figure 1. Location map of the study area, associated geographic features, and hydraulic-head observation wells.



EXPLANATION

- Geologic or hydrogeologic sections from Environmental Restoration
- Yucca Mountain seismic line
- Published seismic data
- Geologic or hydrogeologic sections from published geologic maps
- Model Boundary
- Nevada Test Site Boundary
- State-line Boundary
- Lithologic well data
- Resistivity data for Paleozoic top

Universal Transverse Mercator projection, Zone 11.
 Shaded-relief base from 1:250,000-scale Digital Elevation Model;
 sun illumination from southeast at 30 degrees above horizon

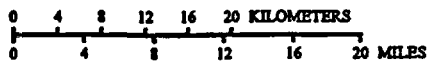


Figure 2. Geologic, geophysical, and well-data locations used in the construction of the hydrogeologic framework model .

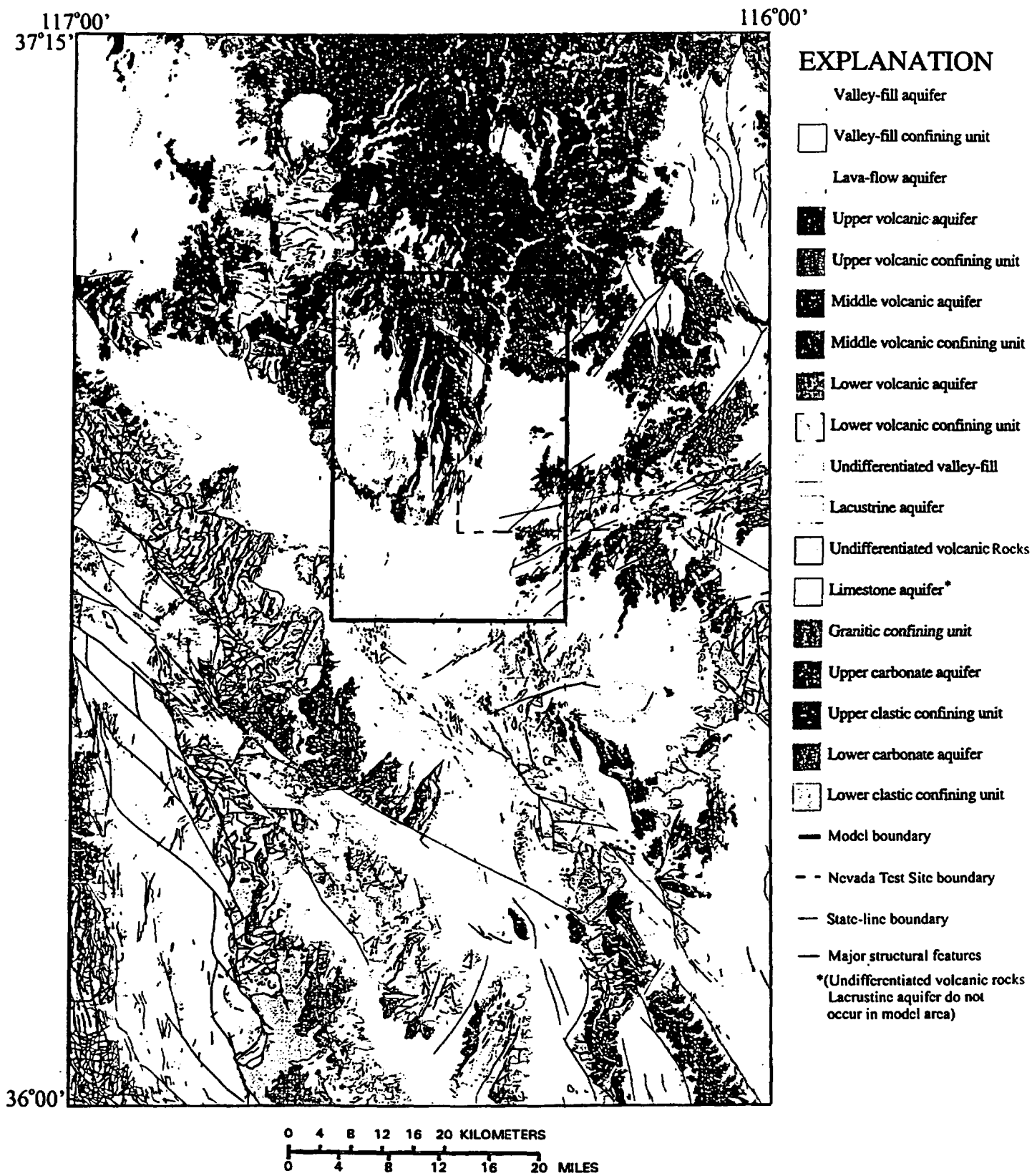


Figure 3(a). Generalized hydrogeologic units with major structural features for region surrounding the area of the site model.

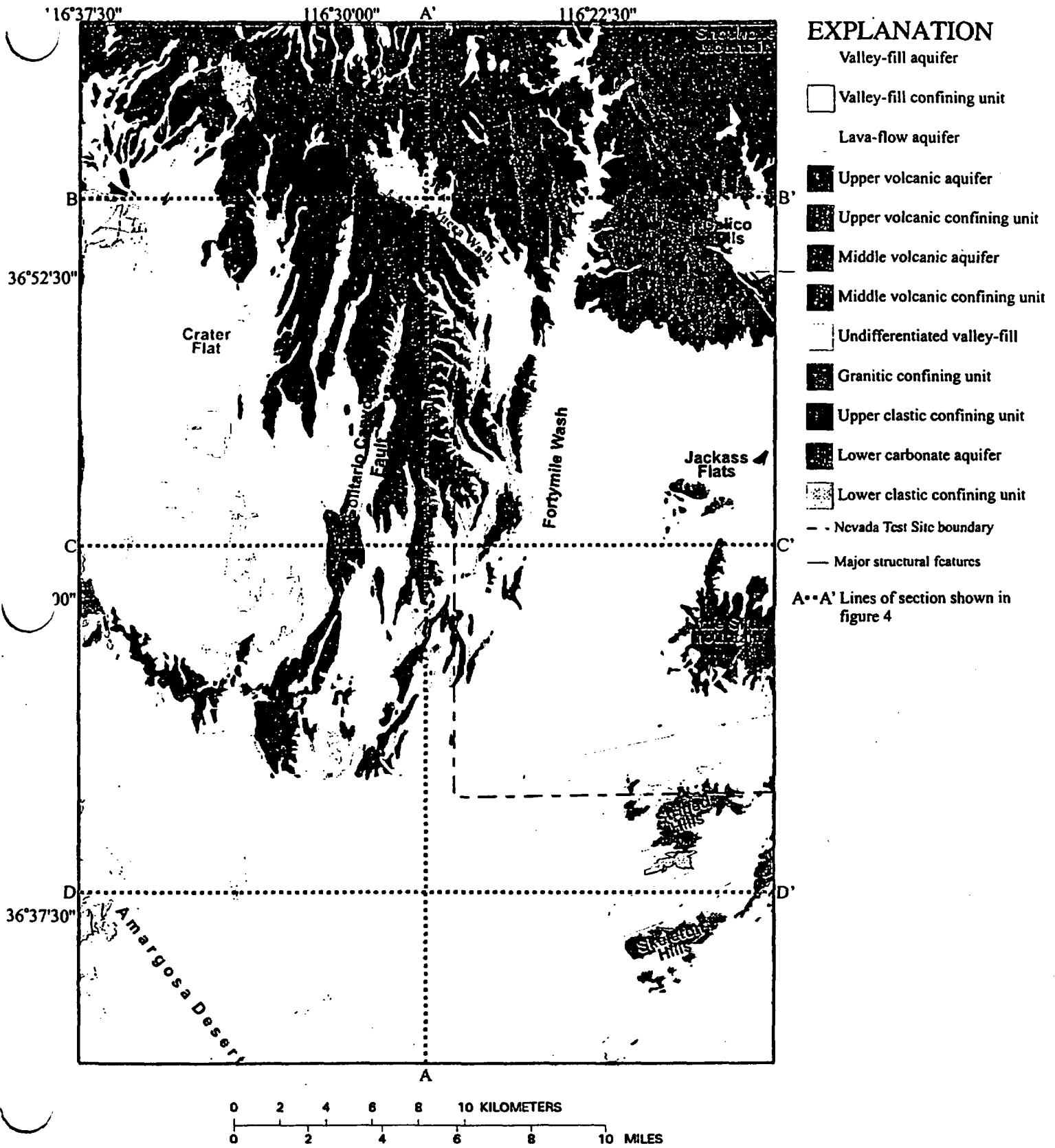
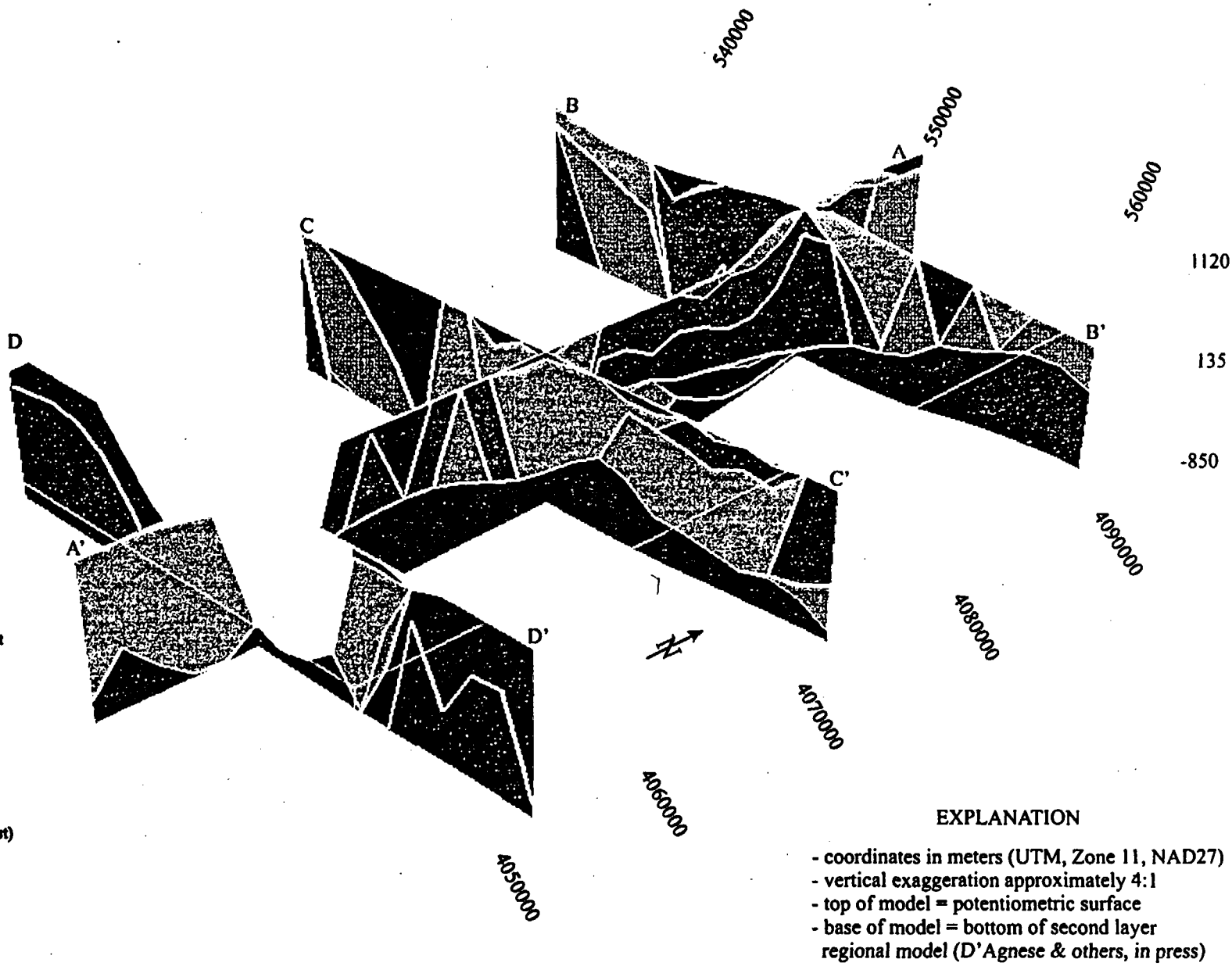


Figure 3(b). Generalized hydrogeologic units with major structural features and lines of section specific to the site model area (limestone aquifer, lower volcanic aquifer, and lower volcanic confining unit do not appear at the land surface).

Explanation color and model unit number

19	Valley-fill aquifer
8	Valley-fill confining unit
17	Limestone aquifer
16	Lava-flow aquifer
15	Upper volcanic aquifer
14	Upper volcanic confining unit
13	Middle volcanic aquifer
12	Middle volcanic confining unit
11	Lower volcanic aquifer
10	Lower volcanic confining unit
9	Undifferentiated valley fill
8	Upper carbonate aquifer
7	Lower carbonate aquifer (thrust)
6	Upper clastic confining unit
5	Lower carbonate aquifer
4	Lower clastic confining unit
3	Lower carbonate aquifer (thrust)
2	Granitic confining unit



EXPLANATION

- coordinates in meters (UTM, Zone 11, NAD27)
- vertical exaggeration approximately 4:1
- top of model = potentiometric surface
- base of model = bottom of second layer regional model (D'Agnes & others, in press)

Figure 4. Fence diagram showing sections along lines shown on figure 3(b) with 1.5 kilometer geologic grid spacing.

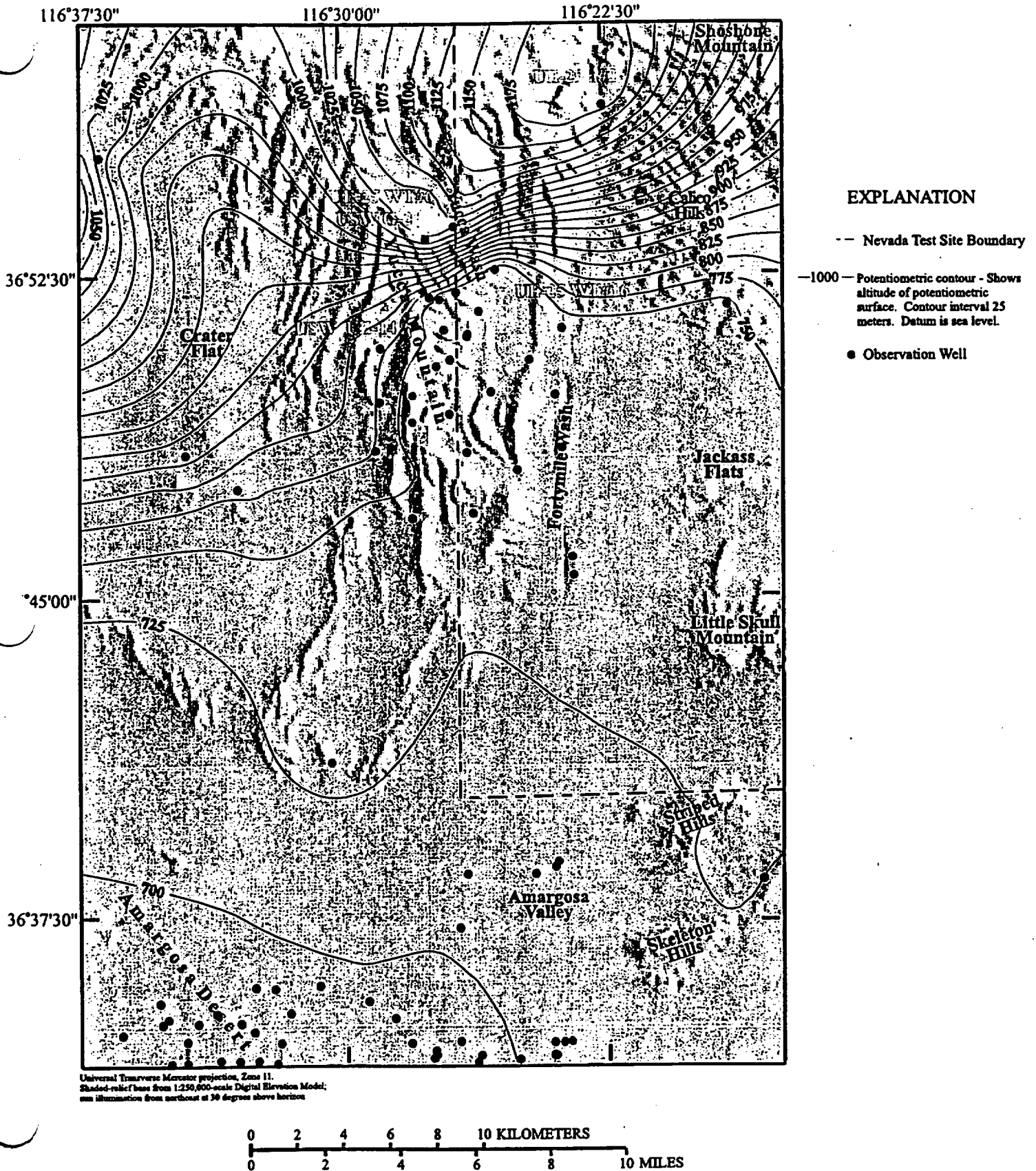


Figure 5. Potentiometric surface that includes the large hydraulic gradient. Water-level altitude data outside the model domain, which were used for control, were obtained from tables 1 and 2 in Ciesnik (1995) (shown on figure 1); those within the model domain are listed in appendix A.

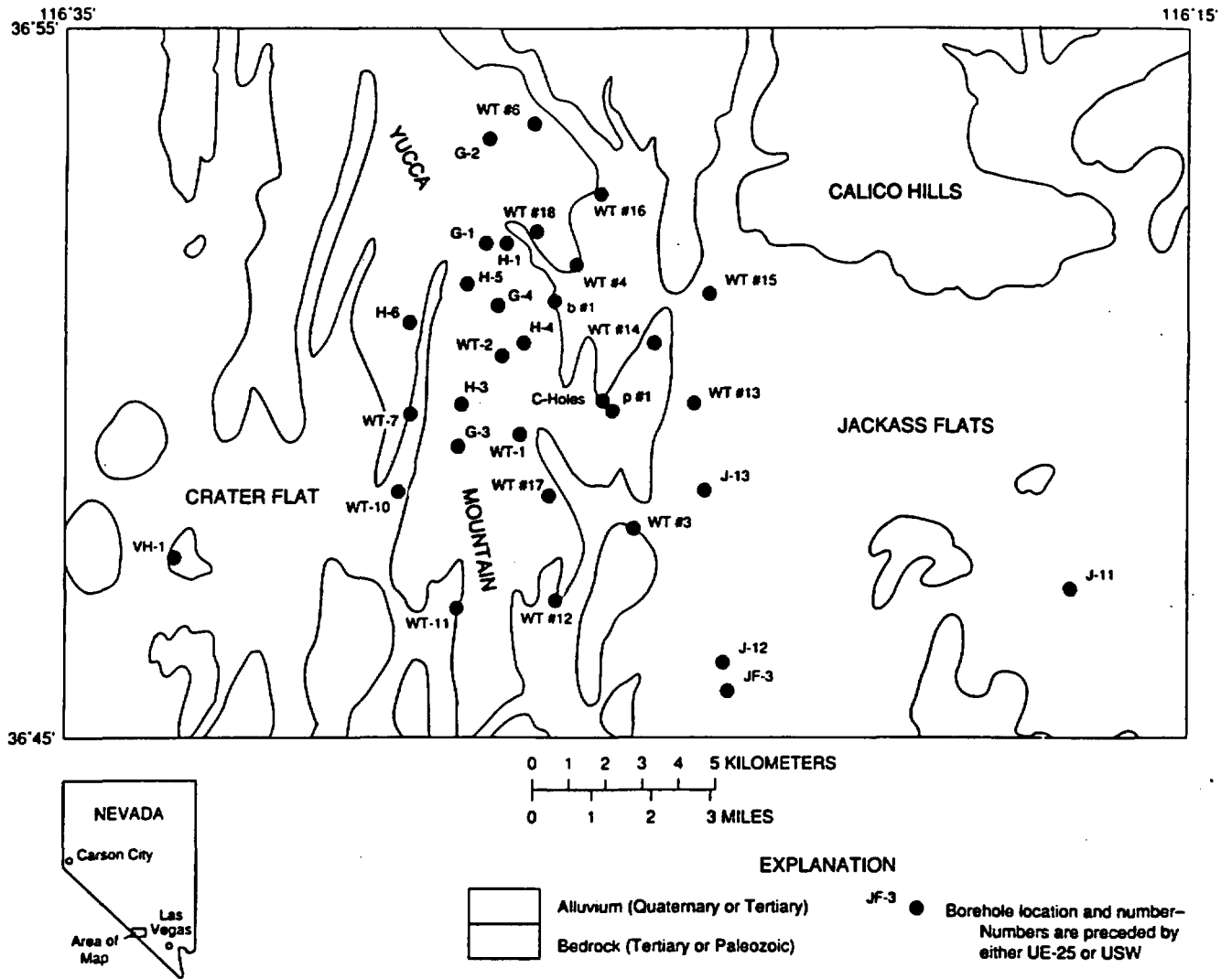


Figure 6. Locations of deep boreholes in the vicinity of Yucca Mountain (from Luckey and others, 1996).

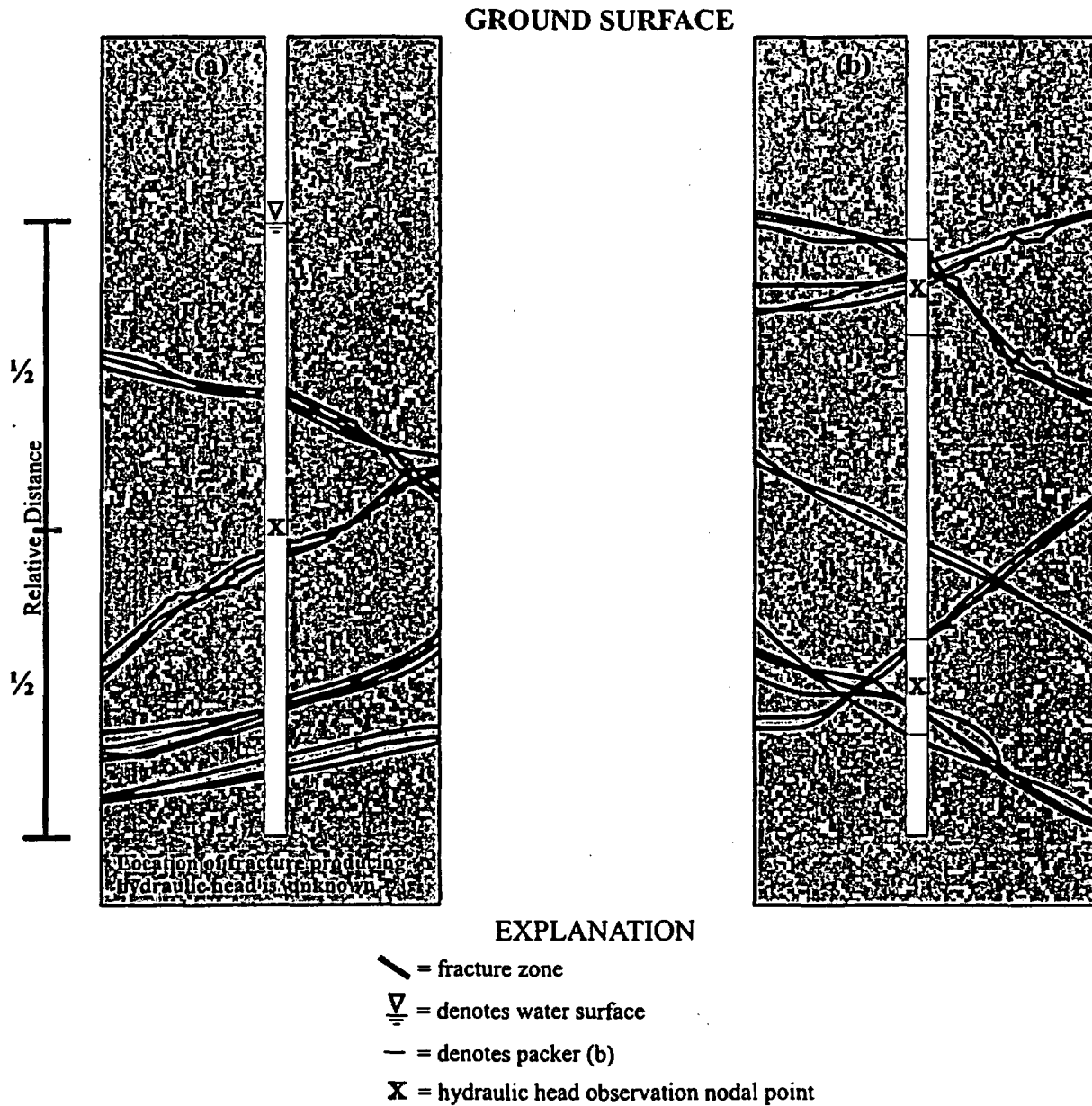


Figure 7. Location of hydraulic-head observation nodal points for (a) uncased or profusely perforated casing (or unknown casing/perforation) of boreholes; (b) packed-off borehole.

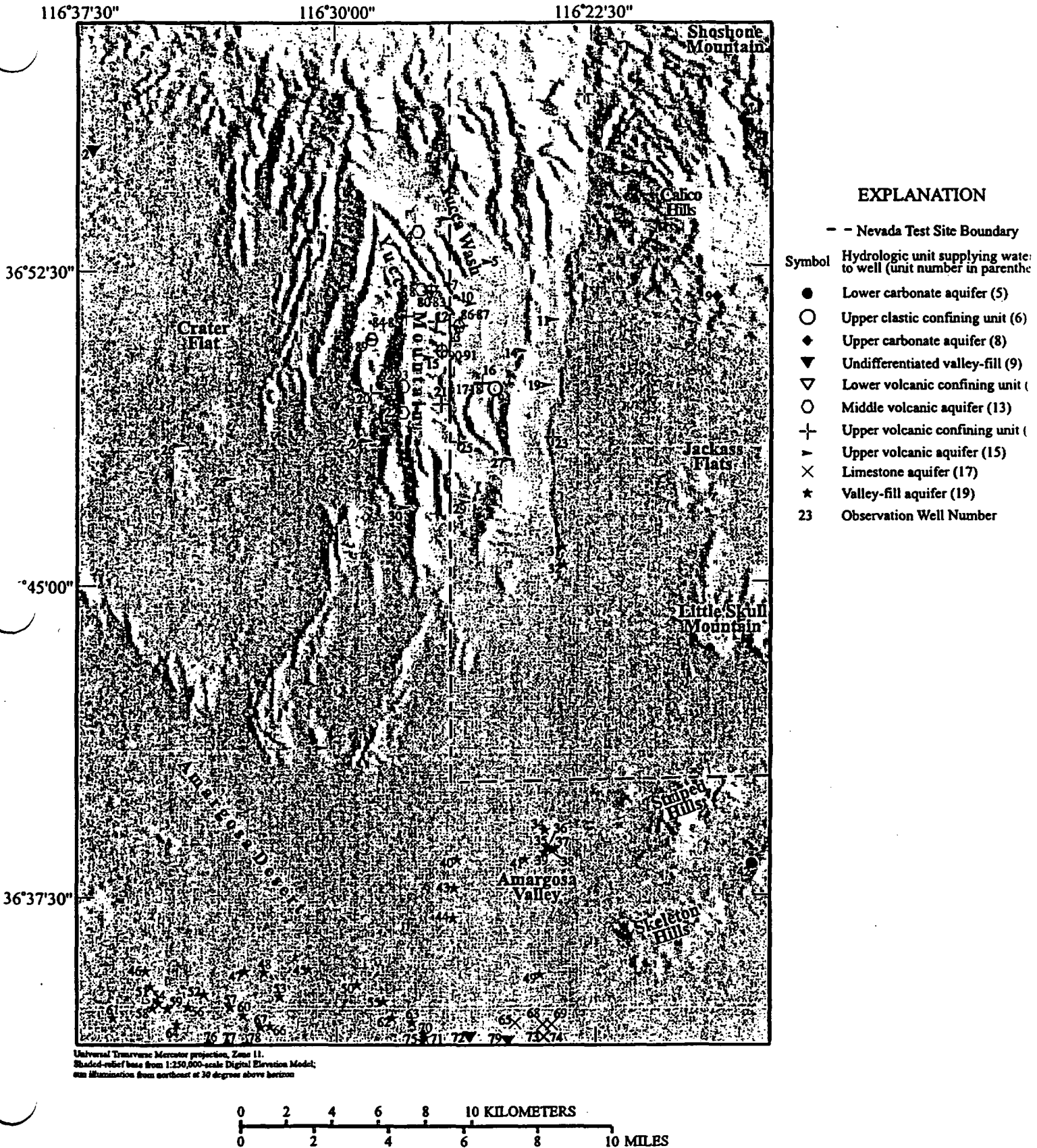


Figure 8. Observation node numbers and associated hydrogeologic units.

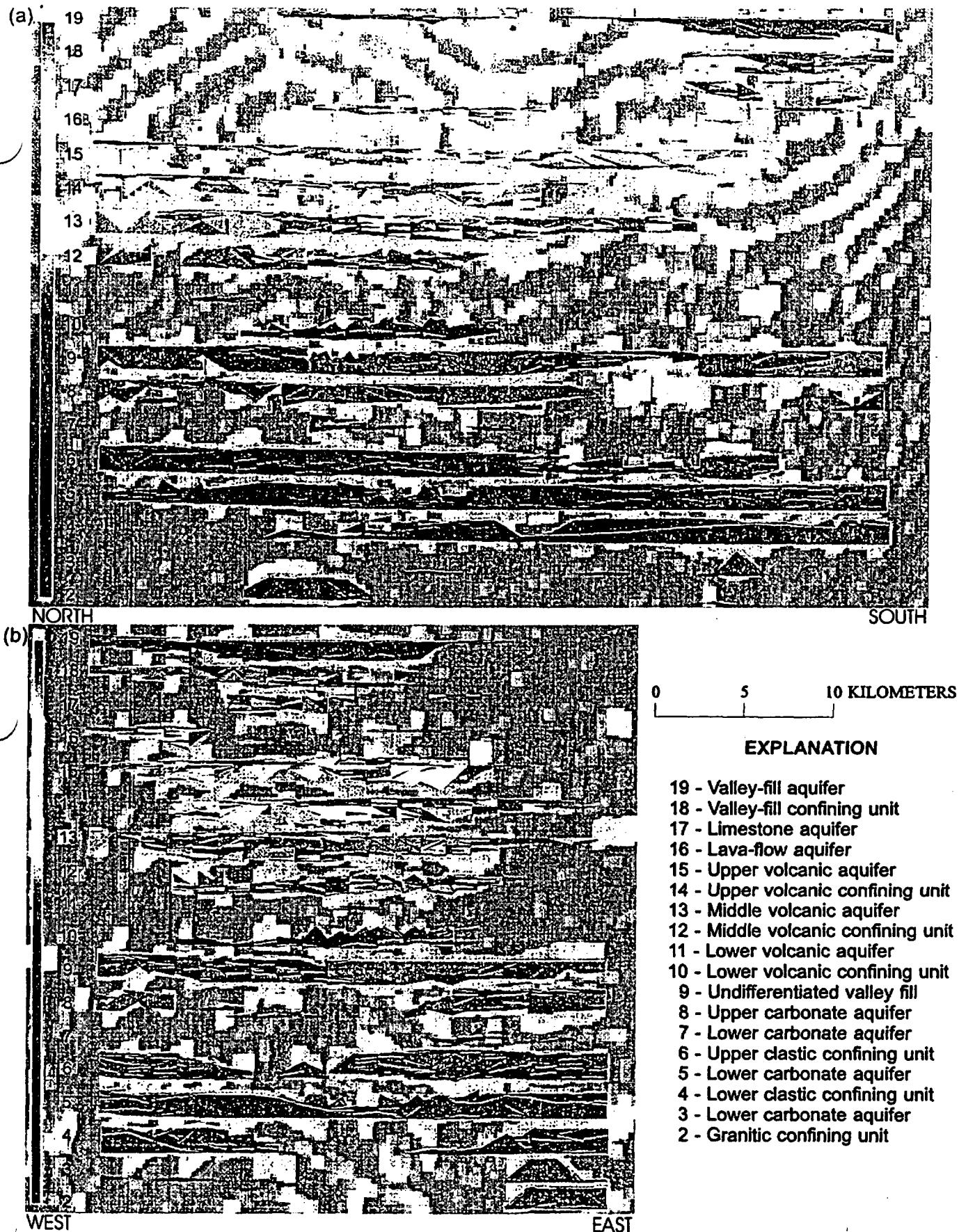


Figure 10. Exploded view of hydrogeologic units as captured with the finite-element model mesh oriented (a) north to south; and (b) west to east. The dark areas of the individual units result from the simulated light angle hitting the faces of the tetrahedral elements comprising each of the hydrogeologic units. The hydrogeologic units are represented as discontinuous, irregularly shaped objects, which interlock with their adjacent units in a 3-dimensional jig-saw puzzle fashion. The rendered objects appear where they would in the horizontal dimension, and are depicted with shading, which emphasizes the faces of individual tetrahedral elements.

(a)

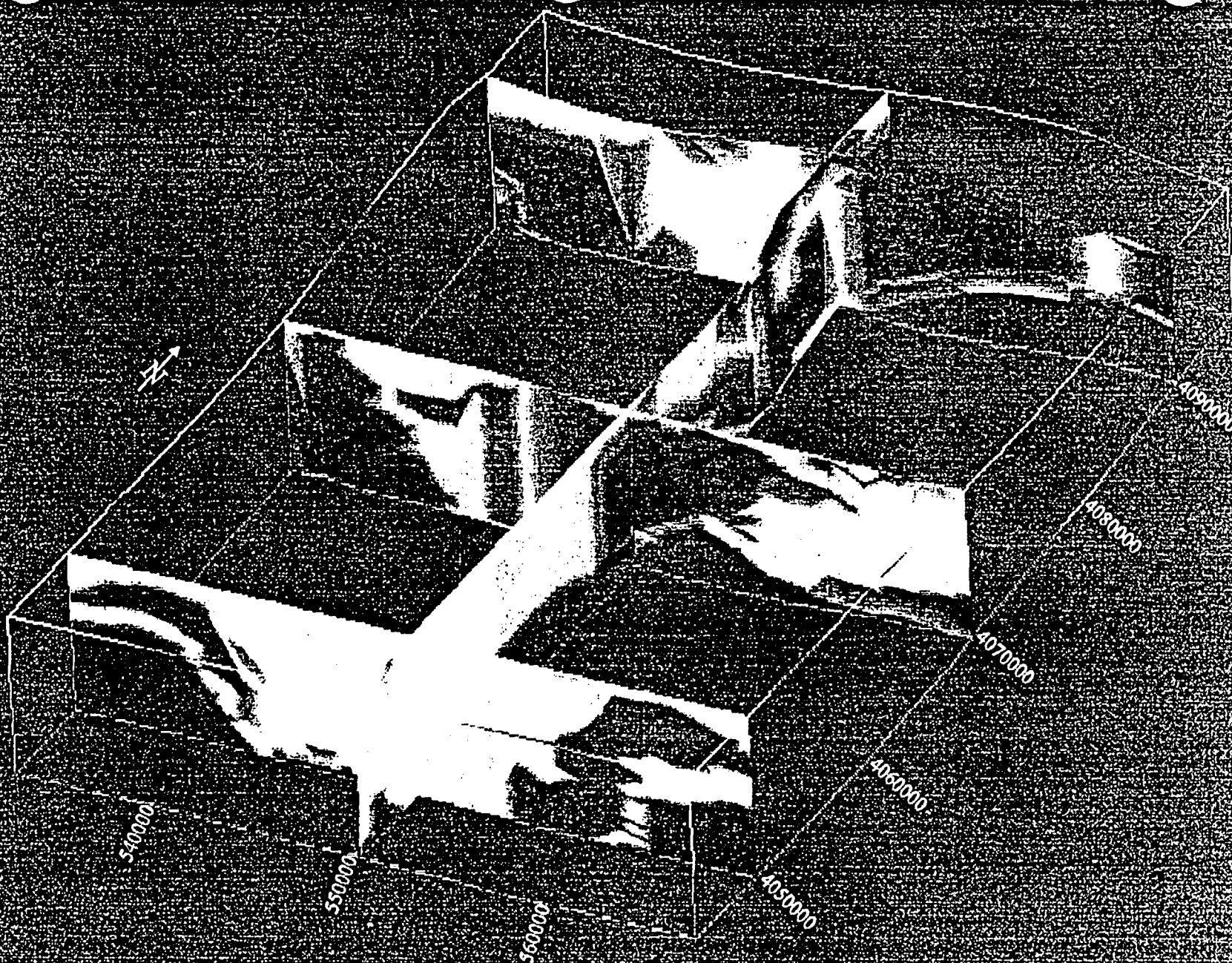
Log of
Permeability
(meters squared)



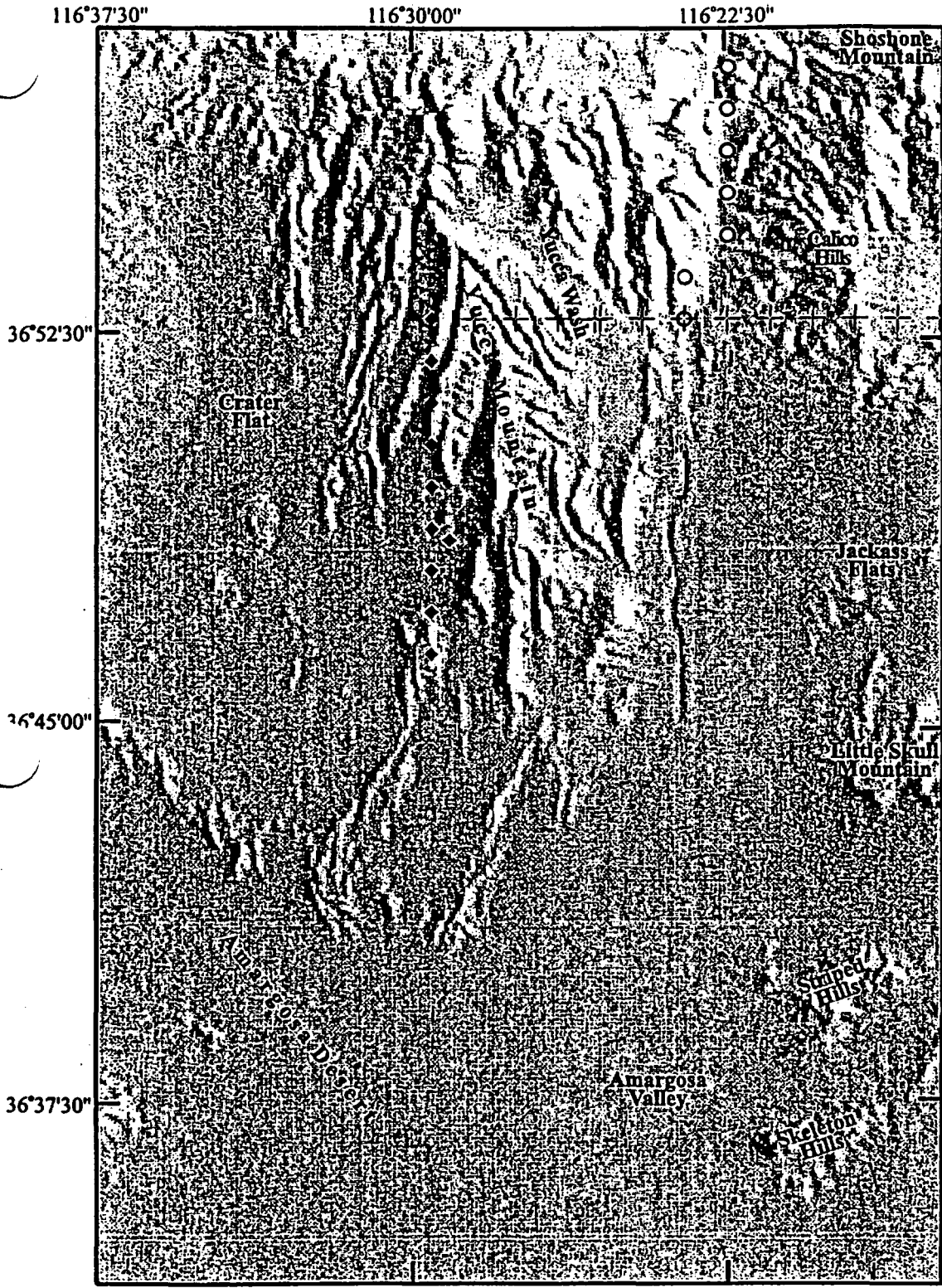
- coordinates in meters (UTM; Zone 11, NAD 27)
- vertical exaggeration approximately 5:1
- - denotes approximate section lines

(b)

Log of
Permeability
(meters squared)



- coordinates in meters (UTM, Zone 11, NAD 21)
- vertical exaggeration approximately 35:1



EXPLANATION

- Fortymile Wash recharge nodes (fm, zone 00079)
- ◆ Solitario Canyon barrier nodes (lkns, zone 00062)
- ⊕ East-West barrier nodes (lkew, zone 00061)

Universal Transverse Mercator projection, Zone 11.
 Shaded-relief base from 1:250,000-scale Digital Elevation Model;
 sun illumination from northeast at 30 degrees above horizon.

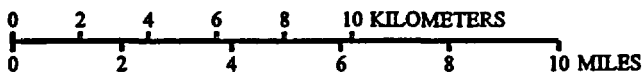


Figure 12. Locations of nodes for recharge in upper Fortymile Wash (zone 00079), the north-south barrier in Solitario Canyon (zone 00062), and the east-west barrier (zone 00061).

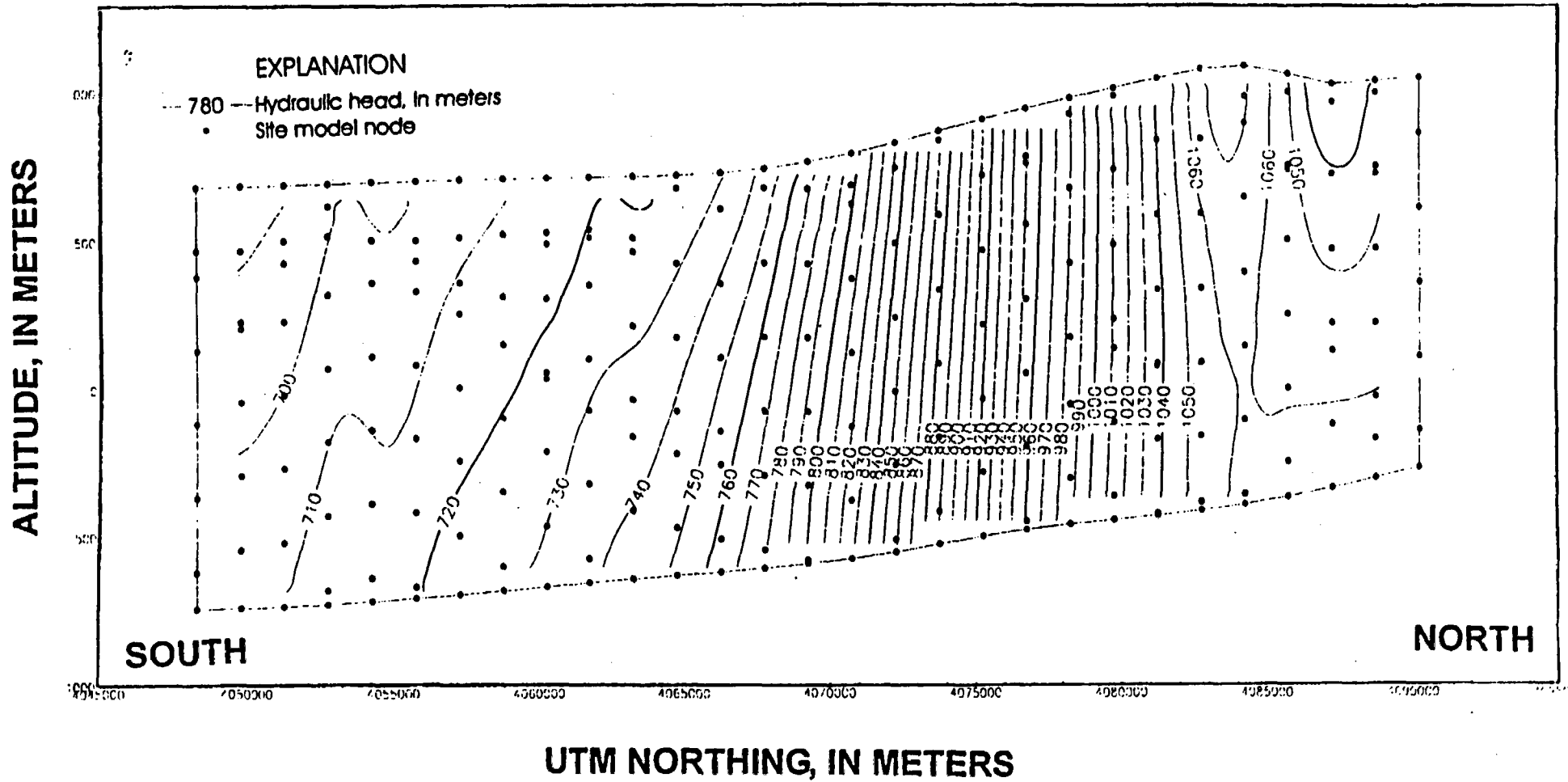


Figure 13. Specified head boundary conditions and nodal distributions for west face of model (zone 00073).

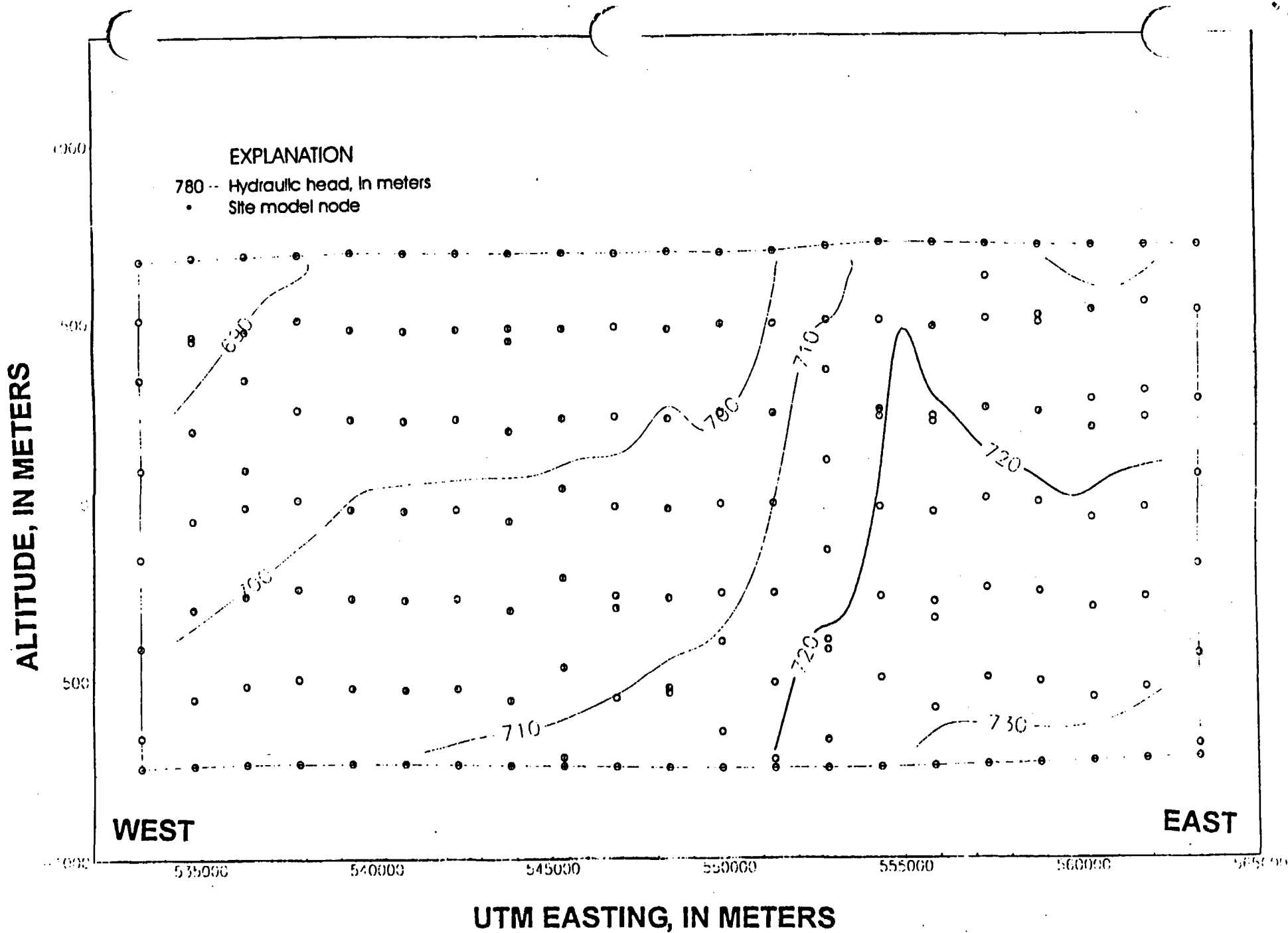


Figure 14. Specified head boundary conditions and nodal distributions for south face of model (zone 00074).

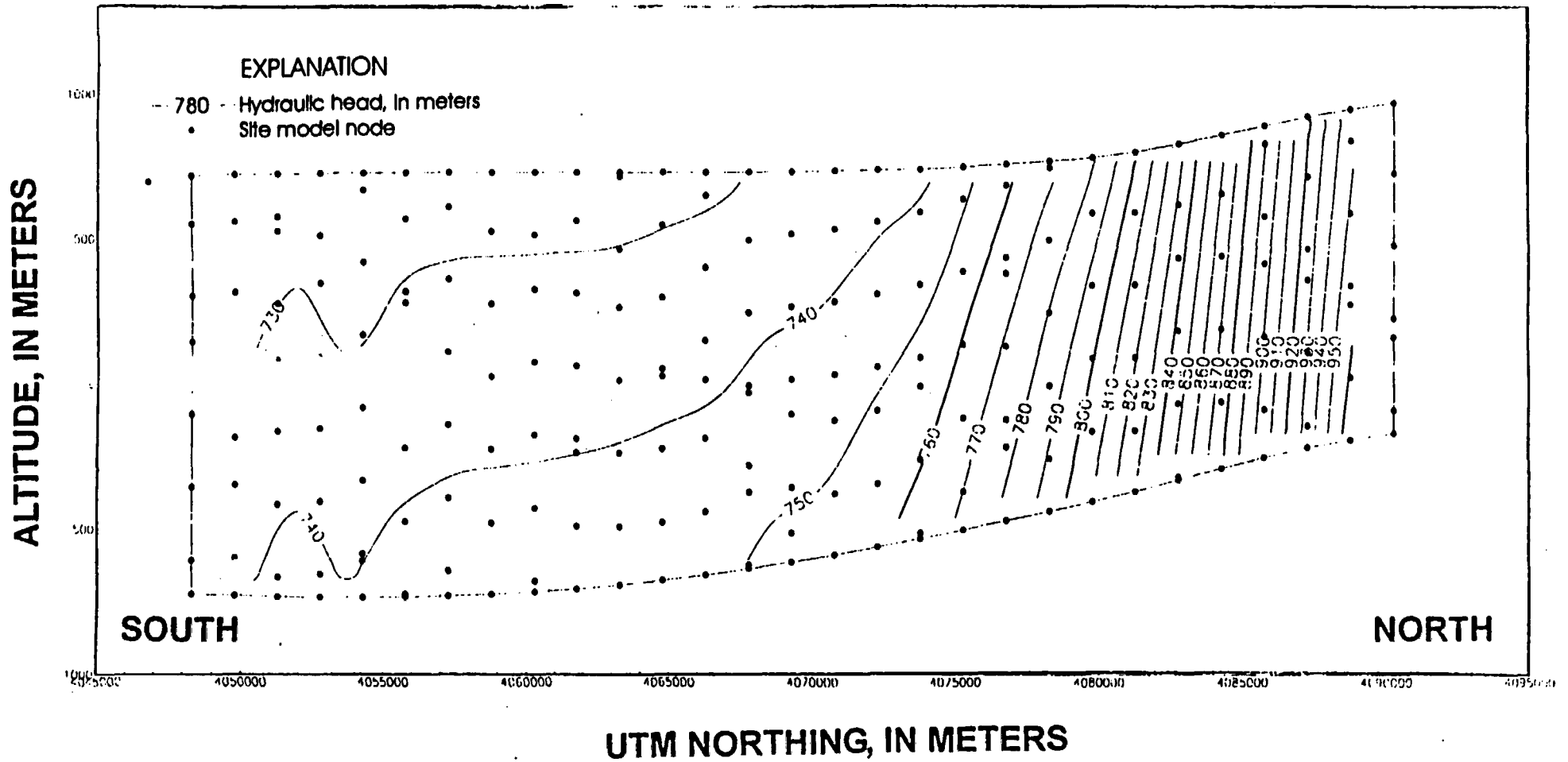


Figure 15. Specified head boundary conditions and nodal distributions for east face of model (zone 00075).

ALTITUDE, IN METERS

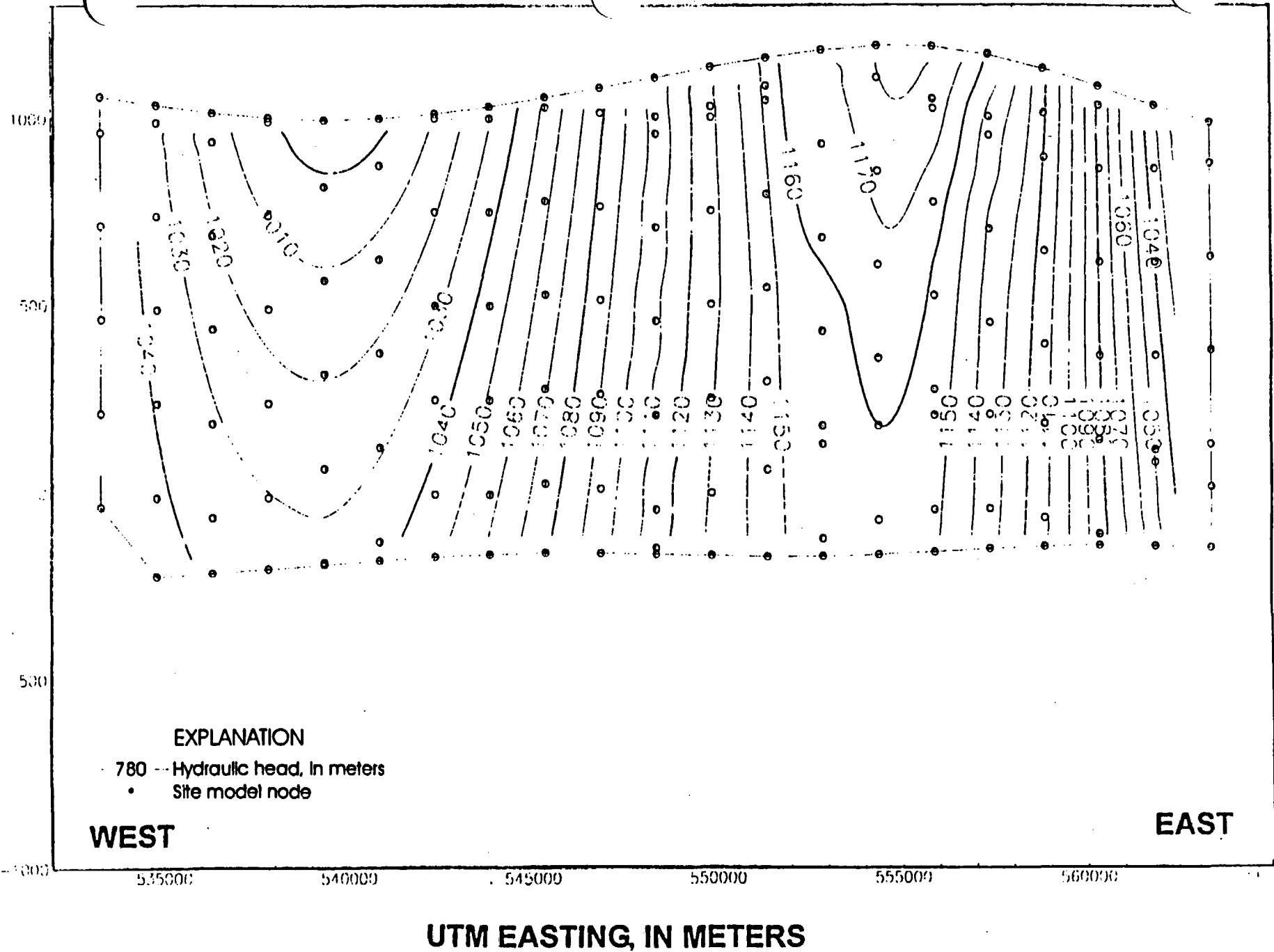


Figure 16. Specified head boundary conditions and nodal distributions for north face of model (zone 00076).

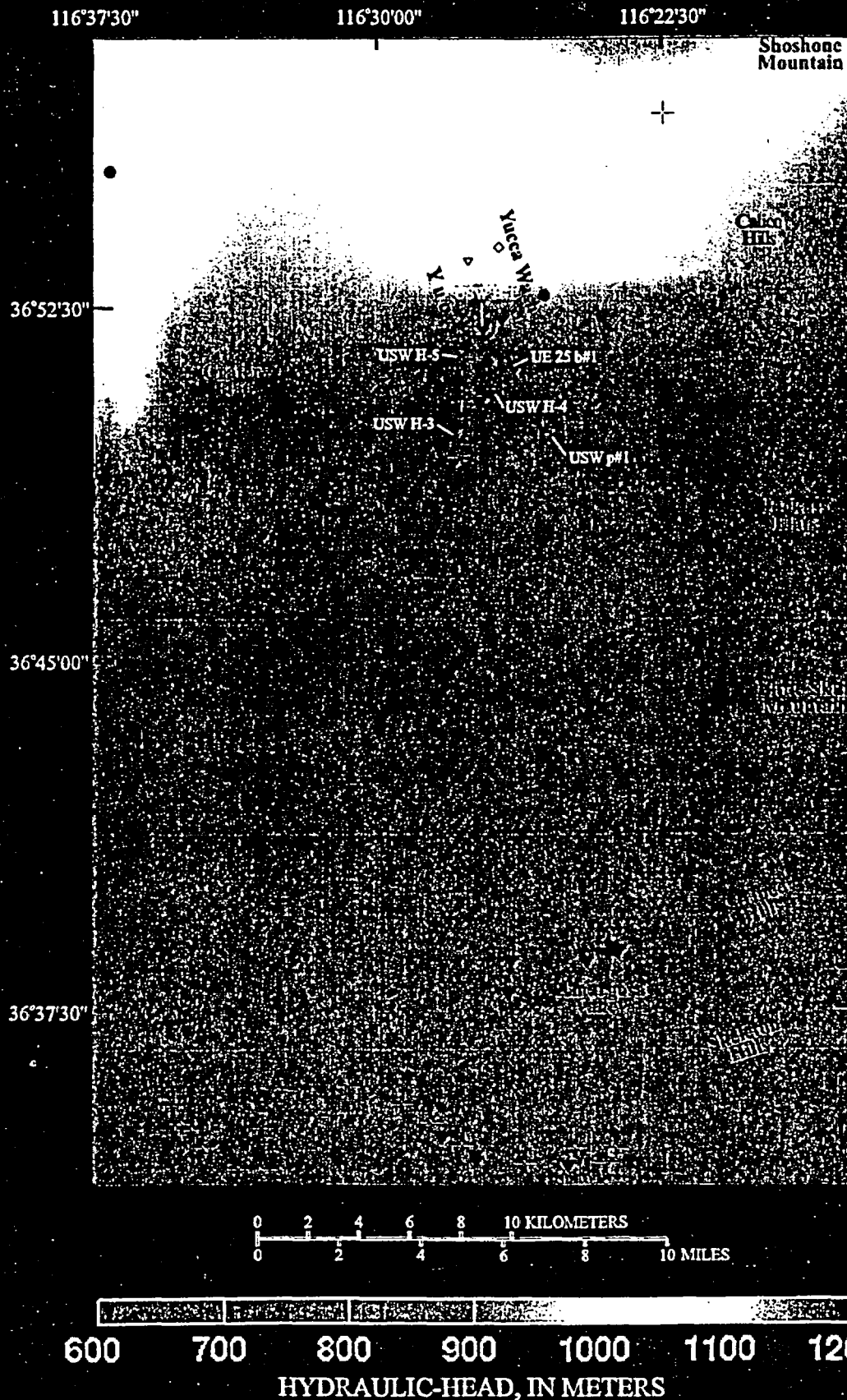


Figure 17. Simulated hydraulic head and residuals. Residuals (the difference between observed and simulated hydraulic-head values) pertain to simulation sequence number 40 in appendix B.

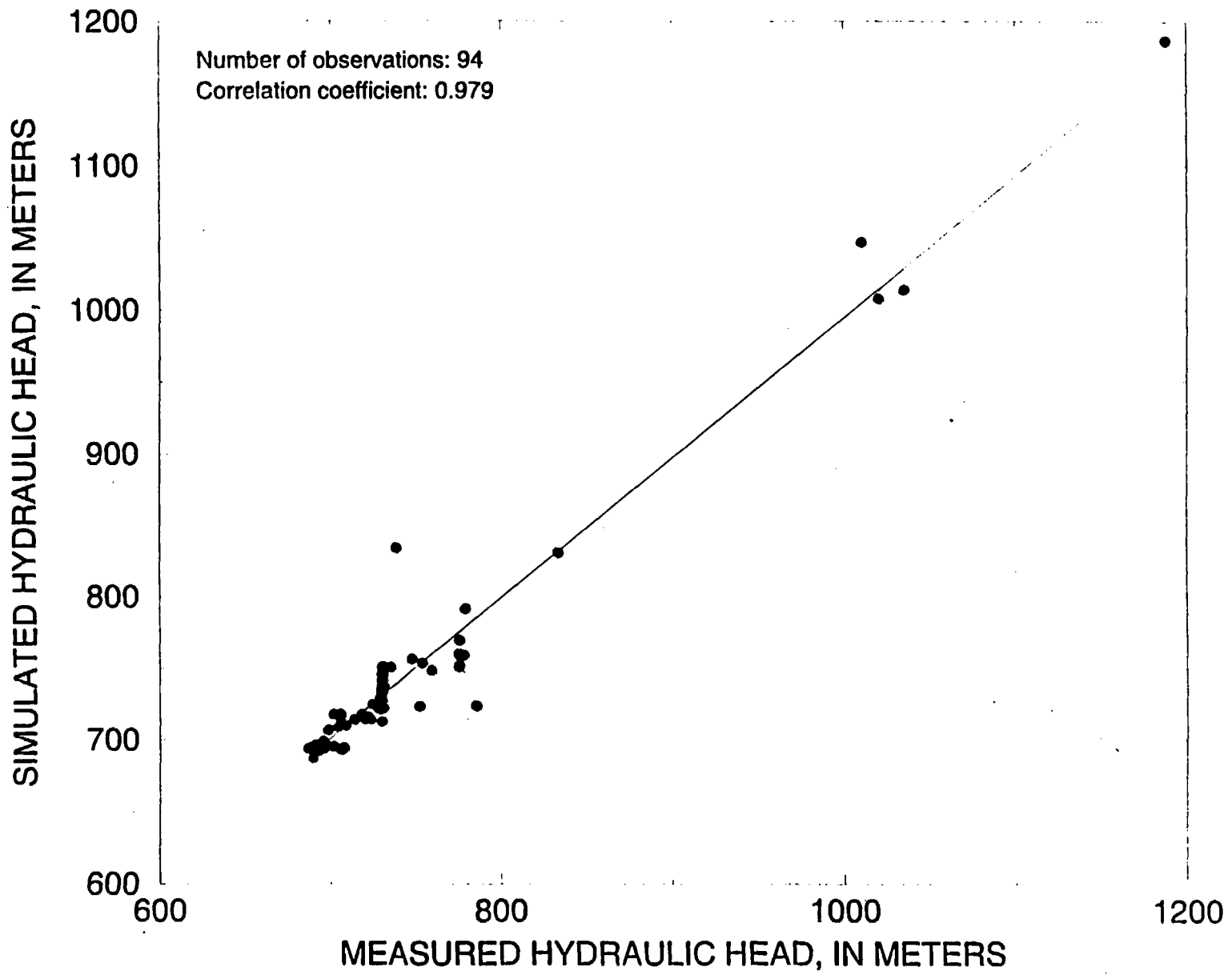


Figure 18. Simulated hydraulic head as a function of measured hydraulic head.

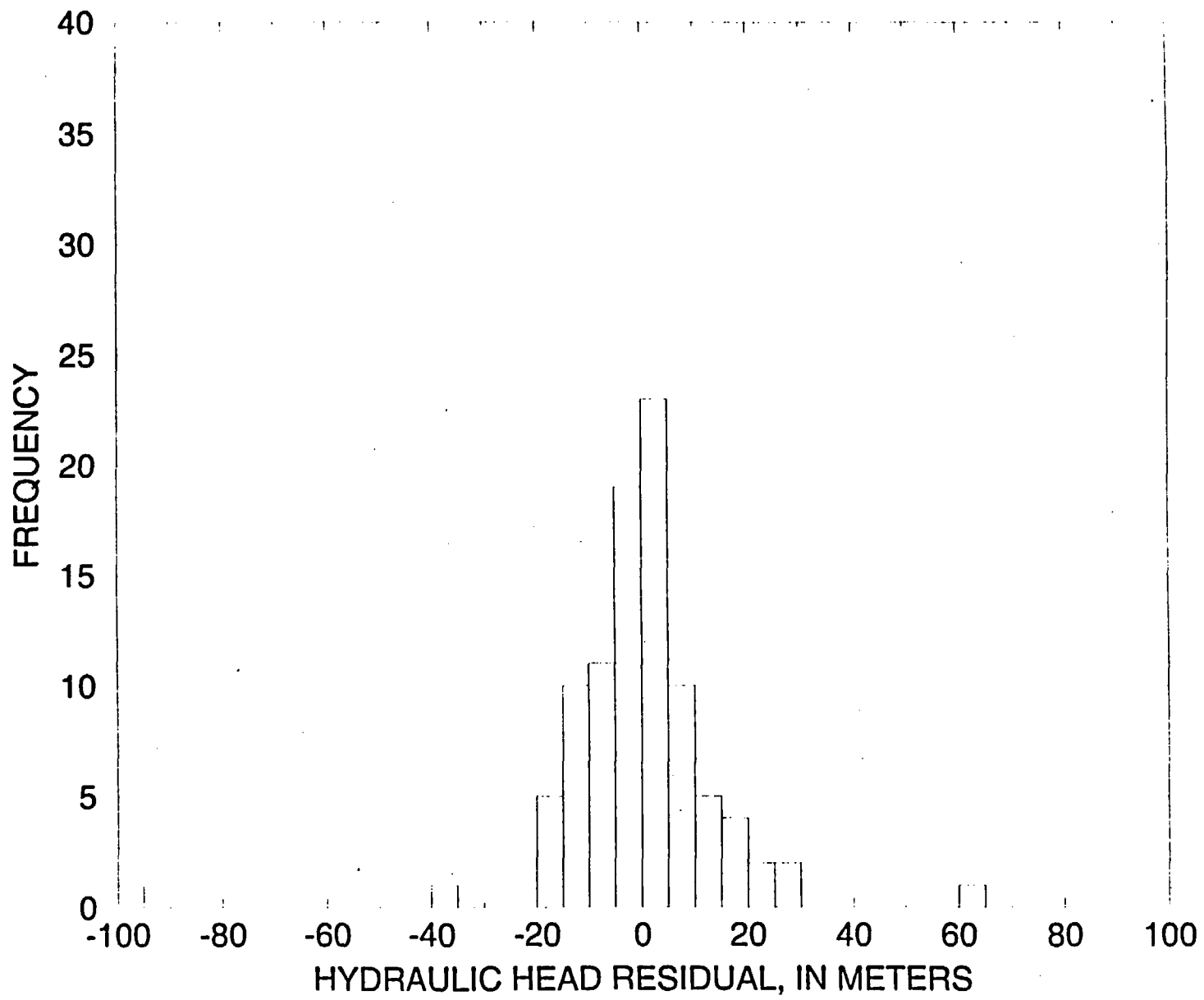


Figure 19. Histogram of hydraulic-head residuals.

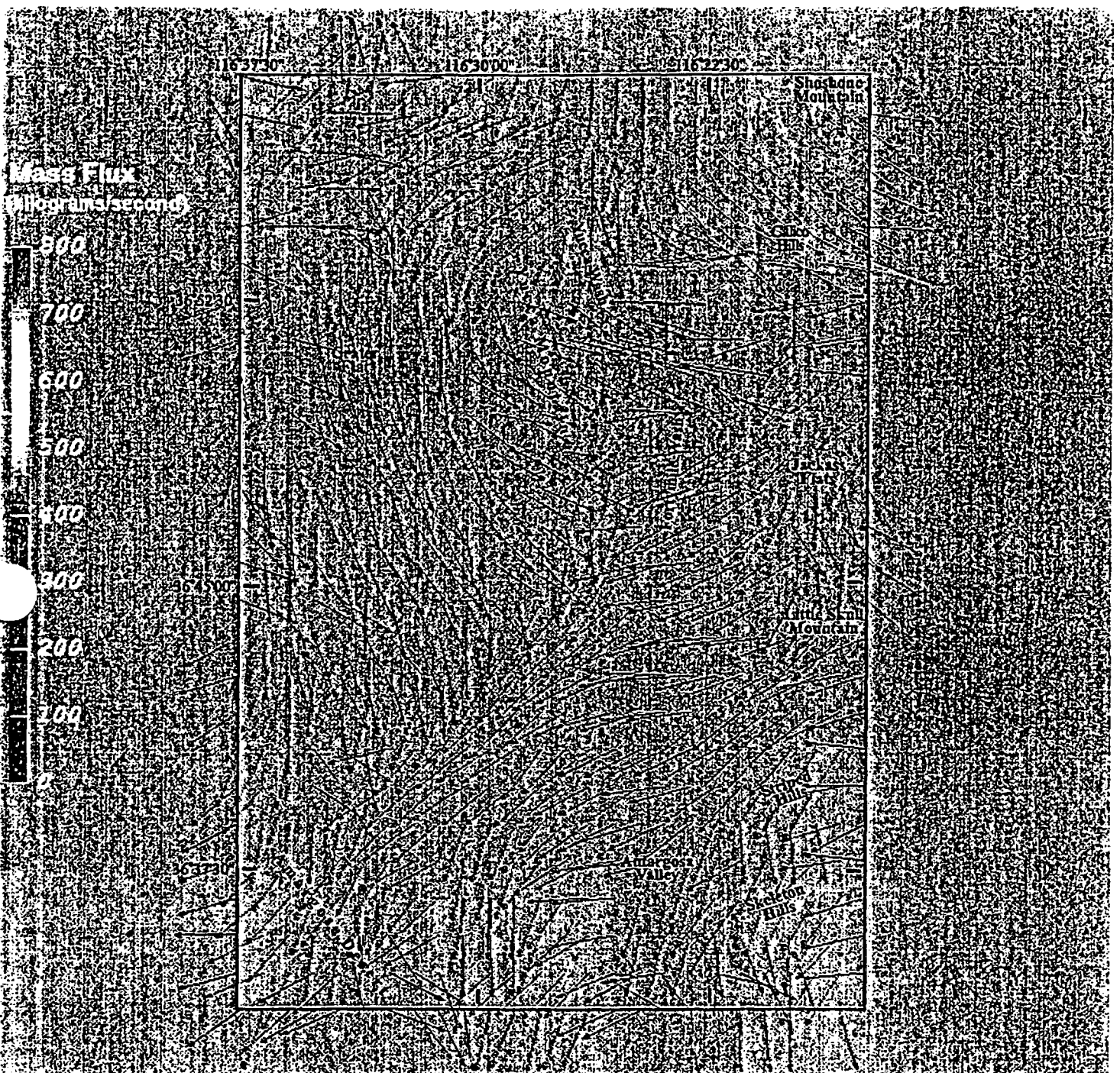


Figure 20. Ground-water flow for normalized vectors.

Appendix A: Observation-well data used in the construction of the Yucca Mountain site saturated-zone model

[well names are those contained in the USGS Ground-Water Site Inventory data base;
midpoint of water column is midpoint of packed off interval for multiply completed wells]

Observation Number	Well Name	Latitude	Longitude	Measuring point altitude (meters)	Altitude of midpoint of water column (meters)	Hydraulic head (meters)	Date of Measurement
1	UE-29a #2	36°56'29"	116°22'26"	1215.39	1024.05	1187.80	02/19/84
2	GEXA Well 4	36°55'20"	116°37'03"	1198.14	860.25	1010.05	03/14/96
3	UE-25 WT 6	36°53'40"	116°26'46"	1314.79	988.57	1034.52	12/04/95
4	USW G-2	36°53'22"	116°27'35"	1553.90	371.53	1019.79	12/11/95
5	UE-25 WT #16	36°52'39"	116°25'34"	1210.91	719.59	738.51	12/04/95
6	USW UZ-14	36°52'08"	116°27'40"	1349.11	724.77	778.43	12/16/96
7	UE-25 WT#18	36°52'07"	116°26'42"	1336.40	721.83	730.26	08/30/95
8	USW G-1	36°52'00"	116°27'29"	1325.91	125.65	754.20	03/23/82
9	UE-25a 3	36°51'47"	116°18'53"	1385.62	681.46	748.28	12/19/79
10	UE-25 WT#4	36°51'40"	116°26'03"	1169.21	711.21	730.84	12/05/95
11	UE-25 WT #15	36°51'16"	116°23'38"	1083.20	698.91	729.15	12/10/96
12	USW G-4	36°51'14"	116°27'04"	1269.49	542.16	730.15	01/26/90
13	UE-25a #1	36°51'05"	116°26'24"	1199.21	583.94	730.97	04/29/85
14	UE-25 WT #14	36°50'32"	116°24'35"	1076.40	704.61	729.98	12/04/95

Appendix A: Observation-well data used in the construction of the Yucca Mountain site saturated-zone model

[well names are those contained in the USGS Ground-Water Site Inventory data base;
midpoint of water column is midpoint of packed off interval for multiply completed wells]

Observation Number	Well Name	Latitude	Longitude	Measuring point altitude (meters)	Altitude of midpoint of water column (meters)	Hydraulic head (meters)	Date of Measurement
15	USW WT#2	36°50'23"	116°27'18"	1301.31	705.16	730.81	12/12/95
16	UE-25c 1 IITII	36°49'47"	116°25'43"	1130.59	479.08	730.09	04/20/84
17	UE-25c 3 IITII	36°49'47"	116°25'43"	1132.30	474.05	730.19	07/13/95
18	UE-25c 2 IITII	36°49'45"	116°25'43"	1132.21	473.65	730.06	01/09/95
19	UE-25 WT #13	36°49'43"	116°23'51"	1032.51	704.06	729.18	12/09/96
20	USW WT#7	36°49'33"	116°28'57"	1196.89	745.78	775.96	12/06/95
21	USW WT# 1	36°49'16"	116°26'56"	1201.40	712.27	730.64	12/12/95
22	USW G-3	36°49'05"	116°28'01"	1480.51	339.02	730.52	06/27/95
23	J-13 WW	36°48'28"	116°23'40"	1011.30	338.19	728.22	12/16/96
24	USW WT#10	36°48'25"	116°29'05"	1123.40	748.36	775.97	12/06/95
25	UE-25 WT #17	36°48'22"	116°26'26"	1124.01	717.00	729.40	06/28/95
26	USW VH-2	36°48'21"	116°34'37"	974.45	294.21	833.17	03/10/85
27	UE-25 WT #3	36°47'57"	116°24'58"	1030.01	708.39	729.66	12/12/95
28	USW VH-1	36°47'32"	116°33'07"	963.50	490.33	779.46	12/17/96
29	UE-25 WT #12	36°46'56"	116°26'16"	1074.69	709.40	729.37	12/13/95

Appendix A: Observation-well data used in the construction of the Yucca Mountain site saturated-zone model

[well names are those contained in the USGS Ground-Water Site Inventory data base;
midpoint of water column is midpoint of packed off interval for multiply completed wells]

Observation Number	Well Name	Latitude	Longitude	Measuring point altitude (meters)	Altitude of midpoint of water column (meters)	Hydraulic head (meters)	Date of Measurement
30	USW WT#11	36°46'49"	116°28'02"	1094.11	704.37	730.68	12/06/95
31	J-12 WW	36°45'54"	116°23'24"	953.54	666.86	727.34	12/05/83
32	JF- 3 Well	36°45'28"	116°23'22"	944.36	662.65	727.80	12/12/96
33	Cind-R-Lite Well	36°41'05"	116°30'26"	830.76	710.18	729.81	12/17/96
34		36°39'07"	116°23'57"	819.91	697.38	718.41	05/20/61
35		36°38'42"	116°23'53"	811.38	676.85	705.40	09/12/90
36		36°38'40"	116°23'50"	813.82	681.99	704.09	02/28/55
37		36°38'40"	116°23'40"	810.77	697.99	705.61	05/03/52
38		36°38'38"	116°23'45"	811.38	679.25	701.65	03/08/55
39	NDOT Well	36°38'35"	116°23'58"	809.79	682.20	705.48	12/16/96
40		36°38'25"	116°26'32"	795.53	663.61	705.44	01/15/87
41	Airport Well	36°38'25"	116°24'33"	804.31	640.53	705.36	12/16/96
42	TW-5	36°38'15"	116°17'59"	931.47	706.30	724.96	12/16/96
43		36°37'44"	116°26'37"	783.95	669.13	706.10	07/12/62
44		36°37'01"	116°26'40"	774.19	671.93	704.39	10/18/58

Appendix A: Observation-well data used in the construction of the Yucca Mountain site saturated-zone model

[well names are those contained in the USGS Ground-Water Site Inventory data base;
midpoint of water column is midpoint of packed off interval for multiply completed wells]

Observation Number	Well Name	Latitude	Longitude	Measuring point altitude (meters)	Altitude of midpoint of water column (meters)	Hydraulic head (meters)	Date of Measurement
45		36°35'49"	116°30'50"	742.19	639.29	695.81	01/07/87
46		36°35'48"	116°35'37"	731.82	674.83	694.03	01/05/60
47		36°35'47"	116°32'43"	735.18	676.37	693.76	01/07/87
48		36°35'45"	116°32'09"	737.01	664.79	693.76	01/08/87
49		36°35'40"	116°24'08"	771.14	699.30	722.25	03/13/73
50		36°35'27"	116°29'25"	744.02	667.13	696.93	01/16/87
51	Davidson Well	36°35'26"	116°35'29"	730.09	673.46	689.98	12/18/96
52		36°35'15"	116°33'55"	740.66	677.24	707.68	07/02/62
53		36°35'11"	116°31'42"	733.65	649.12	693.22	01/07/87
54		36°35'03"	116°35'15"	727.86	684.02	690.46	01/07/87
55		36°35'03"	116°28'40"	740.66	685.95	692.20	01/12/87
56		36°34'57"	116°34'23"	740.66	686.24	705.58	01/07/87
57		36°34'57"	116°33'09"	731.52	666.89	693.69	01/07/87
58	DeFir Well	36°34'56"	116°35'25"	727.07	671.71	690.42	03/24/93
59		36°34'55"	116°34'59"	726.03	667.91	692.99	07/02/62

Appendix A: Observation-well data used in the construction of the Yucca Mountain site saturated-zone model

[well names are those contained in the USGS Ground-Water Site Inventory data base;
midpoint of water column is midpoint of packed off interval for multiply completed wells]

Observation Number	Well Name	Latitude	Longitude	Measuring point altitude (meters)	Altitude of midpoint of water column (meters)	Hydraulic head (meters)	Date of Measurement
60		36°34'45"	116°32'46"	727.86	661.39	692.44	01/07/87
61		36°34'42"	116°36'33"	725.73	676.96	689.15	04/21/82
62		36°34'40"	116°28'24"	731.52	664.60	686.38	06/29/62
63		36°34'34"	116°27'51"	741.88	673.30	696.16	07/15/58
64		36°34'32"	116°34'42"	723.29	653.80	690.07	01/20/84
65		36°34'30"	116°24'52"	762.00	667.22	709.00	06/29/62
66		36°34'29"	116°31'59"	729.08	664.89	692.14	01/07/87
67		36°34'28"	116°32'15"	740.66	679.72	706.56	07/04/62
68	Cooks West Well	36°34'28"	116°24'03"	754.26	689.74	720.32	04/09/91
69	Cooks East Well	36°34'28"	116°23'47"	755.23	695.82	718.41	12/18/96
70		36°34'17"	116°27'30"	740.66	685.53	688.30	01/20/84
71	Amargosa Town C	36°34'11"	116°27'29"	739.14	668.27	688.85	11/19/80
72		36°34'10"	116°26'11"	743.71	615.35	691.20	01/15/87
73		36°34'10"	116°24'03"	748.59	700.81	713.99	03/16/87
74		36°34'10"	116°24'00"	749.81	709.89	723.63	03/16/87

Appendix A: Observation-well data used in the construction of the Yucca Mountain site saturated-zone model

[well names are those contained in the USGS Ground-Water Site Inventory data base;
midpoint of water column is midpoint of packed off interval for multiply completed wells]

Observation Number	Well Name	Latitude	Longitude	Measuring point altitude (meters)	Altitude of midpoint of water column (meters)	Hydraulic head (meters)	Date of Measurement
75	Amargosa Valley	36°34'07"	116°27'33"	737.92	673.91	701.34	12/10/88
76		36°34'05"	116°33'45"	723.90	672.08	696.47	08/15/58
77		36°34'04"	116°33'12"	724.20	662.28	692.40	01/08/87
78		36°34'04"	116°32'39"	724.20	685.61	692.74	02/26/74
79		36°34'04"	116°25'04"	746.76	678.44	698.51	06/29/62
80	USW H-1 Tube1	36°51'57"	116°27'12"	1302.99	-495.50	785.80	12/05/95
81	USW H-1 Tube2			1302.99	192.98	735.25	12/05/95
82	USW H-1 Tube3			1302.99	562.49	730.58	12/05/95
83	USW H-1 Tube4			1302.99	680.39	730.78	12/05/95
84	USW H-5 Upper	36°51'22"	116°27'55"	1478.89	704.15	775.41	02/07/95
85	USW H-5 Lower			1478.89	446.39	775.68	06/14/95
86	UE-25b#1 Lower	36°51'08"	116°26'23"	1200.70	-8.79	730.11	07/18/95
87	UE-25b#1 Upper			1200.70	366.13	730.56	12/05/95
88	USW H-6 Upper	36°50'49"	116°28'55"	1301.71	662.73	775.75	12/06/95
89	USW H-6 Lower			1301.71	315.71	775.63	12/06/95

Appendix A: Observation-well data used in the construction of the Yucca Mountain site saturated-zone model

[well names are those contained in the USGS Ground-Water Site Inventory data base;
midpoint of water column is midpoint of packed off interval for multiply completed wells]

Observation Number	Well Name	Latitude	Longitude	Measuring point altitude (meters)	Altitude of midpoint of water column (meters)	Hydraulic head (meters)	Date of Measurement
90	USW II-4 Upper	36°50'32"	116°26'54"	1248.49	395.33	730.16	12/12/95
91	USW II-4 Lower			1248.49	45.00	730.27	12/12/95
92	USW II-3 Upper	36°49'42"	116°28'00"	1483.19	550.12	731.04	07/26/95
93	USW II-3 Lower			1483.19	316.70	759.33	12/12/95
94	UE-25p#1 PTH	36°49'38"	116°25'21"	1114.20	-410.29	752.62	12/03/96

APPENDIX B: SUPPORTING INFORMATION REGARDING PARAMETER ESTIMATION SEQUENCE

This appendix provides supporting information that pertains to initial parameter-estimation runs. Appendix C lists the sequence of simulations, the parameters estimated, and the sum-of-squared errors for each simulation. No formal sensitivity analyses (that is, incrementally varying one model variable and observing the model response or calculation of composite scaled sensitivities) were done using the model. However, based on the variations in the weighted sum-of-squared errors for hydraulic head, reported during each PEST run, certain model variables were observed to affect calibration more than others. Those that had the largest effects are listed in table 8 in this appendix.

An earlier version of the model finite-element mesh was discovered to have errors that affected simulated flux. The error involved the omission of a term in one of the mesh coefficients, but was identified too late to be incorporated into the parameter-estimation sequence listed in Appendix C.

Some simulations resulted in unacceptable estimates for certain parameters even though the sum of squared residuals were similar. For example, simulations 28 and 29 (Appendix C) produced estimates for aquifer permeability values for the middle volcanic aquifer (mva) and the upper volcanic aquifer (uva), which were considered to be unrealistically small ($5.9e-15 \text{ m}^2$) relative to other units specified in the model (that is, confining units). Values of permeability in table 3 provided guidance as to acceptable estimates. However, the parameter estimation algorithm would sometimes calculate intermediary estimates that would go beyond the ranges given in table 3. If this were to occur during a simulation, the parameter would be fixed at its upper or lower limit, whichever was reached. When this happened, the model specified limits for that parameter were sometimes increased to test whether an estimate within the newly specified limits could be achieved with an acceptable confidence interval (plus or minus one standard deviation).

Permeability of the lower carbonate aquifer (lca) showed a moderately high correlation (greater than 0.7) with the permeability of the alluvial aquifer (qal). Both units are connected spatially in the model. Experience has shown that spatially connected hydrogeologic units with similar permeability that are oriented approximately parallel to the direction of ground-water flow tend to be highly correlated, preventing independent estimates of their associated permeability values. For that reason qal was tied to lca such that both would vary together with a fixed ratio, and lca was the parent parameter.

The final simulation (40) listed in Appendix C used permeability values obtained for the best-fitting simulation (simulation 30, Appendix C) from the initial parameter-estimation sequence except that recharge at Fortymile Wash (fm) and the permeability of the Solitario Canyon fault zone (lkns) were optimized using PEST. The permeability values and fluxes specified in simulation 40 are those listed in table 6. Limitations in the resolution of hydrogeologic units using the current coarse mesh indicate that further optimization of permeability likely is not warranted until a higher-resolution mesh is developed.

Table 8—Key model parameters affecting model calibration

[model parameter abbreviations: lkew, zone of low permeability oriented east to west located at approximate southern end of large hydraulic gradient; lkns, zone of low permeability associated with Solitario Canyon Fault oriented north to south; ecu, Upper Clastic Confining Unit; mvcu, Middle Volcanic Confining Unit; uvcu, Upper Volcanic Confining Unit; lca, Lower Carbonate Aquifer; uca, Upper Carbonate Aquifer; fm, mass flux estimated for Fortymile Wash recharge]

Simulation Sequence Number	Key Model Parameters Affecting Change in Model Objective Function	Change in Model Objective Function From Previous Model Simulation, phi (meters ²)	Comment
5	lkew lkns	-4,249	lkew and lkns added as separate zone lists: not explicitly part of original hydrogeologic framework model
6	ecu mvcu	-4,256	First attempt at estimating permeability of confining units
7	uvcu	-18,250	Single largest improvement; residual for observation 1 had been large up until this adjustment
19	lca uca	-14,196	lca estimate set at upper limit by the regression
34	lca	-16,496	Upper allowable value increased because it had been set at upper limit by regression in previous simulation

Table 8--Key model parameters affecting model calibration

[model parameter abbreviations: lkew, zone of low permeability oriented east to west located at approximate southern end of large hydraulic gradient; lkns, zone of low permeability associated with Solitario Canyon Fault oriented north to south; ecu, Upper Clastic Confining Unit; mvcu, Middle Volcanic Confining Unit; uvcu, Upper Volcanic Confining Unit; lca, Lower Carbonate Aquifer; uca, Upper Carbonate Aquifer; fm, mass flux estimated for Fortymile Wash recharge]

Simulation Sequence Number	Key Model Parameters Affecting Change in Model Objective Function	Change in Model Objective Function From Previous Model Simulation, phi (meters ²)	Comment
40	fm lkns	-22,200	Corrected mesh was used which permitted optimization of flux at Fortymile Wash. Permeability values for 16 hydrogeologic units were those used in simulation 30.

Appendix C. Model-calibration parameter estimates

[All permeability values are in meters²; all parameters pertain to permeability except for fm, mass flux estimated for Fortymile Wash recharge, for which units are kilograms/second per node; model parameter abbreviations: gran, Granite Confining Unit; qcu, Lower Clastic Confining Unit; lca, Lower Carbonate Aquifer; ecu, Upper Clastic Confining Unit; uca, Upper Carbonate Aquifer; lcu, Undifferentiated Valley Fill; lvcu, Lower Volcanic Confining Unit; lva, Lower Volcanic Aquifer; mvcu, Middle Volcanic Confining Unit; mva, Middle Volcanic Aquifer; uvcu, Upper Volcanic Confining Unit; uva, Upper Volcanic Aquifer; b, Lava-Flow Aquifer; llim, Limestone Aquifer; tpla, Valley-Fill Confining Unit; qal, Valley-Fill Aquifer; lkns, zone of low permeability associated with Solitario Canyon Fault oriented north to south; lkew, zone of low permeability oriented east to west located at approximate southern end of large hydraulic gradient; kfm, permeability of zone beneath Fortymile Wash; mvcz, vertical permeability of zone at top of Middle Volcanic Confining Unit; kz, vertical permeability for all nodes at base of uvcu; kzns, vertical permeability for nodes associated with zone of low permeability associated with Solitario Canyon Fault oriented north to south; fixed parameters and values are those not listed in Appendix C. Values that exceed 3 significant figures reflect values extracted directly from a PFST record file and do not imply a higher level of accuracy. Files use the naming convention h^orec^o, and generally follow a naming sequence of letter-number-letter-number (not to four places), and are included for traceability.]

Simulation Sequence Number	File Name	Adjustable Parameters	Initial Value	Estimated Value	95 Percent Confidence Limit		Sum of Squared Residuals (meters ²)	Tied Parameters (Parent)	Estimated Values for Tied Parameters	Fixed Parameters and Values
					Lower Limit	Upper Limit				
1	h2 rec	ku uva	1.0E-11 1.0E-12	8.89E-11 8.27E-14	7.0E-11 7.10E-11	1.01E-12 8.74E-11	5.77E+04	mva (uva) qal (lca)	4.63E-14 1.67E-11	
2	h3 rec	lca uva kz	1.60E-13 1.00E-12 1.00E-16	7.91E-13 3.96E-14 5.00E-12	6.04E-13 7.50E-13 4.99E-12	9.78E-13 8.29E-13 5.01E-12	5.65E+04	mva (uva) qal (lca)	2.22E-14 1.48E-13	
3	h4 rec	lca uva kz fm	1.60E-13 1.00E-12 1.00E-16 -200.000	9.81E-13 4.27E-14 5.00E-12 -10000.0	6.73E-13 7.59E-13 4.99E-12 -165301	1.29E-12 8.44E-13 5.01E-12 145301	5.66E+04	mva (uva) qal (lca)	2.39E-14 1.84E-13	
4	h4a rec	lca uva kz fm	1.60E-13 1.00E-12 1.00E-16 -200.000	3.06E-13 7.13E-14 4.17E-15 -1678.68	-9.23E-15 -7.41E-13 -1.32E-14 -199842	6.22E-13 8.83E-13 2.15E-14 196565	5.68E+04	mva (uva) qal (lca)	3.99E-14 5.74E-14	
5	h4b rec	lca uva kz lkew lkns	1.60E-13 1.00E-12 1.00E-16 1.00E-16 1.00E-16	5.83E-13 1.80E-14 2.29E-15 1.59E-17 3.45E-16	3.73E-13 7.74E-13 -1.02E-14 -7.05E-16 -1.02E-15	7.93E-13 8.10E-13 1.48E-14 7.36E-16 1.71E-15	5.25E+04	mva (uva) qal (lca)	1.01E-14 1.09E-13	
6	h4c rec	ecu mvcu	2.00E-15 1.80E-15	1.00E-18 1.92E-16	-1.95E-14 -5.43E-15	1.95E-14 5.81E-15	4.83E+04	uvcu (mvcu)	1.07E-15	
7	h4d rec	uvcu	1.00E-15	1.00E-18	-2.41E-15	2.41E-15	3.00E+04			
8	h4f rec	ecu	1.00E-19	5.50E-19	-1.87E-17	1.98E-17	2.90E+04			
	h4g rec	uvcu	1.00E-18	1.00E-18	-3.50E-17	3.70E-17	2.90E+04			

Appendix C. Model-calibration parameter estimates

[All permeability values are in meters²; all parameters pertain to permeability except for fm, mass flux estimated for Fortymile Wash recharge, for which units are kilograms/second per node; model parameter abbreviations: gran, Granitic Confining Unit; qcu, Lower Clastic Confining Unit; lca, Lower Carbonate Aquifer; ecu, Upper Clastic Confining Unit; uca, Upper Carbonate Aquifer; lcu, Undifferentiated Valley Fill; lvcu, Lower Volcanic Confining Unit; lva, Lower Volcanic Aquifer; mvcu, Middle Volcanic Confining Unit; mva, Middle Volcanic Aquifer; uvcu, Upper Volcanic Confining Unit; uva, Upper Volcanic Aquifer; b, Lava-Flow Aquifer; llm, Limestone Aquifer; tpla, Valley-Fill Confining Unit; qal, Valley-Fill Aquifer; lkns, zone of low permeability associated with Solitario Canyon Fault oriented north to south; lkew, zone of low permeability oriented east to west located at approximate southern end of large hydraulic gradient; kfm, permeability of zone beneath Fortymile Wash; mvcz, vertical permeability of zone at top of Middle Volcanic Confining Unit; kz, vertical permeability for all nodes at base of uvcu; kzns, vertical permeability for nodes associated with zone of low permeability associated with Solitario Canyon Fault oriented north to south; fixed parameters and values are those not listed in Appendix C. Values that exceed 3 significant figures reflect values extracted directly from a PFST record file and do not imply a higher level of accuracy. Files use the naming convention h*rec*, and generally follow a naming sequence of letter-number-letter-number (out to four places), and are included for traceability.]

Simulation Sequence Number	File Name	Adjustable Parameters	Initial Value	Estimated Value	95 Percent Confidence Limits		Sum of Squared Residuals (meters ²)	Tied Parameters (Parent)	Estimated Values for Tied Parameters	Fixed Parameters and Values
					Lower Limit	Upper Limit				
10	h4h rec	fm	-20	-201.258	-272.187	-134.168	2.90E+04			
11	h4j rec	lkew	1.60E-17	1.60E-17	-9.20E-17	8.40E-17	2.90E+04			
12	h4k rec	lkns	1.40E-16	1.67E-16	-6.79E-17	4.01E-16	2.80E+04			
13	h4k rec 001	lkns	3.40E-16	1.67E-16	-6.79E-17	4.01E-16	2.80E+04			
14	h4k1 rec	mvcu	1.90E-16	1.90E-18	-1.20E-15	1.20E-15	3.91E+04			
15	h4k1 rec 001	lkns	3.40E-16 (Initial value changed)	1.60E-16	-1.16E-16	4.36E-16	3.91E+04			
16	h4k1 rec 002	mvcu	1.90E-16	1.90E-18	-1.20E-15	1.20E-15	3.91E+04			
17	h4k2 rec	lkns	3.40E-16	1.62E-16	-1.16E-16	4.41E-16	3.88E+04			
18	h4l rec	mvcz	1.90E-16	1.90E-18	-2.46E-15	2.46E-15	3.88E+04			
19	h4m rec	lca uca	5.80E-13 5.00E-13	5.00E-12 6.74E-13	3.50E-12 -2.49E-12	6.50E-12 3.84E-12	2.46E+04			
20	h4m rec 001	mva	1.00E-14	1.04E-14	-3.36E-15	2.41E-14	2.83E+04			
21	h4n rec	mva uva	1.00E-14 1.80E-14	3.109193274259 1E-14E-16	-1.94E-14 -4.61E-14	2.00E-14 1.01E-13	2.30E+04			

Appendix C. Model-calibration parameter estimates

[All permeability values are in meters²; all parameters pertain to permeability except for fm, mass flux estimated for Fortymile Wash recharge, for which units are kilograms/second per node; model parameter abbreviations: gran, Granitic Confining Unit; qcu, Lower Clastic Confining Unit; lca, Lower Carbonate Aquifer; ecu, Upper Clastic Confining Unit; uca, Upper Carbonate Aquifer; lcu, Undifferentiated Valley Fill; lvcu, Lower Volcanic Confining Unit; lva, Lower Volcanic Aquifer; mvcu, Middle Volcanic Confining Unit; mva, Middle Volcanic Aquifer; uvcu, Upper Volcanic Confining Unit; uva, Upper Volcanic Aquifer; b, Lava-Flow Aquifer; lfm, Limestone Aquifer; tpla, Valley-Fill Confining Unit; qal, Valley-Fill Aquifer; lkns, zone of low permeability associated with Sollarin Canyon Fault oriented north to south; lkew, zone of low permeability oriented east to west located at approximate southern end of large hydraulic gradient; kfm, permeability of zone beneath Fortymile Wash; mvcz, vertical permeability of zone at top of Middle Volcanic Confining Unit; kz, vertical permeability for all nodes at base of uvcu; kzns, vertical permeability for nodes associated with zone of low permeability associated with Sollarin Canyon Fault oriented north to south; fixed parameters and values are those not listed in Appendix C. Values that exceed 3 significant figures reflect values extracted directly from a PEST record file and do not imply a higher level of accuracy. Files use the naming convention h*rec*, and generally follow a naming sequence of letter-number-letter-number (out to four places), and are included for traceability.]

Simulation Sequence Number	File Name	Adjustable Parameters	Initial Value	Estimated Value	95 Percent Confidence Limit		Sum of Squared Residuals (meters ²)	Tied Parameters (Param)	Estimated Values for Tied Parameters	Fixed Parameters and Values
					Lower Limit	Upper Limit				
22	Mn rec 0 01	ka	1.00E-12	5.57E-12	-1.14E-12	1.49E-11	2.46E+04			
23	Mn rec 0 02	uva	1.00E-14	1.80E-14	2.98E-15	3.34E-14	2.46E+04			
24	Mn rec 0 03	mva	1.00E-14	1.81E-15	-9.90E-15	1.35E-14	2.31E+04			
25	Mn rec 0 04	mva uva	1.00E-14 1.80E-14	3.11E-16 2.74E-14	-1.94E-14 -4.63E-14	2.00E-14 1.01E-13	2.30E+04			
26	h4o rec	mva	6.00E-16	5.72E-15	5.24E-15	6.20E-15	2.34E+04	uva (mva)	5.72E-15	
27	h4o1 rec	mva lkns	6.00E-16 1.70E-16	2.56E-14 8.80E-16	2.46E-14 5.47E-16	2.65E-14 1.22E-15	2.24E+04	uva (mva)	2.56E-14	
28	h4o2 rec	lca mva	5.50E-12 6.00E-16	3.32E-12 5.95E-15	-1.10E-12 5.47E-15	7.74E-12 6.43E-15	2.29E+04	uva (mva) qal(lca)	5.95E-15 6.64E-14	
29	h4o2 rec 002	lca mva	5.50E-12 6.00E-16	3.32E-12 5.95E-15	-1.10E-12 5.47E-15	7.74E-12 6.43E-15	2.29E+04	uva (mva) qal(lca)	5.95E-15 6.64E-14	
30	h4o2 rec 001	lca mva lkns	5.50E-12 6.00E-16 1.70E-16	4.41E-12 1.63E-14 6.98E-16	-1.82E-14 1.53E-14 3.17E-16	8.83E-12 1.73E-14 1.00E-15	2.24E+04	uva (mva) qal(lca)	1.63E-14 8.81E-14	
31	h4o3 rec	lca mva lca	5.50E-12 6.00E-16 2.90E-14	3.36E-12 5.87E-15 3.54E-14	-2.46E-12 5.38E-15 -7.15E-14	9.17E-12 6.35E-15 1.42E-13	2.29E+04	uva (mva) qal(lca)	5.87E-15 6.72E-14	
32	h4o4 rec	kzns	1.70E-16	1.70E-12	1.70E-12	1.70E-12	3.95E+04			uva 6.00E-16

Appendix C. Model-calibration parameter estimates

[All permeability values are in meters²; all parameters pertain to permeability except for fm, mass flux estimated for Fortymile Wash recharge, for which units are kilograms/second per node; model parameter abbreviations: gran, Granitic Confining Unit; qcu, Lower Clastic Confining Unit; lca, Lower Carbonate Aquifer; ccu, Upper Clastic Confining Unit; uca, Upper Carbonate Aquifer; lcu, Undifferentiated Valley Fill; lvcu, Lower Volcanic Confining Unit; lva, Lower Volcanic Aquifer; mvcu, Middle Volcanic Confining Unit; mva, Middle Volcanic Aquifer; uvcu, Upper Volcanic Confining Unit; uva, Upper Volcanic Aquifer; b, Lava-Flow Aquifer; llim, Limestone Aquifer; tpla, Valley-Fill Confining Unit; qal, Valley-Fill Aquifer; lkns, zone of low permeability associated with Solitario Canyon Fault oriented north to south; lkew, zone of low permeability oriented east to west located at approximate southern end of large hydraulic gradient; kfm, permeability of zone beneath Fortymile Wash; mvcz, vertical permeability of zone at top of Middle Volcanic Confining Unit; kz, vertical permeability for all nodes at base of uvcu; kzns, vertical permeability for nodes associated with zone of low permeability associated with Solitario Canyon Fault oriented north to south; fixed parameters and values are those not listed in Appendix C. Values that exceed 3 significant figures reflect values extracted directly from a PEST record file and do not imply a higher level of accuracy. Files use the naming convention h*rec*, and generally follow a naming sequence of letter-number-letter-number (not to four places), and are included for traceability.]

Simulation Sequence Number	File Name	Adjustable Parameters	Initial Value	Estimated Value	95 Percent Confidence Limits		Sum of Squared Residuals (meters ²)	Tied Parameters (Parent)	Estimated Values for Tied Parameters	Fixed Parameters and Values
					Lower Limit	Upper Limit				
13	h3p rec	Rns	1.70E-16	2.48E-16	7.50E-17	4.20E-16	3.96E+04			uvcu 1.00E-19 qal 5.70E-15
14	h3p rec 0 01	ka	4.90E-12	1.81E-11	2.99E-11	4.68E-11	2.27E+04			
15	h3p rec 0 03	ccu	5.90E-16	5.90E-19	-4.77E-15	4.77E-15	2.34E+04			
16	h5 rec	fm ^a	-200	-478.518	-633.247	-323.790	2.34E+04			
17	h5a rec	fm kfm	-200 1.10E-13	-873.008 5.00E-12	-1187.03 4.65E-12	-558.989 5.55E-12	2.56E+04			
18	h6 rec	fm kfm ^b	-200 1.10E-13	-872.313 5.00E-12	-1312.94 4.45E-12	-431.686 5.55E-12	5.05E+04			
19	h6a rec	mva Rns	6.00E-16 1.70E-16	6.02E-16 1.33E-17	-3.10E-16 -3.76E-16	1.51E-15 4.02E-16	5.54E+04	uva(mva)	6.02E-16	kfm 1.10E-11
40	a32 rec ^c	fm Rns	-0.019 1.02 x 10 ⁻¹⁵	-0.012 1.20 x 10 ⁻¹⁵	-0.0197 6.89 x 10 ⁻¹⁶	-0.0245 1.72 x 10 ⁻¹⁵	23,163			

- a. 40 Mile Wash zone reduced to just the topmost nodes
- b. Solitario Canyon Fault barrier specified 1.5km east of previous position
- c. Corrected finite-element mesh used.

Appendix D. Fixed-parameter values used in most of the parameter-estimation runs

[All permeability values are in meters²; all parameters pertain to permeability except for fm, mass flux estimated for Fortymile Wash recharge, for which units are kilograms/second per node; model parameter abbreviations: gran, Granitic Confining Unit; qcu, Lower Clastic Confining Unit; lca, Lower Carbonate Aquifer; ecu, Upper Clastic Confining Unit; uca, Upper Carbonate Aquifer; lcu, Undifferentiated Valley Fill; lvcu, Lower Volcanic Confining Unit; lva, Lower Volcanic Aquifer; mvcu, Middle Volcanic Confining Unit; mva, Middle Volcanic Aquifer; uvcu, Upper Volcanic Confining Unit; uva, Upper Volcanic Aquifer; b, Lava-Flow Aquifer; tim, Limestone Aquifer; tpla, Valley-Fill Confining Unit; qal, Valley-Fill Aquifer; lkns, zone of low permeability associated with Solitario Canyon Fault oriented north to south; lkew, zone of low permeability oriented east to west located at approximate southern end of large hydraulic gradient; mvcz, vertical permeability of zone at top of Middle Volcanic Confining Unit; kz, vertical permeability for all nodes at base of uvcu; kzns, vertical permeability for nodes associated with zone of low permeability associated with Solitario Canyon Fault oriented north to south]

Variable Name	Specified Value	Simulation Sequence Numbers
gran	3.5E-14	all
qcu	2.0E-15	all
lvcu	1.0E-16	all
b	4.5E-14	all
lva	5.0E-13	all
ecu	2.0E-15	1-5
	1.0E-18	7
	5.5E-19	9-32, 34, 36-40
	5.5E-16	33
uca	5.00E-13	1-18,20
	6.70E-13	21-40
mvcu	1.80E-15	1-5
	1.90E-16	7-13,15,17-40
lcu	2.90E-14	1-30,32-40
uvcu	1.00E-14	1-5
	1.00E-18	8,10-32,34-40
tim	1.00E-14	all
tpla	3.00E-16	all
fm	-200.	5-9,11-35,39
lca	5.80E-13	6-18,20
	5.50E-12	21,23-27,32,33,35
	4.40E-12	40

Appendix D. Fixed-parameter values used in most of the parameter-estimation runs

[All permeability values are in meters²; all parameters pertain to permeability except for fm, mass flux estimated for Fortymile Wash recharge, for which units are kilograms/second per node; model parameter abbreviations: gran. Granitic Confining Unit; qcu. Lower Clastic Confining Unit; lca. Lower Carbonate Aquifer; ecu. Upper Clastic Confining Unit; uca. Upper Carbonate Aquifer; lcu. Undifferentiated Valley Fill; lvcu. Lower Volcanic Confining Unit; lva. Lower Volcanic Aquifer; mvcu. Middle Volcanic Confining Unit; mva. Middle Volcanic Aquifer; uvcu. Upper Volcanic Confining Unit; uva. Upper Volcanic Aquifer; b. Lava-Flow Aquifer; ltm. Limestone Aquifer; tpla. Valley-Fill Confining Unit; qal. Valley-Fill Aquifer; lkns. zone of low permeability associated with Solitario Canyon Fault oriented north to south; lkew. zone of low permeability oriented east to west located at approximate southern end of large hydraulic gradient; mvcz. vertical permeability of zone at top of Middle Volcanic Confining Unit; kz. vertical permeability for all nodes at base of uvcu; kzns. vertical permeability for nodes associated with zone of low permeability associated with Solitario Canyon Fault oriented north to south]

Variable Name	Specified Value	Simulation Sequence Numbers
uva	1.80E-14	6-20,22,24
	5.70E-15	33-35
	2.50E-14	36-38
	1.60E-14	40
qal	1.10E-13	6-27,32,34-39
	8.80E-14	40
kz	2.20E-15	6-13,17,19-39
lkew	1.60E-17	6-10,12-40
lkns	3.40E-16	6-11,14,16
	1.70E-16	19-26,28,29,31-34
	8.80E-16	36-39
mva	1.00E-14	6-19,22
	5.70E-15	33-35
	2.50E-14	36-39
	1.60E-14	40

Appendix E. Observed and simulated hydraulic head

Observation Number	Observed Hydraulic Head (meters)	Simulated Hydraulic Head (meters)	Difference Between Observed and Simulated Hydraulic Head (meters)
1	1187.80	1186.68	1.12
2	1010.05	1046.61	-36.56
3	1034.52	1013.56	20.96
4	1019.79	1007.52	12.27
5	738.51	833.54	-95.03
6	778.43	758.51	19.92
7	730.26	737.24	-6.98
8	754.20	752.84	1.36
9	748.28	756.05	-7.77
10	730.84	733.29	-2.45
11	729.15	728.61	0.54
12	730.15	745.42	-15.27
13	730.97	736.55	-5.58
14	729.98	729.36	0.62
15	730.81	745.29	-14.48
16	730.06	727.41	2.65
17	730.09	727.37	2.72
18	730.19	727.36	2.83
19	729.18	728.30	0.88
20	775.96	758.44	17.52
21	730.64	734.40	-3.76
22	730.52	741.31	-10.79
23	728.22	725.23	2.99
24	775.97	751.70	24.27

Appendix E. Observed and simulated hydraulic head

Observation Number	Observed Hydraulic Head (meters)	Simulated Hydraulic Head (meters)	Difference Between Observed and Simulated Hydraulic Head (meters)
25	729.40	727.03	2.37
26	833.17	830.14	3.03
27	729.66	722.43	7.23
28	779.46	791.11	-11.65
29	729.37	721.04	8.33
30	730.68	721.59	9.09
31	727.34	722.35	4.99
32	727.80	721.77	6.03
33	729.81	712.43	17.38
34	718.41	717.27	1.14
35	705.40	716.84	-11.44
36	704.09	716.91	-12.82
37	705.61	717.30	-11.69
38	701.65	717.06	-15.41
39	705.48	716.49	-11.01
40	705.44	712.85	-7.41
41	705.36	715.46	-10.10
42	724.96	724.20	0.76
43	706.10	711.29	-5.19
44	704.39	708.61	-4.22
45	695.81	698.97	-3.16
46	694.03	694.41	-0.38
47	693.76	695.57	-1.81
48	693.76	696.34	-2.58
49	722.25	715.61	6.64

Appendix E. Observed and simulated hydraulic head

Observation Number	Observed Hydraulic Head (meters)	Simulated Hydraulic Head (meters)	Difference Between Observed and Simulated Hydraulic Head (meters)
50	696.93	696.28	0.65
51	689.98	692.99	-3.01
52	707.68	693.76	13.92
53	693.22	694.18	-0.96
54	690.46	691.96	-1.50
55	692.20	694.19	-1.99
56	705.58	692.93	12.65
57	693.69	693.58	0.11
58	690.42	691.69	-1.27
59	692.99	692.10	0.89
60	692.44	693.26	-0.82
61	689.15	687.11	2.04
62	686.38	693.28	-6.90
63	696.16	693.86	2.30
64	690.07	691.07	-1.00
65	709.00	709.27	-0.27
66	692.14	692.26	-0.12
67	706.56	692.48	14.08
68	720.32	714.02	6.30
69	718.41	715.16	3.25
70	688.30	694.25	-5.95
71	688.85	694.28	-5.43
72	691.20	696.00	-4.80
73	713.99	713.42	0.57
74	723.63	713.79	9.84

Appendix E. Observed and simulated hydraulic head

Observation Number	Observed Hydraulic Head (meters)	Simulated Hydraulic Head (meters)	Difference Between Observed and Simulated Hydraulic Head (meters)
75	701.34	694.97	6.37
76	696.47	694.86	1.61
77	692.40	694.05	-1.65
78	692.74	692.66	0.08
79	698.51	706.24	-7.73
80	785.80	723.09	62.71
81	735.25	750.00	-14.75
82	730.58	750.26	-19.68
83	730.78	750.31	-19.53
84	775.68	759.63	16.05
85	775.68	750.31	25.37
86	730.11	733.33	-3.22
87	730.56	736.93	-6.37
88	775.75	769.11	6.64
89	775.63	769.15	6.48
90	730.27	735.41	-5.14
91	730.16	741.11	-10.95
92	731.04	747.76	-16.72
93	759.33	747.78	11.55
94	752.62	722.69	29.93

Appendix 1.--Correlation of RIB and ISM2.0 to Hydrogeologic Units

Site Saturated Zone Hydrogeologic Unit	Geologic/Lithologic Stratigraphy (RIB Item 1.1.2.1)						ISM2.0
	Definition/Buesch (1996)	Group	Formation	Member	Zone	Subzone	
Valley-Fill Aquifer							
Valley-Fill Confining Unit							
Limestone Aquifer							
Lava-Flow Aquifer							
Upper Volcanic Aquifer	Timber Mountain Group	Tm					
Upper Volcanic Aquifer	Rainier Mesa Tuff		Tmr				44tmr
Upper Volcanic Aquifer	Paintbrush Group	Tp					
Upper Volcanic Aquifer	Post tuff unit "x" bedded tuff			Tpbt6			
Upper Volcanic Aquifer	Tuff unit "x"			Tpkl (informal)			44tpk
Upper Volcanic Aquifer	Pre-tuff unit "x" bedded tuff			Tpbt5			44tpc
Upper Volcanic Aquifer	Tiva Canyon Tuff		Tpc				
Upper Volcanic Aquifer	Crystal-Rich Member			Tpcr			
Upper Volcanic Aquifer	Vitric zone				Tpcrv		
Upper Volcanic Aquifer	Nonwelded subzone					Tpcrv3	
Upper Volcanic Aquifer	Moderately welded subzone					Tpcrv2	
Upper Volcanic Aquifer	Densely welded subzone					Tpcrv1	
Upper Volcanic Aquifer	Nonlithophysal zone				Tpcm		
Upper Volcanic Aquifer	Subvitrophyre transition subzone					Tpcm4	
Upper Volcanic Aquifer	Pumice-poor subzone					Tpcm3	
Upper Volcanic Aquifer	Mixed pumice subzone					Tpcm2	
Upper Volcanic Aquifer	Crystal transition subzone (not always present)					Tpcrn1	
Upper Volcanic Aquifer	Lithophysal zone				Tpcrl		
Upper Volcanic Aquifer	Crystal transition subzone (not always present)					Tpcrl1	
Upper Volcanic Aquifer	Crystal-Poor Member			Tpcp			
Upper Volcanic Aquifer	Upper lithophysal zone				Tpcpl		
Upper Volcanic Aquifer	Spherulite-rich subzone					Tpcpl1	
Upper Volcanic Aquifer	Middle nonlithophysal zone				Tpcpm		
Upper Volcanic Aquifer	Upper subzone					Tpcpm3	
Upper Volcanic Aquifer	Lithophysal subzone					Tpcpm2	
Upper Volcanic Aquifer	Lower subzone					Tpcpm1	
Upper Volcanic Aquifer	Lower lithophysal zone				Tpcpl1		
Upper Volcanic Aquifer	Hackly-fractured subzone					Tpcpl1h	
Upper Volcanic Aquifer	Lower nonlithophysal zone				Tpcpln		
Upper Volcanic Aquifer	Hackly subzone					Tpcplnh	
Upper Volcanic Aquifer	Columnar subzone					Tpcplnc	
Upper Volcanic Aquifer	Vitric zone				Tpcpv		
Upper Volcanic Aquifer	Densely welded subzone					Tpcpv3	44tpcv3
Upper Volcanic Aquifer	Moderately welded subzone					Tpcpv2	44tpcv12
Upper Volcanic Aquifer	Nonwelded subzone					Tpcpv1	44tpcv12
Upper Volcanic Aquifer	Pre-Tiva Canyon bedded tuff			Tpbt4			44tpbt4
Upper Volcanic Aquifer	Yucca Mountain Tuff		Tpy				44tpy
Upper Volcanic Aquifer	Pre-Yucca Mountain bedded tuff			Tpbt3			44tpbt3
Upper Volcanic Aquifer	Pah Canyon Tuff		Tpp				44tpp
Upper Volcanic Aquifer	Pre-Pah Canyon bedded tuff			Tpbt2			44tpbt2
Upper Volcanic Aquifer	Topopah Spring Tuff		Tpt				

Appendix 1.--Correlation of RIB and ISM2.0 to Hydrogeologic Units

Site Saturated Zone Hydrogeologic Unit	Geologic/Lithologic Stratigraphy (RIB Item 1.1.2.1)						ISM2.0
	Definition/Buesch (1996)	Group	Formation	Member	Zone	Subzone	
Upper Volcanic Aquifer	Crystal-Rich Member			Tpr			
Upper Volcanic Aquifer	Vitric zone				Tprv		
Upper Volcanic Aquifer	Nonwelded subzone					Tprv3	44tprv23
Upper Volcanic Aquifer	Moderately welded subzone					Tprv2	44tprv23
Upper Volcanic Aquifer	Densely welded subzone					Tprv1	44tprv1
Upper Volcanic Aquifer	Nonlithophysal zone				Tprm		44tprm
Upper Volcanic Aquifer	Dense subzone					Tprm3	
Upper Volcanic Aquifer	Vapor-phase corroded subzone					Tprm2	
Upper Volcanic Aquifer	Crystal transition subzone (not always present)					Tprm1	
Upper Volcanic Aquifer	Lithophysal zone				Tprl		
Upper Volcanic Aquifer	Crystal transition subzone (not always present)					Tprl1	44tprl
Upper Volcanic Aquifer	Crystal-Poor Member			Tpp			
Upper Volcanic Aquifer	Lithic-rich zone			Tptpl or Tptpf			44tptf
Upper Volcanic Aquifer	Upper lithophysal zone				Tptpul		44tptpul
Upper Volcanic Aquifer	Middle nonlithophysal zone				Tptpma		44tptpma
Upper Volcanic Aquifer	Nonlithophysal subzone					Tptpma3	
Upper Volcanic Aquifer	Lithophysal-bearing subzone					Tptpma2	
Upper Volcanic Aquifer	Nonlithophysal subzone					Tptpma1	
Upper Volcanic Aquifer	Lower lithophysal zone				Tptpl		44tptpl
Upper Volcanic Aquifer	Lower nonlithophysal zone				Tptpln		44tptpln
Upper Volcanic Aquifer	Vitric zone				Tptpv		
Upper Volcanic Aquifer	Densely welded subzone					Tptpv3	44tptpv3
Upper Volcanic Aquifer	Moderately welded subzone					Tptpv2	44tptpv12
Upper Volcanic Aquifer	Nonwelded subzone					Tptpv1	44tptpv12
Upper Volcanic Aquifer	Pre-Topopah Spring bedded tuff				Tpbtl		44tpbt
Upper Volcanic Confining Unit	Calico Hills Formation		Ta				44tac
Upper Volcanic Confining Unit	Bedded tuff				Ttbt		44tact
Middle Volcanic Aquifer	Crater Flat Group	Tc					
Middle Volcanic Aquifer	Prow Pass		Tcp				44tcpnw, 44cpnw, 44tcpw
Middle Volcanic Aquifer	Bedded tuff				Tcpbt		44tcpbt
Middle Volcanic Aquifer	Bullfrog Tuff		Tcb				44tcbnw, 44tcbunw, 44tcbw
Middle Volcanic Aquifer	Bedded tuff				Tcbbt		44tcbbt
Middle Volcanic Aquifer	Tram Tuff		Tct				44tct
Middle Volcanic Aquifer	Bedded tuff				Tcibt		44tcbt
Middle Volcanic Aquifer	Lava and flow breccia (informal)				Tl		
Middle Volcanic Aquifer	Bedded tuff				Tlibt		
Middle Volcanic Aquifer	Lithic Ridge Tuff		Tr				
Middle Volcanic Aquifer	Bedded tuff				Tlrbt		
Middle Volcanic Aquifer	Lava and flow breccia (informal)				Tl12		
Middle Volcanic Aquifer	Bedded tuff				Tl2bt		
Middle Volcanic Aquifer	Lava and flow breccia (informal)				Tl13		
Middle Volcanic Aquifer	Bedded tuff				Tl3bt		
Middle Volcanic Aquifer	Older tuffs (informal)				Ti		
Middle Volcanic Aquifer	Unit a (informal)				Tia		
Middle Volcanic Aquifer	Unit b (informal)				Tib		

Appendix 1.--Correlation of RIB and ISM2.0 to Hydrogeologic Units

Site Saturated Zone Hydrogeologic Unit	Geologic/Lithologic Stratigraphy (RIB item 1.1.2.1)						ISM2.0
	Definition/Buesch (1996)	Group	Formation	Member	Zone	Subzone	
Middle Volcanic Aquifer	Unit c (informal)			Tic			
Middle Volcanic Aquifer	Sedimentary rocks and calcified tuff (informal)			Tca			
Middle Volcanic Aquifer	Tuff of Yucca Flat (informal)			Tyf			
Middle Volcanic Confining Unit							
Lower Volcanic Aquifer							
Lower Volcanic Confining Unit							
Undifferentiated Valley-Fill							
Upper Carbonate Aquifer							
Upper Clastic Confining Unit							
Lower Carbonate Aquifer	Lone Mountain Dolomite		Slm				palcozoicGrav (not used)
Lower Carbonate Aquifer	Roberts Mountain Formation		Srm				palcozoicGrav (not used)
Lower Clastic Confining Unit							
Granitic Confining Unit							

**HYDROGEOLOGY AND PRELIMINARY
THREE-DIMENSIONAL FINITE-ELEMENT
GROUND-WATER FLOW MODEL OF THE SITE
SATURATED ZONE, YUCCA MOUNTAIN, NEVADA**

**U.S. Geological Survey
Yucca Mountain Project Milestone Report SP23NM3**

**Prepared in cooperation with the
NEVADA OPERATIONS OFFICE of the
U.S. DEPARTMENT OF ENERGY, under
Interagency Agreement DE-AI08-92NV10874**